Imperial College London

Department of Electrical and Electronics Engineering

Adaptive Protection and Control for Wide-Area Blackout Prevention

Mohd Aifaa bin Mohd Ariff

November 2014

Submitted in part of fulfilment of the requirements for the degree of Doctor of Philosophy in Electrical Engineering of the Imperial College London

I hereby declare that all the work in the thesis is my own. The work of others has been properly acknowledged.

Dedicated to my family, especially my wife, Sofia Najwa

"My project was retarded by laws of nature. The world was not prepared for it. It was too far ahead of time. But the same laws will prevail in the end and make it a triumphal success."

Nikola Tesla

Abstract

Technical analyses of several recent power blackouts revealed that a group of generators going out-of-step with the rest of the power system is often a precursor of a complete system collapse. Out-of-step protection is designed to assess the stability of the evolving swing after a disturbance and take control action accordingly. However, the settings of out-of-step relays are found to be unsatisfactory due to the fact that the electromechanical swings that occurred during relay commissioning are different in practice. These concerns motivated the development of a novel approach to recalculate the out-of-step protection settings to suit the prevalent operating condition. With phasor measurement unit (PMU) technology, it is possible to adjust the setting of out-of-step relay in real-time.

The setting of out-of-step relay is primarily determined by three dynamic parameters: direct axis transient reactance, quadrature axis speed voltage and generator inertia. In a complex power network, these parameters are the dynamic parameters of an equivalent model of a coherent group of generators. Hence, it is essential to identify the coherent group of generators and estimate the dynamic model parameters of each generator in the system first in order to form the dynamic model equivalent in the system.

The work presented in this thesis develops a measurement-based technique to identify the coherent areas of power system network by analysing the measured data obtained from the system. The method is based on multivariate analysis of the signals, using independent component analysis (ICA). Also, a technique for estimating the dynamic model parameters of the generators in the system has been developed. The dynamic model parameters of synchronous generators are estimated by processing the PMU measurements using unscented Kalman filter (UKF).

Contents

Acknowledgements

I would like to thank my supervisor Professor Bikash Pal for his dedicated guidance, encouragement and financial support. I also wish to thank Professor Arun Phadke and Professor James Thorp, of Virginia Polytechnic Institute and State University (Virginia Tech) who helped me with the work on protection system. I am thankful to Dr. Martin Clark and Abhinav Kumar Singh for their support direction and constructive criticism during parts of my research. I would also like to acknowledge the Ministry of Education Malaysia through the Universiti Tun Hussein Onn Malaysia and SLAI Program for funding my PhD research. Finally, I would like to thank my families and friends for their support and understanding during my PhD study.

List of Figures

List of Tables

List of Nomenclature

$\boldsymbol{x}(t)$	Continuous state variables,
$\boldsymbol{x}_k$	Discrete state variables,
$\boldsymbol{y}(t)$	Continuous output variables,
$\boldsymbol{y}_k$	Discrete output variables,
$\boldsymbol{u}(t)$	Continuous input variables,
$\boldsymbol{u}_k$	Discrete input variables,
$\boldsymbol{v}(t)$	Continuous process noise variables,
$\boldsymbol{v}_k$	Discrete process noise variables,
$\boldsymbol{w}(t)$	Continuous measurement noise variables,
$\boldsymbol{w}_k$	Discrete measurement noise variables,
$\boldsymbol{f}(.)$	State update function,
$\boldsymbol{h}(.)$	Measurement function,
$\hat{\boldsymbol{x}}_k$	Estimated mean of the state,
$\boldsymbol{P}_{x_k}$	Estimated covariance matrix of the state,
$\boldsymbol{Q}$	Process noise covariance,
$\boldsymbol{R}$	Measurement noise covariance,
$\boldsymbol{x}_k^a,\ \boldsymbol{X}_k$	Augmented state variables,
$\hat{\boldsymbol{X}}_k$	Estimated mean of augmented state,
$\boldsymbol{P}_{\boldsymbol{X}_k}$	Estimated covariance of augmented state,
$\boldsymbol{\psi}$	Parameters vector,
Δt	Time step,
L	Dimension of state vector,
$\boldsymbol{\chi}$	Sigma points of state vector,
$\boldsymbol{\chi}^-$	Predicted sigma points of state vector,
n	Length weight of sigma points,
W	Associated weight of sigma points,
$\hat{\boldsymbol{X}}_k^-$	Weighted mean of predicted sigma points,
$\boldsymbol{P}_{\boldsymbol{X}_k}^-$	Covariance of predicted sigma points,

$\boldsymbol{\gamma}^-$	Sigma points of predicted measurement,
$\hat{\boldsymbol{y}}_k^-$	Weighted mean sigma points of predicted measurement,
$\boldsymbol{P}_{\boldsymbol{y}_k}^-$	Covariance of sigma points of predicted measurement,
$\boldsymbol{P}_{\boldsymbol{x}_k\boldsymbol{y}_k}^-$	Cross-correlation matrix,
$\boldsymbol{K}_k$	Kalman gain,
δ	Rotor angle (rad),
ω	Rotor speed (pu),
ω_0	Synchronous speed (pu),
ω_B	Base speed (rad/s),
P_m	Mechanical input power (pu),
T_m	Mechanical input torque (pu),
T_e	Electrical input torque (pu),
E'_d	d-axis transient voltage,
E'_q	q-axis transient voltage,
i_d	d-axis armature current,
i_q	q-axis armature current,
v_d	d-axis terminal voltages,
v_q	q-axis terminal voltages,
P_g	Active power (pu),
Q_g	Reactive power (pu),
P_L	Active power component of the load (pu),
Q_L	Reactive power component of the load (pu),
P_{L0}	Nominal value of active power component of the load (pu),
Q_{L0}	Nominal value of reactive power component of the load (pu),
V_g	Voltage magnitude (pu),
θ_g	Phase angle (rad),
V_L	Voltage magnitude at load terminal (pu),
a_P	Constant power fraction for active power component,
b_P	Constant power fraction for reactive power component,
a_I	Constant current fraction for active power component,
b_I	Constant current fraction for reactive power component,
a_Z	Constant impedance fraction for active power component,
b_Z	Constant impedance fraction for reactive power component,
E_q	Generator internal voltage (pu),
x_d	d-axis synchronous reactance (pu),
x_q	q- axis synchronous reactance (pu),

x'_d	d-axis transient reactance (pu),
x'_q	q-axis transient reactance (pu),
T'_{d0}	d-axis transient time constant (pu),
T'_{q0}	q-axis transient time constant (pu),
R_a	Stator resistance (pu),
E_{fd}	Excitation field voltage (pu),
H	Inertia constant (s),
M	Inertia coefficient (pu),
V_g^u	Pseudo input for voltage magnitude V_g,
P_g^u	Pseudo input for active power P_g,
V_g^w	Pseudo process noise for voltage magnitude V_g,
P_g^w	Pseudo process noise for active power P_g.

Chapter 1

Introduction

The advent of global electrification drives the world advancement in technology in every industrial sector. The modern alternate current (ac) power system began with the early design and implementation of high voltage ac generation and transmission system by Nikola Tesla, dated back to 1885. After more than a century of development, power system networks have grown in size and complexity. With thousands of generating units all interconnected by a complex network consisting of ac, transformers, high voltage direct current (dc) system and other complex equipment, the daily operation delivering safe, reliable and high quality electric power energy to the user is a very complicated task. It requires continuous planning work on top of the constant monitor and action of the operator. Increasing numbers of recent wide-area system blackouts have been a constant reminder of the fact that the prevalent modus operandi on delivering power to customers is not sufficient in maintaining the security of the power system during operation. Fig. 1.1 illustrates a visual summary of the blackouts and major power system disturbances of the past several decades in the world [1]. All these blackouts and disturbances cause tremendous loss of generations and loads in the networks leading to disastrous impact on customers and the economy in general. Usually, these disturbances happen when the power systems are heavily loaded and a number of multiple outages occur within a short period. As a result, these events initiate power oscillations between neighbouring utility systems and reduce network voltages, consequently causing voltage and angular instability in the system.

Power system stability is an overriding concern in power system operation. The power system operates very close to its nominal frequency at all times and

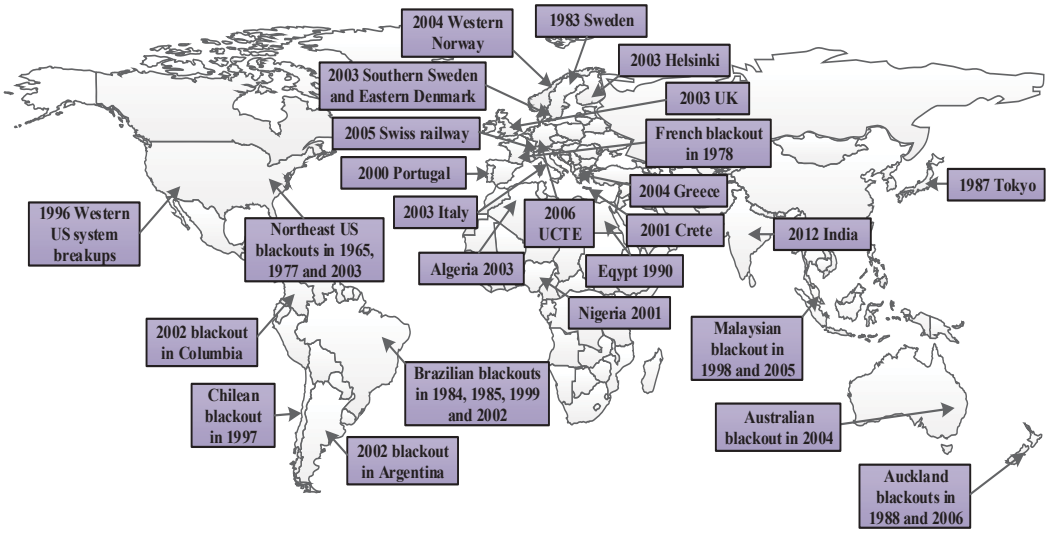

Figure 1.1: Major system disturbances and blackouts

all synchronous machines connected to the system are in step with each other and operate at the same average speed. The generator speed governors maintain the average machine speed close to its nominal value while continuous changes in load and network configuration are constantly taking place, providing small disturbance to the network. However, when faults occur in the system, the resulting disturbances are no longer small, causing severe oscillations in machine rotor angles and consequent power flow swing in the system. Depending on the severity of the disturbance and the system protection and control action, a power swing may evolve into a stable or an unstable power swing. A stable power swing implies that the system may remain stable and return to synchronous operation following a disturbance. On the other hand, an unstable power swing may cause the system to lose synchronism, with groups of machines accelerating or decelerating away from the synchronous speed. Nevertheless, the protective relays must be able to discriminate between the fault, stable power swing and out-of-step conditions.

The detection function to discriminate between the fault, stable power swing and out-of-step condition is served by the conventional out-of-step protection system, which has multiple characteristics. A fault in the system causes the apparent impedance to lie inside the characteristic of a distance relay, and so does the power swing. Therefore, the protection system must be able to distinguish between a fault and a power swing. The primary aspect of distinction is the speed at which the two phenomena occur: a fault trajectory moves into a zone almost instantaneously

(within a few milliseconds), while a power swing moves more gradually. Typically, a power swing oscillates at the frequency less than 1 Hz, with oscillations of 0.5-0.8 Hz being common [2]. This gives a period of oscillation greater than 1 second, which is a rather long time for observation of the phenomenon. Typically, a power swing oscillation is observed on a complex impedance plane (R-X plane) with the x-axis represents resistance (R) and the y-axis represents reactance (X). Therefore, if the trajectory speed of the impedance locus in the R-X plane travels relatively quickly, it is treated to be a fault, and take the corresponding action. However, if the transition is gradual, the phenomenon is identified as a power swing. Therefore, for out-of-step relay applications, extensive stability studies with different operating conditions are performed to determine the rate and the trajectory of the possible power swing. The relay characteristic should be set such that for all stable swings, the impedance trajectory comes no closer than a certain minimum distance from its origin in the R–X plane. Thus, an additional zone with a setting smaller than this minimum distance should be chosen to detect an unstable swing. If the impedance trajectory encroaches upon this additional impedance zone, an unstable swing is declared. On the other hand, if a power swing does not encroach into this additional zone, the swing is determined as a stable swing. Upon detecting an unstable swing, an out-of-step condition is declared, and appropriate tripping or blocking action should be initiated depending upon the requirements of the system.

In the context of 14^{th} August 2003 blackout in the Northeast of United States and Southeast Canada, the conventional out-of-step protection relay is found to be unsatisfactory in highly interconnected power networks [3]. This is because the operating conditions and modelling details assumed during relay commissioning do not represent the prevalent dynamic behaviour of the system. Hence, the power swings that occur in the system are quite different from those simulated in the study when the relay is set. Consequently, the conventional out-of-step relay fails to determine correctly the stability the evolving power swing following a disturbance. This may cause the relay to either mal-operate or miss-operate depending on the nature of disturbance and the characteristic of the relay [4]. Mal-operation is a condition when a relay operates although its operation is not required. On the other hand, miss-operation is a condition when a relay fails to operate although its operation is required. Consequently, the inaccurate corresponding control actions exacerbate the impact of the initial disturbance to the system by triggering cascading event. This is a very difficult challenge given that the power system

network involves rapid switching of the lines and load variation during operation. Moreover, increasing addition of power electronics interfaced renewable generation at transmission level also influence the apparent impedance seen by the out-of-step relay during power swing. All these uncertainties and variations demand regular update of the relay setting to adapt to the prevailing operating situation.

1.1 Adaptive philosophy in protection system

The advancement and application of computer-based protection in power systems has opened the possibility for the protection system to permit automatic changes within the protection system itself as the power system undergoes normal or abnormal changes during operation. Therefore, with the concept of adaptive relaying, it is not necessary to anticipate all contingencies during relay commissioning. Adaptive relaying is defined as follows: "*it permits and seeks to make adjustments automatically in various protections in order to make them attuned to prevailing power system conditions*" [5]. The key concept is to change something in a protection system in response to the changes in the power system caused by load variations, network switching operations, or faults. To a certain extent, all existing protection systems must accommodate power system changes. Typically, this is realised by making the relay settings suitable for all plausible assumption of network conditions. However, such consideration usually causes deficiencies in the conventional protection system because it is almost impossible to anticipate all possible system contingencies during the commissioning of the protection system.

It is also worth noting that the application of adaptive protection functions closes the gap between control and protection functions in power system operation. Many protection systems have already incorporated control functions in their operation. As the protection system adapts its characteristic based on the change of operating conditions in power system, the adaptive protection systems utilise the classic concept of feed-back control. Indeed, adaptive relaying is in fact a feed-back control system [6].

Since adaptive protection system implies that the relays must adjust their characteristic to accommodate the change in the system conditions, computer relays with communication links are required. Subsequently, some adaptive protection systems adapt their characteristic using the local substation measurements

while others require real-time data measured from the remote locations. Among other options, fibre optic communication links are one of the feasible options for such voluminous data transfers. The modern wide area measurements (WAMS) technology is able to facilitate all these requirements for the application of adaptive protection system in practice [7]. Eventually, as the installations of WAMS technology become more commonplace, many more adaptive relaying concepts are likely to be implemented by the industry.

1.2 Roles of PMU in improving power system monitoring

The electric power system is one of the largest machines ever invented by men. It is spread over a large geographical area. Therefore, effectively monitoring the system requires measurements gathered from different locations to a central location. Additionally, the time synchronisation of the measurements taken at different locations is also an important factor in monitoring such a large system. Accurate time synchronisation is vital, especially during post-mortem analysis after a severe disturbance, validating simulation models or in real-time monitoring, protection and control. The recent advent of the WAMS technology based on synchronized phasor measurements has provided a solution to this problem.

The WAMS technology offers precise measurements of positive sequence voltages and currents at remote locations using Phasor Measurement Units (PMUs). Fig.1.2 illustrates a generic PMU structure. The basic structure of a PMU is similar with structure of computer relay. The utilisation of voltage and current measurements as input signals are sampled and converted to positive sequence quantities. The measurements are time-tagged using a GPS clock and can be refreshed as frequently as once every cycle. Reference [7, 8] provides detailed information about WAMS.

The time-synchronized outputs of the PMU are available for local substation utilisation or they can be transferred to remote location through communication hubs known as Phasor Data Concentrators (PDCs). Fig. 1.3 shows the hierarchical arrangement of WAMS. The PDCs organize time-synchronized measurement data received from various PMU according to their corresponding time-tags so that a synchronized data stream is available for various power system applications and for

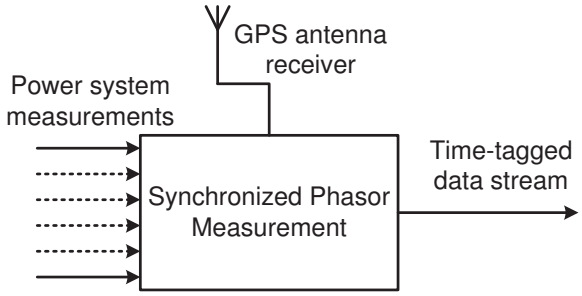

Figure 1.2: A generic PMU

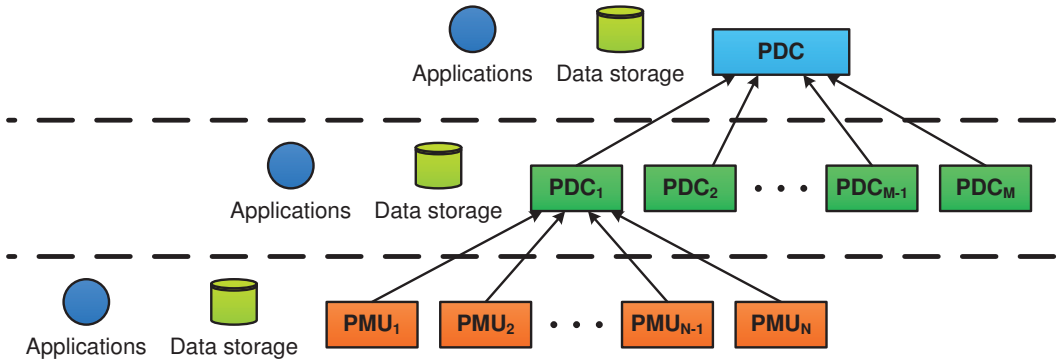

Figure 1.3: Hierarchy of PMUs and PDCs

communication with the upper level of hierarchy for further data concentration. The PDCs and PMUs are capable of storing archival data which are useful for post-mortem analysis of major system events. The PMU data measured from the system can be utilised at any level of the WAMS hierarchical structure. It is clear that the volume of data collected increases at the higher level of WAMS hierarchy. Hence, the utilisation of the data at various level of the hierarchy is only suitable for certain selection of applications. Since the measurements are locally available, relatively fast application can be taken at the PMU level. On the other hand, power system applications that require data from wide areas need more time in order to achieve acceptable performance of their functions. This distinction in applications is true for system monitoring and control applications, as well as for the protection applications using WAMS.

The work reported in this thesis focuses on the protection application using WAMS for stability enhancement emphasizing on the out-of-step relay application. The out-of-step relay is engineered to detect the condition following a large disturbance that may cause generators in one part of the system to accelerate

while generators in another part of the system decelerate, thereby creating a condition where two parts of the system are likely to separate. In order to monitor the generator behaviour after a large disturbance effectively, dynamic properties of generators in the system need to be monitored in real-time. Time-synchronized network quantities such as voltage magnitude, voltage angle, active power, and reactive power measurements at near to large generation units or grid supply points in the system need to be gathered at a centralised control centre. The out-of-step relay characteristic in the system would be available to the centralised control centre. The method proposed in this thesis tracks the change of dynamic properties in the system that influences the sensitivity of out-of-step relay settings to the system operating condition. Subsequently, out-of-step relay settings (supervisory mho characteristic, blinder settings, and time delay to traverse both blinders) are re-calculate and re-tune to adapt with the change in the operating condition of the system. This out-of-step relay setting adaptation prevents the mal-operation of the relay following a disturbance in the system that often initiates the cascading tripping event.

1.3 Adaptive out-of-step protection

The wide-area measurement system provides accurate time-synchronized phasor measurement. It further motivates the researchers to explore the potential application of adaptive protection in power system. Therefore, many of the ideas of adaptive protection become particularly appealing with the availability of WAMS. However, not every protection system is suitable to be re-designed to be adaptive. The adaptive protection function which is based on WAMS is intended for non-instantaneous protection due to the delays in gathering data at WAMS (typically of the order of 30–100 milliseconds) [9]. Thus, the application of adaptive function using WAMS data is ideal for the backup and system protection system. Several ideas of adaptive protection system can be found in the literature [10]. Among these, one is adaptive out-of-step relaying. The application of adaptive out-of-step protection system involves the general problem in trying to predict the instability of a power swing as it is developing following a disturbance. A power swing evolves in a relatively long period of time; it may take a few seconds. Therefore, the adaptive schemes are particularly suited for the out-of-step protection

system and potentially huge benefits can be achieved by embracing the adaptive protection philosophy.

Typically, out-of-step relays are utilised in the systems to assess the stability between two or more regions and initiate appropriate actions corresponding to the outcome of an evolving power swing in the system after a disturbance. Fig.1.4 shows the generic apparent impedance trajectory seen by the relays in R-X plane during a power swing in the system. Depending on the severity of the disturbance, the distance relay at a bus may see impedance trajectory of Y-Y or Z-Z. The impedance trajectory of Y-Y and Z-Z correspond to a stable power swing and an unstable power swing, respectively. The shaded area represents the tripping zone of the relay. In any case, these impedance trajectories may encroach one of the trip zones of the relay as illustrated in Fig. 1.4. The function of the out-of-step relay is to discriminate between the movements of impedance trajectory representing a fault and the movement of impedance trajectory representing a stable power swing as they enter the trip zone of the relay. Conventionally, this is realised by using the movement speed of impedance trajectory criterion. In the case of fault, the impedance trajectory travels almost instantaneously while the impedance trajectory represent a stable power swing moves at relatively slow speed. Consequently, the detection of an out-of-step condition indicates that the controlled separation of the system is necessary in response to a system disturbance that will lead to wide-area instability. Hence, the out-of-step protection system should initiate selective tripping to separate the system into several sustainable islands with a reasonable balance between the generation and load within each island. At present, the trip locations for controlled separation are pre-determined. The pre-determined trip location is established based upon simulations studies performed during system commissioning. However, a whole new research area dedicated to determine the desirable locations for controlled separation in real time can be found in the literature which is beyond the scope of this thesis. Therefore, it is not being discussed in detail here.

This thesis focuses on the first part of the problem in out-of-step relays which is determining whether the system with developing power swing following a disturbance is able to return to synchronized operation. It is an interesting yet challenging problem in power system operation especially in a large interconnected power system network. The issue with the conventional method in determining the stability of the developing power swing are found to be inadequate in highly

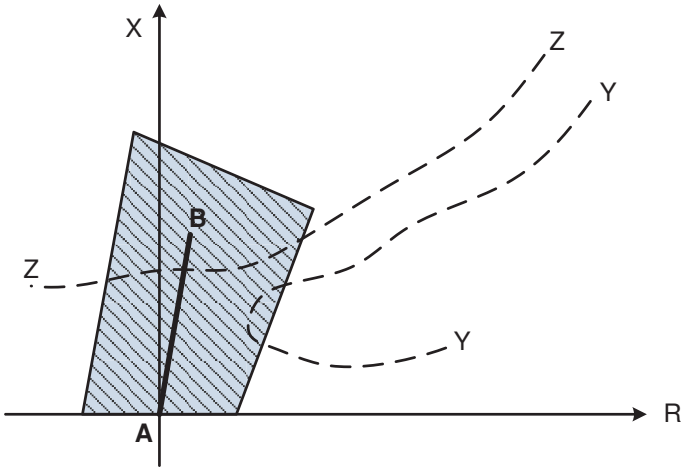

Figure 1.4: Power swing excursion into the trip zone of relay

interconnected power networks. Since the setting of out-of-step relays are determined based on model-based simulation studies over large number of operating scenarios, there will always be some risk involved as in practice. The dynamic behaviour of large interconnected power networks can never be closely represented through model-based simulation. The famous WECC blackout in 1996 corroborated this fact, where measured response in the period just preceding the blackouts did not match with simulated results using the planning model. Consequently, the conventional out-of-step relays often mal-operate. The relays failed to assess the stability of the evolving electromechanical swing, resulting erroneous control actions of the relays. Thus, an out-of-step relay which adapts itself to changing system conditions is believed to be an elegant solution to this problem.

It is clarified in the previous section that in out-of-step relay operation, the behaviour of the evolving power swing is translated into the trajectory of the impedance locus in R-X plane. The speed and path of the apparent impedance trajectory are primarily influenced by the dynamic parameters seen by the out-of-step relay. In a large interconnected power networks, these parameters are the dynamic parameters of an equivalent model of a coherent group of generators. The equivalent dynamic model of coherent group of generators is a single generating unit that exhibits the similar time trend of angular speed, voltage, and electrical and mechanical power as the generators in a coherent group during any perturbation. Therefore, it is essential to identify the coherent groups and to estimate the dynamic model parameters of the individual generating units in the system

first in order to form the dynamic equivalent of the system. The identification of coherent groups in the system also helps in identifying the critical location of the out-of-step relays that are prone to mal-operate during power swing. When the dynamic equivalent of the system has been determined, the setting of the out-of-step protection can be recalculated and retuned to suit the prevailing system operating condition.

1.4 Research objectives

The following list clarifies the research objectives of this thesis.

- *To develop a WAMS supported measurement-based technique to identify the coherent areas of power system network by analysing the measured data obtained from the system.* The method is based on multivariate analysis of the signals, using independent component analysis (ICA). Like other existing methods, the proposed method is able to identify the correct coherency group of generators and buses in the system. The ICA is preferred compared to the other methods because it is simple, accurate, and robust in filtering out the effect of noise in practical measured signals. The effectiveness of the proposed method is validated in a simulated data from 16-machine 68-bus test system model and PMU data from UK university-based WAMS system. The coherency property helps in developing the adaptive out-of-step protection in a large interconnected power system. It also helps in identifying the critical location of the relays which are prone to mal-operate during power swing.

- *To develop a technique for estimating the dynamic model parameters of the individual generating units in the system.* The dynamic model parameters of synchronous generators are estimated by processing the PMU measurements using unscented Kalman filter (UKF). It calculates the statistics of random variables that undergo a non-linear transformation. The UKF method is simple, accurate, fast and robust in filtering out the effect of noise in the estimated parameters. Validation is performed on the simulated data from 16-machine 68-bus test system model. It is demonstrated that the approach is able to estimate accurate dynamic model parameters even with the presence of noise in the measured data. Moreover, the UKF is completely data

driven and recursive thus offering real opportunity of fast estimation in real time. The dynamic parameters estimated using this approach influence the setting of out-of-step relays. In practice, the variation and uncertainties of these parameters expose the secure and accurate operation of out-of-step relays. Therefore, these parameters require continuous estimation in order to recalculate and retune the setting of out-of-step relay to suit the prevalent operating situation.

- *To develop a novel approach to recalculate and retune the out-of-step protection settings to suit the prevalent operating condition.* The stability of the evolving swing resulting from a disturbance needs to be assessed and appropriate control action needs to be taken in order to contain the disturbance. Out-of-step system protection is designed to serve this purpose. The out-of-step relay assesses the stability of an evolving swing by monitoring the trajectory and speed of the apparent impedance in the system. This is realised through the out-of-step relay settings characterized by the supervisory mho element, the blinders elements, and the time delay for the apparent impedance to traverse across the relay's blinders elements. However, these settings are found to be frequently unsatisfactory. This is because the condition assumed during the commissioning of the relay becomes out-of-date rather quickly. Furthermore, the electromechanical swings that occurred after a disturbance during operation are different in practice from its planning model. The thesis proposes an out-of-step protection system which adapts itself to the prevalent system operating condition. The method is based on the application of extended equal area criterion (EEAC) using real time dynamic representation of the system to determine the adaptive setting of the out-of-step relay. It is demonstrated that the adaptive setting of out-of-step relay is able to detect an out-of-step condition accurately even with the changes in the system operating condition.

1.5 Thesis contributions

- The technical investigation of recent wide area blackout shows that the maloperation of the protection system during power swing is often a cause for a complete system blackout. Hence, the investigation and analysis of the

impact of electromechanical oscillation following a disturbance to the performance of protection system is presented.

- A measurement-based coherency identification technique using ICA method to determine the coherent group of generator and buses following a disturbance is proposed. The proposed method is completely data driven, accurate and robust in the present of noise in the measured data. The novel contribution of this method is to deal with the order inconsistency of ICs in the ICA algorithm by sorting ICs and their corresponding mixing matrix according to their dominance. The application of the proposed coherency identification method on simulated data and actual WAMS data is also presented.

- The setting of out-of-step protection system is primarily determined by the dynamic model parameters of the system. A method that continuously estimate the dynamic parameters to tailor the setting of out-of-step protection system to suit with the system prevailing operating condition is presented. Novel contribution of the dynamic model parameter estimations technique proposed in this research has been made in the augmentation of the state, the set of unknown model parameters, and the process noise covariance into a higher order state vector in the UKF algorithm for the dynamic model parameter estimations of the system. The sigma point distribution in UKF algorithm applied in this research is considered as one of the novel contributions in this study. This is because it has never been applied in the application of UKF algorithm in power system prior to the work reported in this thesis. The performance of the proposed method is demonstrated on simulated data.

- A novel approach of recalculating the setting of out-of step protection is proposed. The proposed method is based on the application of the EEAC method using real-time dynamic representation of the system to provide vital information for out-of-step relay setting calculations. The novel feature of the proposed adaptive out-of-step protection system is the formulation of the algorithm to calculate the setting of an out-of-step protection relay online based on the timely estimations of the dynamic characteristics of the system. It is shown that the proposed method adapts the out-of-step protection setting to suit the prevailing system condition, hence ensures the correct and

secure operation of out-of-step protection. Ensuring the appropriate protection and control actions of the relay prevents the relay mal-operation which often to be the cause of a wide-area blackout.

- A modelling guide for multi-machine power system model for transient stability analysis is presented.

1.6 Outline

The thesis is organized as follows:

The thesis is organised as follows. Following the introduction, **Chapter 2** presents the modelling details of different components of the power system and phasor measurement unit consideration used in the remainder of work. **Chapter 3** presents the coherency identification technique using ICA proposed in this thesis. The application of ICA on the generator speed and bus angle data, simulated data from 16-machine 68-bus system model and actual PMU data gathered through UK University-based Wide-Area Measurement System is presented in this chapter. The results obtained using the proposed method are presented, analysed and discussed in this chapter as well. **Chapter 4** seeks to continuously estimate the dynamic parameters of the system. The application of UKF to estimate the dynamic model parameters in the system using PMU data is presented. Validation is performed on the simulated data from 16-machine 68-bus test system model. **Chapter 5** presents the proposed method to recalculate and retune the out-of-step protection system. It is based on the application of EEAC using real time dynamic representation of the system to determine the adaptive setting of the out-of-step relay. In this chapter, the simulated data from 16-machine 68-bus system model is used to demonstrate the performance of the proposed method in ensuring the accurate and secure operation of the out-of-step relay during an electromechanical oscillation. Finally, the conclusions of key results are presented in **Chapter 6**. Future research directions in line with the work presented in the thesis are also presented in this final chapter.

1.7 Publications

The following list of journal publications represent the work reported in this thesis.

1. Ariff, M. A. M. and Pal, B. C., "Coherency Identification in Interconnected Power System—An Independent Component Analysis Approach", IEEE Transactions on Power Systems, vol. 28, no. 2, pp.1747-1755, May 2013.

2. Ariff, M. A. M.; Pal, B. C.; and Singh, A. K., "Estimating Dynamic Model Parameters for Adaptive Protection and Control in Power System", IEEE Transactions on Power Systems, vol. PP, no. 99, pp.1-11, July 2014.

Chapter 2

Modelling details and considerations

The main sources of electrical power energy are the synchronous generators. In power system stability studies, the primary challenge is to ensure the synchronism of the interconnected synchronous generators after a disturbance. All the generating units are interconnected by a myriad of transmission lines, transformers and other complex transmission equipment. Hence, the stability of the system is also dependent on these components. Consequently, accurate understanding of the fundamental characteristic and modelling of these components are important for stability studies and protection design. In this chapter, a brief overview of power system modelling is given. The technical considerations of PMU used in this thesis are also included in this chapter.

2.1 Modelling of multi-machine system

Precise modelling of the synchronous generators is crucial for studying the dynamic behaviour of power systems. Besides synchronous generators, other components such as the loads, transmission lines, transformers need to be modelled as well. Generally, the dynamic behaviour of these components is described through a set of differential equations. On the other hand, the power flow in the network is represented by a set of algebraic equations. Thus, a set of differential-algebraic equations (DAE) is used to describe the behaviour of power system. There are various

models reported in the literature for each component depending on their application. However, only the relevant equations governing the dynamic behaviour of specific types of models used in this study are described. The modelling presented in this section has been well described in [11, 12, 13] and is included here to extend the discussion of ideas presented.

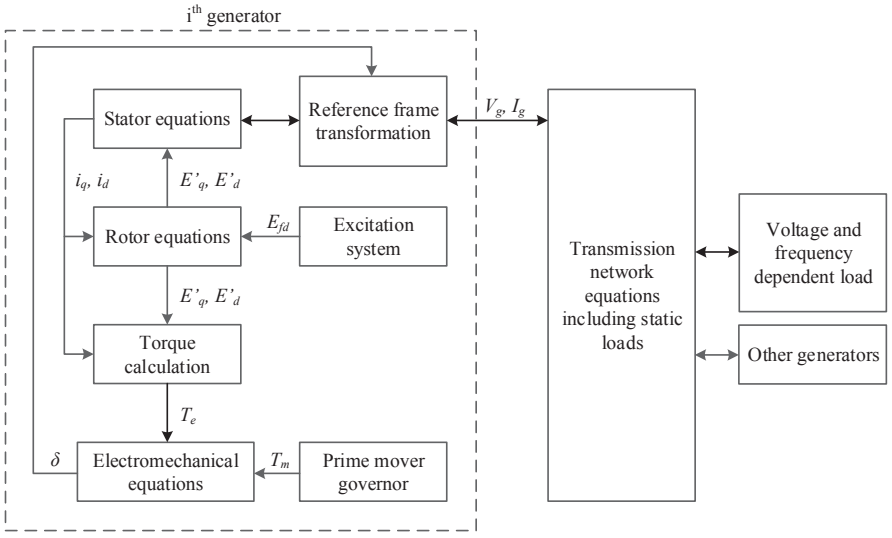

Figure 2.1: The general structure of power system model

Fig. 2.1 depicts a commonly used structure of a power system model for transient stability studies. The overall power system model includes models for the following individual components:

1. Synchronous generator, associated excitation system and prime mover governor,
2. Interconnecting transmission network including static loads,
3. Voltage and frequency dependent loads.

2.1.1 Generator modelling

In this thesis, the synchronous generator model is represented by a model consisting of a field coil on the d-axis and a damper coil on the q-axis (model 1.1). For simplification, the turbine governor and excitation system dynamics are neglected, resulting in mechanical input torque T_m and excitation field voltage E_{fd} being a

constant, respectively. Consequently, the individual machine electromechanical, rotor and stator equations are given in (2.1), (2.2) and (2.3), respectively.

Electromechanical equations

$$\frac{d\delta}{dt} = \omega_B \left(\omega - \omega_0\right) \tag{2.1a}$$

$$\frac{d\omega}{dt} = \frac{1}{2H} \left[T_m - T_e - D\left(\omega - \omega_0\right)\right] \tag{2.1b}$$

Rotor equations

$$\frac{dE'_q}{dt} = \frac{1}{T'_{d0}} \left[-E'_q + \left(x_d - x'_d\right) i_d + E_{fd}\right] \tag{2.2a}$$

$$\frac{dE'_d}{dt} = \frac{1}{T'_{q0}} \left[-E'_d + \left(x_q - x'_q\right) i_q\right] \tag{2.2b}$$

Stator equations

$$v_q = E'_q + x'_d i_d - R_a i_q \tag{2.3a}$$

$$v_d = E'_d - x'_q i_q - R_a i_d \tag{2.3b}$$

Electrical torque is calculated using (2.4).

$$T_e = E'_q i_q + E'_d i_d + \left(x'_d - x'_q\right) i_d i_q \tag{2.4}$$

where,

δ	Generator rotor angle,
ω	Generator rotor speed,
ω_0	Synchronous speed,
ω_B	Base speed,
H	Inertia constant,
T_m, T_e	Mechanical and electrical input torque, respectively,
E'_d, E'_q	d- and q- axis transient voltage, respectively,
i_d, i_q	d- and q- axis armature current, respectively,
v_d, v_q	d- and q- axis terminal voltages, respectively,
x_d, x_q	d- and q- axis synchronous reactance, respectively,
x'_d, x'_q	d- and q- axis transient reactance, respectively,
T'_{d0}, T'_{q0}	d- and q- axis transient time constant, respectively,
R_a	Stator resistance,

E_{fd} Excitation field voltage.

It is to be noted that the generator is modelled with respect to the individual generator reference frame (*d-q* frame). However, all individual generators have to be interfaced to the network in order to perform system studies. Hence, v_q and v_d for each generator have to be transformed into a common reference frame. Equation (2.5) shows the relationship between the *d-q* frame and the common reference frame.

$$(F_q + jF_d) = (F_Q + jF_D)\, e^{-j\delta} \tag{2.5}$$

Equation (2.5) can be written in matrix notation as:

$$\begin{bmatrix} F_q \\ F_d \end{bmatrix} = \begin{bmatrix} \cos\delta & \sin\delta \\ -\sin\delta & \cos\delta \end{bmatrix} \begin{bmatrix} F_Q \\ F_D \end{bmatrix} \tag{2.6}$$

Note that, F in (2.6) represents voltages or currents. Also, the subscript d and q are referred as the variables in individual generator *d-q* frame while the subscript D and Q are referred as the variables in common reference frame.

From the stator equations in (2.3), i_q and i_d are solved using (2.7):

$$\begin{aligned} \begin{bmatrix} i_q \\ i_d \end{bmatrix} &= \underbrace{\frac{1}{{R_a}^2 + x'_d x'_q}}_{Y_g} \begin{bmatrix} R_a & x'_d \\ -x'_q & R_a \end{bmatrix} \begin{bmatrix} E'_q - v_q \\ E'_d - v_d \end{bmatrix} \\ &= Y_g \begin{bmatrix} R_a & x'_d \\ -x'_q & R_a \end{bmatrix} \begin{bmatrix} E'_q - v_q \\ E'_d - v_d \end{bmatrix} \end{aligned} \tag{2.7}$$

Using the relationship in (2.6), equation in (2.7) is reformulated in common reference frame as follows:

$$\begin{bmatrix} i_Q \\ i_D \end{bmatrix} = Y_g^{DQ}(t) \begin{bmatrix} E'_Q - v_Q \\ E'_D - v_D \end{bmatrix} \tag{2.8}$$

where,

$$Y_g^{DQ}(t) = Y_g \begin{bmatrix} \cos\delta & -\sin\delta \\ \sin\delta & \cos\delta \end{bmatrix} \begin{bmatrix} R_a & x'_d \\ -x'_q & R_a \end{bmatrix} \begin{bmatrix} \cos\delta & \sin\delta \\ -\sin\delta & \cos\delta \end{bmatrix}$$

It is noted that the rotor angle δ is varying with time. Since $Y_g^{DQ}(t)$ in (2.8) is a function of delta, the term is considered as time varying matrix. Therefore, the evaluation of i_Q and i_D in (2.8) requires the solution for a time varying algebraic equation. This implies that the network matrix has to be factorised at every time step to solve for i_Q and i_D, which increases the computational complexity. Hence, the dummy coil approach [13] is applied to eliminate the solution of time varying algebraic equations and to develop an approximate equivalent circuit. Using this approach, the stator equations are rewritten as follow:

$$v_q = E'_q + x'_d i_d - R_a i_q \tag{2.9a}$$

$$v_d = E'_d + E'_{dc} - x'_d i_q - R_a i_d \tag{2.9b}$$

where,

$$E'_{dc} = -\left(x'_q - x'_d\right) i_q \tag{2.10}$$

In (2.10), E'_{dc} is a function of i_q. Therefore, it requires the solution of network equations. In the dummy coil approach, E'_{dc} is approximated by considering the term as a fictitious voltage source proportional to a flux linkage of a dummy coil in the q-axis of the armature that has no coupling with other coils. E'_{dc} is considered as a state variable and the differential equation for the term is expressed as follows:

$$\frac{dE'_{dc}}{dt} = \frac{1}{T_c}\left[-E'_{dc} - \left(x'_q - x'_d\right) i_q\right] \tag{2.11}$$

where T_c is the open circuit constant of the dummy coil. For acceptable accuracy, T_c is typically set to 0.01 [13].

Equations (2.1) to (2.11) represent the synchronous generator model with a field circuit with one equivalent damper on q-axis (model 1.1). Simpler model is conveniently achieved by modifying the generator parameters of model 1.1. For classical model, the generator parameters of model 1.1 are altered as follows:

$$x'_q = x_q = x'_d \tag{2.12a}$$

$$x_d = 6x'_d \tag{2.12b}$$

$$T'_{q0} \neq 0 \tag{2.12c}$$

$$T'_{d0} = \text{Large value (say 1000s)} \tag{2.12d}$$

Modification in (2.12) forces E'_d to remains at zero while E'_q remains constant.

2.1.2 Load modelling

The active and reactive components of load powers are represented as polynomial function of static voltage dependent models separately, given as follows:

$$P_L = a_P P_{L0} + a_I \left(\frac{P_{L0}}{V_{L0}}\right) V_L + a_Z \left(\frac{P_{L0}}{{V_{L0}}^2}\right) {V_L}^2 \tag{2.13a}$$

$$Q_L = b_P P_{L0} + b_I \left(\frac{Q_{L0}}{V_{L0}}\right) V_L + b_Z \left(\frac{Q_{L0}}{{V_{L0}}^2}\right) {V_L}^2 \tag{2.13b}$$

where,

P_L, Q_L	Active and reactive power component of the load, respectively,
P_{L0}, Q_{L0}	Nominal value for active and reactive power component of the load, respectively,
V_L	Voltage magnitude at load terminal,
a_P, b_P	Constant power fraction for active and reactive power component of the load, respectively,
a_I, b_I	Constant current fraction for active and reactive power component of the load, respectively,
a_Z, b_Z	Constant impedance fraction for active and reactive power component of the load, respectively.

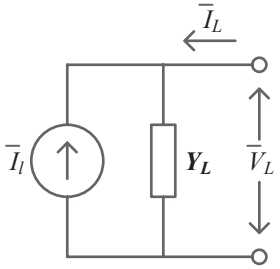

Figure 2.2: Load equivalent circuit

Fig. 2.2 represents the equivalent circuit of the load at a bus. From the figure, the load admittance Y_l is calculated using the nominal value of active and reactive power components of the load (P_{L0} and Q_{L0}) at nominal voltage V_{L0}, as

follows:

$$Y_l = \frac{P_{L0} - jQ_{L0}}{{V_{L0}}^2} \tag{2.14}$$

During a transient, $\overline{I}_L$ is given by:

$$\begin{aligned} -\overline{I}_L &= \left(\frac{P_L + jQ_L}{\overline{V}_L}\right)^* - Y_l \overline{V}_L \\ &= \overline{I}_l - Y_l \overline{V}_L \end{aligned} \tag{2.15}$$

If both active and reactive power components of the load are modelled as constant impedance type, $\overline{I}_l$ will be equal to zero. Otherwise, $\overline{I}_l$ will be zero only during initial operating point.

2.1.3 Network modelling

A transmission network mainly consists of transmission lines and transformers. Since the time constants of these elements are relatively small compared to the mechanical time constants, the network transients are neglected. Also, it is assumed that the network is symmetric. Hence, the positive sequence network is adequate to represent the network. The transmission network is represented by an algebraic equation given in (2.16):

$$(\boldsymbol{Y}_N)\,\overline{V} = \overline{I}_N \tag{2.16}$$

where $\boldsymbol{Y}_N$ is a network bus admittance matrix, $\overline{V}$ is a vector of bus voltages and $\overline{I}_N$ is a vector of injected bus currents. The generator and load equivalent circuits at all the buses are integrated into the network and the overall system algebraic equation is given by:

$$(\boldsymbol{Y})\,\overline{V} = \overline{I} \tag{2.17}$$

From (2.17), $\boldsymbol{Y}$ is the complex admittance matrix. It is obtained by augmenting the shunt admittance at the generator $\boldsymbol{Y}_g$ in (2.7) and the shunt admittance at the load $\boldsymbol{Y}_l$ in (2.14) into the network admittance matrix $\boldsymbol{Y}_N$. On the other hand, $\overline{I}$ is the vector of complex current sources of the j^{th} element which is expressed by:

$$\overline{I}_j = \overline{I}_{g_j} + \overline{I}_{l_j} \tag{2.18}$$

2.1.4 Simulation of faults

The fault at or near a bus is simulated by correspondingly changing the bus admittance matrix in the system. For a bolted three phase fault, the faulted bus has the potential equal to zero. This is realized by placing infinitely high shunt admittance at the faulted bus. Hence, a sufficiently high shunt admittance matrix (say 10^6 per unit) is used so that voltage at the faulted bus is zero. The fault is cleared by using a bus admittance matrix corresponding to the post fault system configuration. If a line trip is required, the respective line is removed from the pre-fault admittance matrix. However, if a line trip is not required, the pre-fault bus admittance matrix itself is used as the post-fault bus admittance matrix.

2.2 Phasor measurement units

The advent of PMU technology permits high resolution time-synchronized measurements across power system networks. The applications of PMU technology pushes transmission capability limits and improves the network capability of identifying various phenomena in power system greatly. The phasor of the PMU is estimated by comparing the input signals with the corresponding ideal sinusoidal waveform with the system nominal frequency. However, frequency deviations and waveform distortions are unavoidable in practice. Thus, the phasor estimated by a PMU might be affected due to the deviations in the system frequency and the distortion of waveform during transients. These situations will affect the performance of the control and protection system developed in this thesis because it requires the measurements gathered during transient periods when they are prone to the phasor estimation errors because of system frequency deviation and waveform distortion. The IEEE Standard C37.118-2011 on Synchrophasor Measurements for Power Systems [8] has addressed various issues and considerations on PMU applications. However, to extend the discussion of the problem investigated in this thesis, some of the important considerations relevant to the application of synchrophasor technology are discussed in this section.

2.2.1 PMU measurements

In power system analysis, a sinusoidal waveform is commonly defined by using phasor representation. The time varying sinusoidal signal $x(t)$ is defined as:

$$\begin{aligned} x(t) &= X_m \cos(\omega_0 t + \phi) \\ &= X_m \cos(2\pi f_0 t + \phi) \end{aligned} \tag{2.19}$$

In 2.19, f_0 represents the nominal angular system frequency (50 Hz or 60 Hz). In general cases, the amplitude and the frequency are function of time denoted as $X_m(t)$ and $f(t)$, respectively. The difference between the actual and nominal frequency is defined in 2.20:

$$\Delta f(t) = f(t) - f_0 \tag{2.20}$$

Therefore, for general cases, the sinusoidal signal in (2.19) is reformulated as in (2.21):

$$\begin{aligned} x(t) &= X_m(t) \cos\left(2\pi \int f(t)\, dt + \phi\right) \\ &= X_m(t) \cos\left[2\pi \int (f_0 + \Delta f(t))\, dt + \phi\right] \\ &= X_m(t) \cos\left[2\pi f_0 t + \left(2\pi \int \Delta f(t)\, dt + \phi\right)\right] \end{aligned} \tag{2.21}$$

The synchrophasor representation for (2.21) is shown in (2.22):

$$\boldsymbol{X}(t) = \left(\frac{X_m(t)}{\sqrt{2}}\right) e^{j\left(2\pi \int \Delta f(t) dt + \phi\right)} \tag{2.22}$$

During steady-state power system operation, the magnitude of the phasor $X_m(t)$ and the difference between the actual and nominal frequency $\Delta f(t)$ are constant, the definition of synchrophasor in (2.21) is simplified as in (2.23):

$$\boldsymbol{X}(t) = \left(\frac{X_m(t)}{\sqrt{2}}\right) e^{j(2\pi \Delta f t + \phi)} \tag{2.23}$$

2.2.2 Reporting rates

It is suggested that the PMU reports at sub-multiples of the nominal system frequency [8]. Table 2.1 shows the required PMU reporting rates for 50 Hz and 60 Hz systems. However, it is permissible to use other reporting rates. The use of

Table 2.1: Required PMU reporting rates

System frequency	50 Hz			60 Hz					
Reporting rates (F_s)	10	25	50	10	12	15	20	30	60

higher rates like 100 or 120 Hz is highly recommended [8]. In this thesis, both 50 Hz and 60 Hz systems are considered. The 16-machine 68-bus test system model and the UK University-based WAMS are used in this thesis. These systems are originated from the United States (US) and United Kingdom (UK) network grid, respectively. The nominal system frequency for the 16-machine 68-bus system is 60 Hz, while for the University-based WAMS is 50 Hz. Hence, the reporting rates for PMU considered for each system are different.

In the following chapters, the reporting rate of 120 Hz is considered for the application involving measured data simulated from the 16-machine 68-bus test system model. On the other hand, the reporting rate of 100 Hz is considered for the application involving measured data gathered from the UK University-based WAMS.

2.2.3 PMU during transients

Given the dynamic and complexity of power system, it is almost impossible to find ideal sinusoidal waveforms of voltage and current, particularly during transients.

Switching operations and faults during power system operation may cause a step changes in the magnitude and phase angles of the voltage and current waveforms [14]. These transients cause the power system network to produce additional high frequencies in the measurements. An anti-aliasing filter is used to attenuate the high frequency signals to an insignificant level [7]. However, since the estimation of the phasor is generally performed over one period of the nominal system frequency, the step changes in the input signals might occur within the data window [14]. This may affect the performance of the phasor estimation in the PMU.

Another transient event that may affect the phasor estimation in the PMU is the rotor of the synchronous generator movement after a disturbance [14]. The rotor movement after a disturbance causes the frequency of the generated voltage to deviate from its nominal value. The superposition of voltages with slightly

different frequencies leads to resultant voltage and current waveforms which show magnitude and phase angle modulation.

These spurious additional frequency components introduced during transient events in the input signals are likely to cause a phasor estimation error in the PMU measurements. It may affect the performance of any measurement-based technique in power system. Thus, it is important to consider PMU errors during transient in the context of developing the measurement-based protection and control in power system.

2.2.4 Effect of signal noise in PMU

Noise is always present in the practical measured signals. An unwanted frequency component which is different from fundamental frequency signal or induced electrical noise picked up in the wiring of the input signals is considered to be noise. The presence of noise in the input signals causes error in the PMU phasor estimation. The error in phasor estimation depends on the difference in amplitude and phase between the theoretical values of a PMU representation of a sinusoid with the values obtained from an input signals. This error is measured by a quantity defined as Total Vector Error (TVE) and is defined as follows [8]:

$$\mathrm{TVE}(n) = \sqrt{\frac{\left[\hat{X}_r(n) - X_r(n)\right]^2 + \left[\hat{X}_i(n) - X_i(n)\right]^2}{\left[X_r(n)\right]^2 + \left[X_i(n)\right]^2}} \tag{2.24}$$

where $\hat{X}_r$ and $\hat{X}_i$ are the sequences of the estimated values of the input signals, while X_r and X_i are the sequences of theoretical values of the input signal at the instants of time n assigned by the unit to those values.

Fig. 2.3 illustrates the 1% TVE of PMU phasor estimation. The maximum magnitude error is 1% when the error in phase is zero, and the maximum error in angle is under 0.573, provided that the observed samples do not lie outside the circle. According to [8, 15] the PMU must maintain TVE less than 1% under steady-state condition and TVE less than 3% under dynamic condition. Since the scope of this thesis covers the steady state, as well as the dynamic aspect of the study system, the TVE of 3% is considered. In this thesis, the noise in the input signal is approximated by using a zero-mean, Gaussian noise process. This is a good approximation for the electrical noise picked up in the wiring and spurious

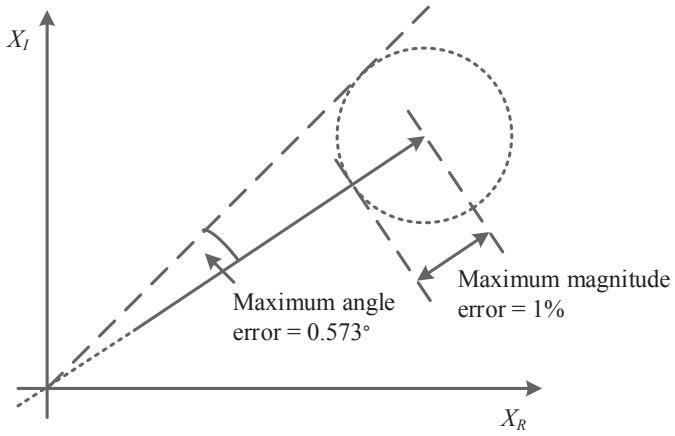

Figure 2.3: Example of 1% TVE

frequency component in the input signals that cause errors in phasor estimation [7].

2.3 Chapter summary

A simulation model is vital for power system protection and control studies. This model is used to analyse the response of the system following a disturbance in the network. In this chapter, mathematical functions have been used to represent the simulation model of power system. These functions describe the characteristics of different components in the system. The simulation model is defined in the form of algebraic and differential equations. These equations describe the static and the dynamic behaviour of the system, respectively. The modelling of power system presented in this chapter has been well described in [11, 12, 13]. It is explained here to provide better discussion and understanding of the ideas presented in this thesis. The technical considerations of PMU used in this thesis have also been incorporated in this chapter.

Chapter 3

Coherency identification in power system

This chapter proposed an approach to the coherency identification technique in interconnected power system using Independent Component Analysis (ICA). The chapter begins with an overview of coherency identification techniques in power system and the motivation behind this research. This is followed by a section of the state of the art in coherency identification techniques. Next, the approach used to utilize ICA for coherency identification in interconnected power system is presented. Subsequently, the proposed approach is applied to measurement data simulated from 16-machine 68-bus system model and actual WAMS data gathered through UK University-based Wide-Area Measurement System. Then, the results obtained using the proposed method are validated and compared with the results obtained using the direction cosine and PCA approach. Additionally, the performance robustness of the proposed algorithm to measurement noise is also tested. The results presented in this chapter have been published by IEEE Transaction on Power Systems in a journal titled, "Coherency Identification in Interconnected Power System - An Independent Component Analysis Approach".

3.1 Overview

A power system network is formed by the interconnection of two or more commercial areas via inter utility transmission links. After a system perturbation, some generators in the system have tendency to swing in unison. These generators are

clustered into a coherent group, which has similar time-domain response trends. The coherent groups of generators are identified by observing the generator rotor angle and bus voltage angle, which have the most consistent pattern over the low frequency electromechanical oscillatory mode [16]. This low frequency electromechanical oscillatory mode is also known as inter-area mode. Additionally, coherency identification techniques can be extended to identify the buses which oscillate coherently with the generator angles. This extension segregates the interconnected power system network into sets of coherent generators and buses. However, with the changes in the system operating condition and network configuration, the elements in the set of coherent generators and buses tend to vary. The accuracy of the system parameters (generator, loads and networks) also influences the accuracy of the technique to obtain coherent areas in the system. These concerns motivated researchers to look for measurement-based coherency identification tools. In measurement-based techniques, all the system quantities and variables such as generator speed, output power, and voltage at all nodes are measured continuously and a snapshot is utilised to find the coherent groups. The technology of wide-area measurement is available to gather time-synchronized measurements across the whole network [7]. It transmits the data to the transmission control centre on a time-scale of milliseconds so that the tool to identify coherency properties has input data available in less than a second's time interval.

3.2 State of the Art

The initial aim of coherency identification in an interconnected power system is to aid the dynamic reduction of the models [17, 18, 19]. It is useful for computational convenience. Conventionally, a model-based approach is used to determine the coherent areas in the power network by observing the generator rotor angle and bus voltage angle, which have the most consistent pattern over all the inter-area modes. This is realized with the help of the direction cosine method [16, 20]. The direction cosine method works on the assumption that the coherent groups of generators are independent of the size of the disturbance. Therefore, the coherent groups of generators are identified by performing an eigenvalue analysis of the linearised model of the system in order to obtain row eigenvectors corresponding to generator angles. Consequently, these row eigenvectors are used to calculate the direction cosine with respect to the inter-area mode of oscillation. The phase

angles of the eigenvectors for coherent group of generators are close to each other. Different coherent groups have more than 90 degrees of angle separating them. Although this technique has a strong theoretical foundation of coherency identification, the accuracy of this method is reliable if the knowledge of the prevailing system condition and various parameters are accurate. In practice, it is not always possible. Furthermore, small variations of load and generation have insignificant impact on the coherent group of generators [21]. Nevertheless, the changes in topology and significant load variation influence the "loosely coherent" generators switching from one group to the other. Hence, as the operating condition and the system topology vary noticeably with time, the coherent areas need to be tracked. The continuation method is used in [22] to address this issue. However, besides being model-based, it is also computationally intensive.

The accuracy of the measurement-based coherency identification techniques does not rely on the accuracy of the system parameters. There are several references in the literature on the measurement-based coherency identification. The methodologies underlying these approaches are diverse, e.g. artificial neural network (ANN) [23], particle swarm optimization and k-means (PSO-KM) algorithm [24], graph theory [25], partitioning around medoids (PAM) [26], hierarchical clustering [27], self-organizing feature maps [28], Fast-Fourier transform (FFT) [29, 30], Hilbert-Huang transform (HHT) [31] and Principal Component Analysis (PCA) [32, 33]. Despite having advantages over model-based approaches, these techniques have some limitations, for instance, the ANN algorithm requires excessive off-line training data to train the neural network in order to identify the coherent generators. The PSO-KM, graph theory based and PAM algorithms on the other hand suffer from high computation burden in order to achieve coherent groups of generator in the system reasonably fast. The FFT approach has been used to determine coherent areas of power system but this technique assumes that the system is linear and the data results from a stationary process, which is usually not the case in practice. The HHT provides solution to nonlinear and non-stationary process, however, it is difficult to visualise the coherent groups of generators using the proposed approach for large power system. The PCA approach proposed in [32, 33] used a multivariate analysis technique on the measured data obtained from the system. It uses PCA to identify the coherent groups of generators and buses, hence coherent areas of the interconnected power system. PCA highlights the clusters of generators and buses displaying common features in the measurements. However, the approach is unable to identify the

accurate coherent areas without *a-priori* information of inter-area mode of the system. Hence, the PCA method requires the help of Hilbert transform (HT) technique and empirical mode decomposition (EMD) to extract the instantaneous attributes of inter-area oscillations. The method is simple and does not require detailed system modelling information.

Although some of measurement-based coherency identification techniques in the literature are reliable in clustering the coherent group of generators in near real time, none of these approaches demonstrate their accuracy and robustness in the presence of noise. The existence of noise in measured signals affects the accuracy of the coherency identification technique. This is an important issue because the measured signals from the system have significant noise. Therefore, it is important to ensure that the coherency identification technique is robust in the presence of measurement noise in the signals.

In this chapter, the coherent groups of generators and buses are obtained by analysing the measurements using ICA, a multivariate analysis tool that is better than PCA. The ICA extracts a set of independent signals from its input signals while PCA finds a set of uncorrelated signals from a set of mixtures. Lack of correlation is a weaker property than independence. Independence implies a lack of correlation but a lack of correlation does not imply independence. This advantage allows better extraction of frequency components from the measured signal. Thus, ICA is able to obtain accurate coherent groups of generators and buses without prior knowledge of modal characteristic of the system. The technique is completely data driven and adaptive.

3.3 Coherency Identification using ICA

Independent Component Analysis is a data driven computation method that recovers a set of data, without any prior information about either the sources or the mixing parameters of the system that has the data as its output. ICA aims to estimate the sources by assuming that the output are dominated by a set of hidden sources which are statistically independent of each other and contribute to each output. Unlike other multivariate analysis techniques, ICA looks for components that are both statistically independent and non-Gaussian. ICA has earlier been

applied to compute the damping and frequency of low oscillatory mode in power systems [34].

A variation of ICA known as spectral ICA [35] is used to determine the coherent areas in interconnected power system. In spectral ICA, different independent components (ICs) consist of different spectral peaks. A component with a single spectral peak is more dominant in terms of non-Gaussianity than a component with multiple peaks. Thus, maximising the non-Gaussianity of ICs in spectral ICA will result in the preferential decomposition of single-peak and narrow-band ICs. Thus, by using this method, a spectrum can be extracted into a combination of spectrum-like and single-peak ICs.

The spectral ICA approach uses a set of the normalised power spectra of measured time trend signals, sampled at different measurement points as input in the analysis. The approach decomposes these signals into their sources such that each of resulting estimated sources or ICs is a narrowband spectrum with one sharp peak in the frequency domain. Each IC corresponds to a frequency of the estimated oscillatory source. Therefore, the ICA decomposition on the power spectra of the signal is able to separate measured signals into their various frequency components. The extraction of the dominant narrow-band peaks from the power spectra of the signal using the spectral ICA is superior to the extraction of the oscillatory sources by time-domain ICA. This is because, unlike time-domain ICA, spectral ICA is invariant to the time delays and phase lags [36].

There are other means in obtaining dominant mono-frequency components of signals such as masking signal-based Empirical Mode Decomposition (EMD) [37] or other band-pass filtering techniques. However, spectral ICA is preferred over these methods because it does not require *a-priori* knowledge of modes presented in the signal. Spectral ICA decomposes the entire frequency spectrum of signals into the mono-frequency components for further analysis. The main aim of this approach is to determine independent sources of similar spectral signature, which represent slow oscillatory modes of the system.

As formulated in [35], row vectors of data matrix for the spectral ICA model,

are single sided power spectra of mean centred time trends over a range of frequency, up to the Nyquist frequency:

$$\boldsymbol{X(f)} = \begin{pmatrix} P_1(f_1) & \cdots & P_1(f_N) \\ \vdots & \ddots & \vdots \\ P_m(f_1) & \cdots & P_m(f_N) \end{pmatrix} \tag{3.1}$$

The power spectrum can be obtained using Discrete Fourier Transform (DFT) to the mean centred time trend. Then, each power spectrum is normalised such that:

$$\sum_{k=1}^{N} P_i(f_k) = 1, \qquad i = 1, 2, \cdots m \tag{3.2}$$

Each vector in $\boldsymbol{X}$ is a linear mixture of hidden and independent process. Each process forms a row vector in $\boldsymbol{S}$. Each row in $\boldsymbol{S}$ is an IC. These processes are represented by an ICA mixing model given by:

$$\boldsymbol{X(f)} = \boldsymbol{A}_{m\times n} \begin{bmatrix} s_1 \\ s_2 \\ \vdots \\ s_n \end{bmatrix} = \boldsymbol{A}_{m\times n}\boldsymbol{S} \tag{3.3}$$

where, $\boldsymbol{A}$ is an unknown $m \times n$ matrix of full rank, called the *mixing matrix*. The main aim of ICA is then to estimate $\boldsymbol{S}$ and the mixing matrix, $\boldsymbol{A}$ from the observed normalised power spectrum, $\boldsymbol{X}$. Estimating the mixing matrix $\boldsymbol{A}$ can be simplified by performing a preliminary sphering or prewhitening the observed data, $\boldsymbol{X}$. The observed data $\boldsymbol{X}$ is linearly transformed to $\boldsymbol{V}$ given by:

$$\boldsymbol{V} = \boldsymbol{MX} = \boldsymbol{MAS} = \boldsymbol{BS} \tag{3.4}$$

The correlation matrix $E\{\boldsymbol{VV}^T\}$ is a unit matrix which means that the elements of $\boldsymbol{V}$ are mutually uncorrelated. The problem of finding an arbitrary full-rank matrix $\boldsymbol{A}$ has been reduced to the simpler problem finding an orthogonal matrix $\boldsymbol{B}$. If the i-th column of $\boldsymbol{B}$ is denoted by $\boldsymbol{b}_i$, the i-th IC can be computed from the observed $\boldsymbol{V}$ as:

$$\boldsymbol{s}_i = (\boldsymbol{b}_i)^T\boldsymbol{V} \tag{3.5}$$

The fast fixed-point algorithm [38] is used to estimate the value of $\boldsymbol{b}_i$ which maximises the kurtosis of $(\boldsymbol{b}_i)^T\boldsymbol{V}$. This algorithm uses a very simple yet highly efficient fixed point iteration technique.

However, the sign, the magnitude and the order of ICs obtained are not unique. So, additional constraints are imposed on the ICA mixing model for physically meaningful results. All ICs are adjusted to have positive peak values to enhance visualisation. The mixing matrix is also scaled so that relationships between the spectral signatures and ICs are easily identified. The order of ICs is also sorted in order to properly visualise the coherency property of the system.

3.3.1 Sign modification

First, the sign of ICs is manipulated by introducing additional constraints on the ICs and incorporating this change into $\boldsymbol{A}$ to preserve the original relationship. Now, spectral signatures are reformulated as shown in (3.6).

$$\boldsymbol{X} = \boldsymbol{Q}\boldsymbol{P} \tag{3.6}$$

where,

$$\boldsymbol{Q} = \boldsymbol{A}diag(SN_1, SN_2, \ldots, SN_n) \tag{3.7a}$$

$$\boldsymbol{P} = diag(SN_1, SN_2, \ldots, SN_n)\boldsymbol{S} \tag{3.7b}$$

The $\boldsymbol{SN_j}$ $(j = 1, \ldots, n)$ signifies the sign of the dominant peak of every IC. The reason for implementing the sign modification on ICs is because the amplitude of a physical oscillation source is positive by definition. Therefore, it must have a positive magnitude in the frequency domain.

3.3.2 Scaling

Following the sign modification on ICs, the mixing matrix $\boldsymbol{S}$ now is represented by $\boldsymbol{Q}$. The modified mixing matrix $\boldsymbol{Q}$ represents relative ratios in which spectral source frequencies exist in measured signals. Nevertheless, it will be more meaningful if the mixing ratio of one signal is relatively compared to other signals for each spectral source. This is realised by normalising the maximum value of each

column of $\boldsymbol{Q} = [q_1 \quad q_2 \quad \dots \quad q_n]$ to unity as given in (3.8).

$$\boldsymbol{T} = \boldsymbol{Q} diag(\triangle_1^{-1}, \triangle_2^{-1}, \dots, \triangle_n^{-1}) \tag{3.8a}$$

$$\boldsymbol{C} = diag(\triangle_1, \triangle_2, \dots, \triangle_n)\boldsymbol{P} \tag{3.8b}$$

where,

$$\triangle_j = \|\boldsymbol{q}_j\|_\infty, \qquad j = 1, \dots n \tag{3.9}$$

hence,

$$\boldsymbol{X} = \boldsymbol{T}\boldsymbol{C} \tag{3.10}$$

$\boldsymbol{C}$ is the modified and sign corrected $\boldsymbol{S}$. Each row of $\boldsymbol{X}$ is the weighted combination of all rows in $\boldsymbol{C}$, which represent the ICs. Therefore, $\boldsymbol{X}$ is the weighted combination of all ICs. The weight coming from the corresponding row element of $\boldsymbol{T}$ is used to plot the coherent groups of generators and buses in the system.

3.3.3 Order sorting

The order inconsistency in the ICA algorithm may affect the consistency of the coherency plot that represents the system under study. This is particularly relevant in the presence of noise in the measured data. This limitation of the ICA algorithm [39] affects the performance of the coherency identification technique. This is because coherency properties depend on electromechanical modes of the system that are represented by ICs. The order of ICs needs to be consistent at every ICA convergence in order to obtain a consistent coherency plot that accurately represents coherency properties of the system. The work presented in the previous application of ICA in the power system [34] is focused on the detection of oscillatory modes in the system. The issue of the order inconsistency in the ICA algorithm has not been discussed extensively. In this thesis, a novel contribution has been made in sorting ICs and their corresponding mixing matrix according to their dominance to preserve the consistency of coherency plot from one ICA convergence to another. Consequently, the performance of the proposed method in identifying coherent groups of generators and buses is not affected by the limitation of the ICA algorithm. To deal with this issue, the dominance ratio is used as a measure of the significance of each source calculated by ICA. It is defined in

[35] and is given in (3.11):

$$\text{Dominance ratio } D(j) = \frac{\left\|\boldsymbol{t}_j \boldsymbol{c}_j^T\right\|_{\text{sum}}}{\|\boldsymbol{TC}\|_{\text{sum}}} \tag{3.11}$$

Referring to (3.11), the total energy of all the power spectra in $\boldsymbol{X}$ is approximated by $\|\boldsymbol{TC}\|_{\text{sum}}$, which is interpreted as the total energy carried by all dominant oscillatory ICs. On the other hand, the total energy related to the j^{th} IC is $\left\|\boldsymbol{t}_j \boldsymbol{c}_j^T\right\|_{\text{sum}}$. Each dominant IC is associated with a ratio which reflects the dominance of that IC. Consequently, ICs (after peak adjustment and scaling) are sorted according to their associated dominance ratio.

The number of dominant components to be considered in the analysis can be determined by using a robust and structured approach such as Cumulative Percent Variance (CPV), Akaike's Information Criterion (AIC) or the Minimum Description Length (MDL) as discussed in [40]. However, the number of dominant ICs considered in the proposed method is adopted from the research reported in [32, 33]. In [32, 33], three dominant components are considered to determine coherent groups of generators and buses using measured data obtained from the 16-machine 68-bus test system model. These dominant components represent inter-area modes of the system. Hence, only three most dominant ICs are being considered in this analysis. Therefore, the ICA decomposition is rewritten as shown (3.12).

$$\boldsymbol{X} = \begin{pmatrix} \boldsymbol{t}_{1,1} \\ \vdots \\ \boldsymbol{t}_{i,1} \end{pmatrix} \boldsymbol{c}_1' + \begin{pmatrix} \boldsymbol{t}_{1,2} \\ \vdots \\ \boldsymbol{t}_{i,2} \end{pmatrix} \boldsymbol{c}_2' + \begin{pmatrix} \boldsymbol{t}_{1,3} \\ \vdots \\ \boldsymbol{t}_{i,3} \end{pmatrix} \boldsymbol{c}_3' + \boldsymbol{E} \tag{3.12}$$

where,

$$\boldsymbol{E} = \begin{pmatrix} \boldsymbol{t}_{1,4} \\ \vdots \\ \boldsymbol{t}_{i,4} \end{pmatrix} \boldsymbol{c}_4' + \cdots \begin{pmatrix} \boldsymbol{t}_{1,n} \\ \vdots \\ \boldsymbol{t}_{i,n} \end{pmatrix} \boldsymbol{c}_n'$$

The first part in (3.12) involving c_1', c_2' and c_3' represents three most dominant ICs. The last part, $\boldsymbol{E}$ represents the rest of the process. The three-tuple ($t_{i,1}$, $t_{i,2}$ and $t_{i,3}$) is a point in three-dimensional dominant IC space. The IC space has the advantage of displaying coherent groups as tightly formed clusters. All three-tuples from different rows of $\boldsymbol{T}$ are plotted in the IC space. The three-tuples

that are close to each other in the IC space represent coherent signals. Since each row signifies a signal from a generator or bus, all generators or buses captured in the cluster form coherent groups. This formation of clusters is used to identify coherent areas in the system. Apart from this graphical way of obtaining coherent groups, there are ways of quantitatively determining coherent groups from the coherency plot such as through k-mean clustering method.

3.4 Application, results and analysis

In order to analyse the performance of the proposed method in identifying coherent areas of the system, the ICA is applied on the simulated data from a test system model and the actual WAMS. Also, results obtained from the simulated data are discussed and analysed in this section.

3.4.1 Application on simulated data

In order to demonstrate the effectiveness of the proposed method in identifying coherent areas in the large interconnected power system, the ICA approach is applied to a test system model. The 16-machine 68-bus system model is considered as the test system. Bus data, line data and dynamic characteristics of the system are obtained from [16, 41] and listed in Appendix A as well. Fig. 3.1 shows the single line diagram of the system. Nonlinear dynamic simulations of the test system are performed in MATLAB Simulink. The disturbance considered for this study is ten percent increment of the mechanical input torque for 80 ms to each generator. Since the coherency property is a slow post-fault dynamic process, a small perturbation is adequate to simulate them. For the coherency identification, generator speed signals from 16-machines subjected to the disturbance are recorded accordingly. The coherency primarily initiated from electromechanical swings of generators following a disturbance. It extends beyond transient stability time scale of 3-5 s particularly in a large interconnected power system with poorly damped or undamped inter-area modes. Therefore, a 20 s time window is sufficient to monitor the system behaviour after a disturbance effectively [42]. The choice of the sampling frequency is also important. In this study, the frequency sampling of 120 Hz is considered as recommended in the recent IEEE Standard for Synchrophasor Measurements for Power Systems C37.118.1-2011 [8]. The time

trends shown in Fig. 3.2 are used to construct the data matrix. The proposed

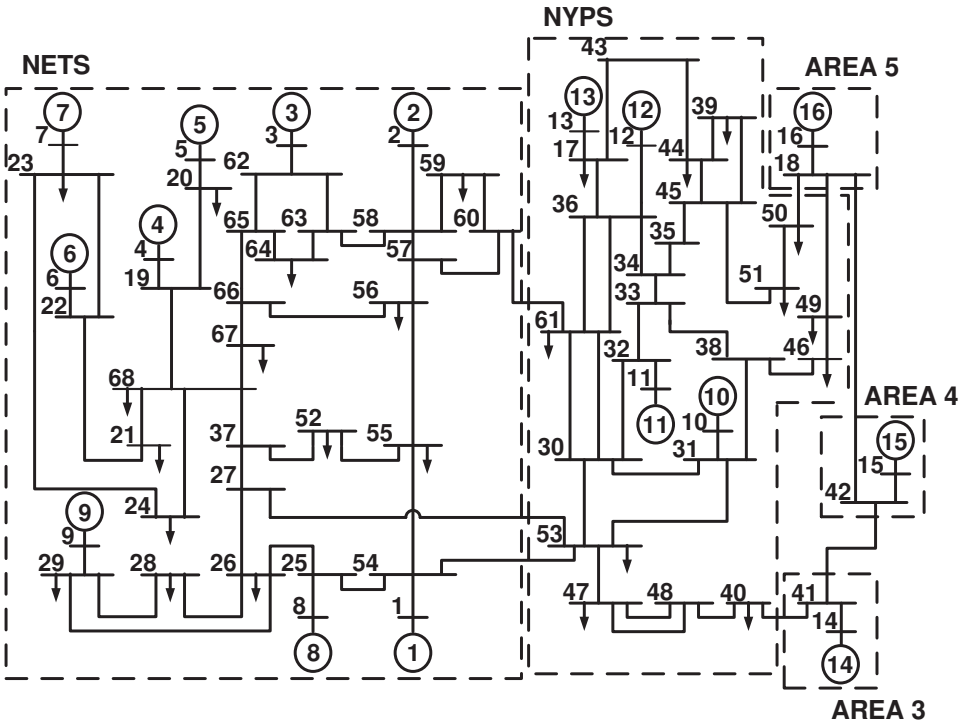

Figure 3.1: 16-machine 68-bus test system model

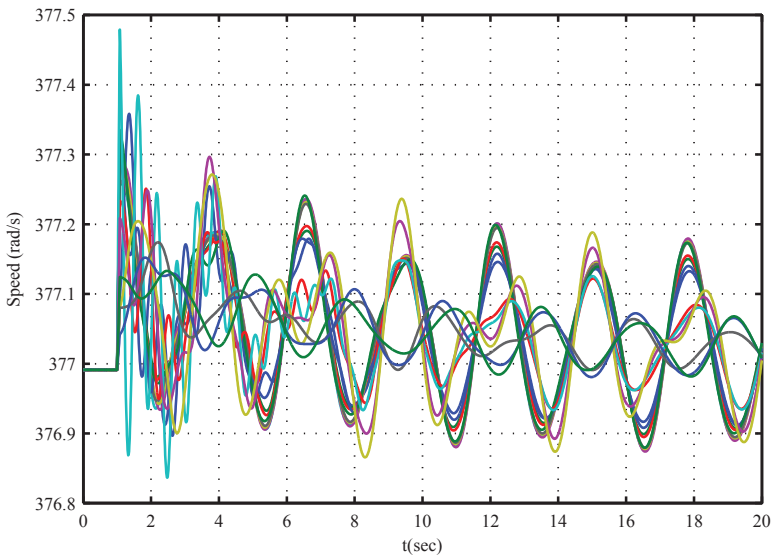

Figure 3.2: The speed response of the generators

method is applied on the measured data to obtain matrices $\boldsymbol{T}$ and $\boldsymbol{C}$ in (3.10). Fig. 3.3 displays three most dominant ICs of the system. Physically, the three most dominant ICs are the slowest mode of the oscillation in the system. The peak of IC_1, IC_2 and IC_3 are at 0.05 Hz, 0.34 Hz and 0.54 Hz, respectively. The

peak of IC_1 represents the stationary mode of the system while the peak of IC_2 and IC_3 represent the low frequency inter-area mode of oscillations. The inclusion of the stationary mode to identify the coherency is necessary [16, 20]. Each spectral signature of the generator speed data is the combination of one or more of these ICs. Columns of the mixing matrix $\boldsymbol{T}$ represent the weighted amount of each IC in each spectral signature of input data. The plot of elements of $\boldsymbol{T}$ in a three-dimensional plot helps to identify coherent groups in the system.

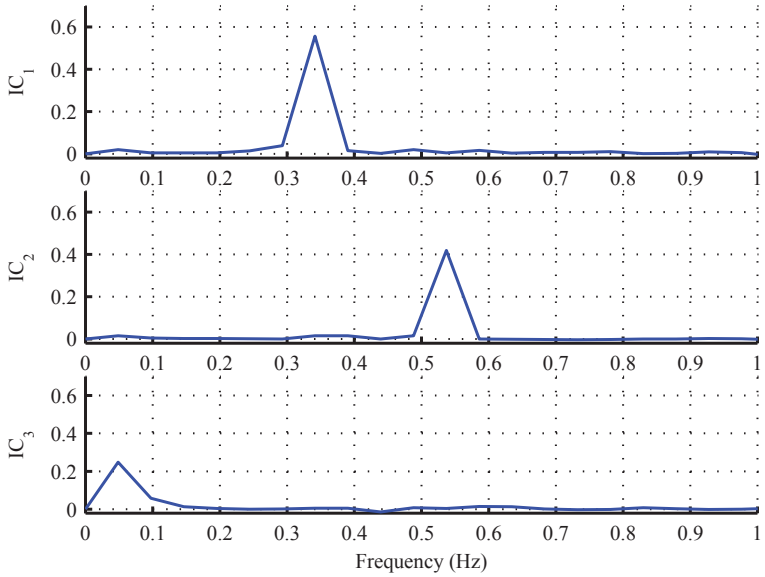

Figure 3.3: Three most dominant ICs

3.4.1.1 Generator coherency

Fig. 3.4 represents the three-dimensional plot of the modified mixing matrix $\boldsymbol{T}$. From the figure, it is observed that the first nine generators, G1 to G9 are well separated from other generators. This set of generators formed a coherent group namely Area 1 (NETS). The location of the first nine generators in the three-dimensional space has relatively similar ratio in three most dominant ICs. On the other hand, G10 to G13 are close to each other and form another group of coherent generators namely Area 2 (NYPS). Other three equivalent machines: G14, G15 and G16 form three separate coherent groups at the far end of the three-dimensional plot namely Area 3, Area 4 and Area 5 accordingly. Cluster of coordinates of the mixing matrix $\boldsymbol{T}$ in the three-dimensional plot represent coherent groups of generators in the system.

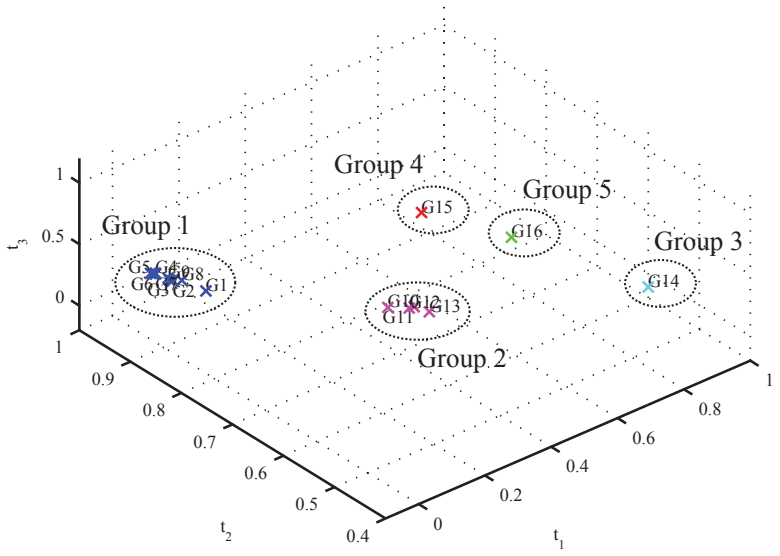

Figure 3.4: Coherent groups of generators using proposed method

Table 3.1: Summary of coherent areas for the 16-machine 68-bus system model

Group	Coherent Generators	Coherent Buses
1	1, 2, 3, 4, 5, 6, 7, 8 ,9	1, 2, 3, 4, 5, 6, 7, 8, 9, 19, 20, 21, 22, 23, 24, 25, 26, 27, 28, 29, 37, 52, 54, 55, 56, 57, 58, 59, 60, 62, 63, 64, 65, 66, 67, 68
2	10, 11, 12, 13	10, 11, 12, 13, 17, 30, 31, 32, 33, 34, 35, 36, 38, 39, 40, 43, 44, 45, 46, 47, 48, 49, 50, 51, 53, 61
3	14	14, 41
4	15	15, 42
5	16	16, 18

3.4.1.2 Bus coherency

The proposed method is also applied on the phase angle of bus voltage measurements to identify the bus coherency of the test system. Fig. 3.5 illustrates the bus coherency of 16-machine 68-bus system model identified using the proposed method. It is clearly seen from the figure that there are five clusters of phase angle measurements, namely as Area 1, Area 2, Area 3, Area 4 and Area 5 respectively. Area 1 and Area 2 consist of large number of buses while the other three clusters (Area 3, Area 4 and Area 5) only contain a pair of buses. Also, it is observed that some of buses from Area 2 are moving towards Area 3. These buses demonstrate weak dynamic coupling with other buses in Area 2. In addition, these buses are also electrically and physically close to buses in Area 3. Table 3.1 concludes the coherent group of generators and buses for the 16-machine 68-bus test system model identified using the proposed ICA method

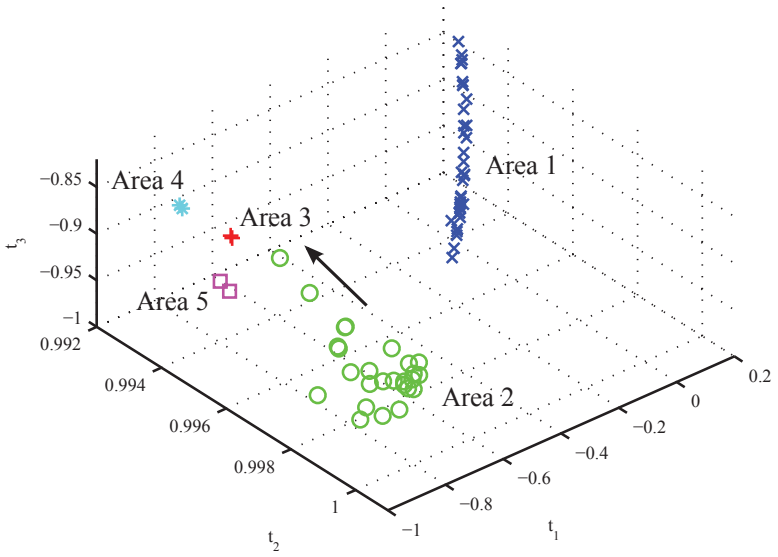

Figure 3.5: Bus coherency plot of the test system using the proposed method

3.4.2 Application on actual WAMS data

The proposed method is applied on the PMU data from United Kingdom University-based WAMS [43]. The WAMS consists of four main PMUs situated at the respective research laboratory of University of Strathclyde in Glasgow, (UoS), University of Birmingham in Midland (UoB), The University of Manchester in Manchester (UoM) and Imperial College London in London (ICL). Fig. 3.6 illustrates the geographical location of PMUs in United Kingdom. Phasor Data Concentrator (PDC) for the WAMS is installed in Ljubljana (Slovenia) and gathers data from all PMUs using standard internet communication network. On 2nd September 2010, a sudden mismatch in load-generation occurred. Fig. 3.7 represents recorded wide area measurements capturing this event measured from PMUs at ICL, UoB and UoS, respectively. Unfortunately, the PMU at UoM was not in service during this particular time. From Fig. 3.8, it can be clearly observed that the measurement can be classified into two different coherent groups. Group 1 consists of PMU measurement located at UoS while Group 2 consists of PMU measurements located at UoB and ICL. Fig. 3.9 shows angle differences between ICL and UoS, UoB and UoS, ICL and UoB. The sampling frequency is set at 100 Hz. However, the system frequency hovers around 50 Hz. This frequency variation led to the time variation in the phase angle recording as shown in Fig. 3.7. The time window of 20 seconds starting from 30^{th} second until 50^{th} second (since the disturbance occurred during this particular time window) is chosen to construct the data matrix. Fig. 3.8 represents the coherency plot of the actual WAMS data using the ICA method. It

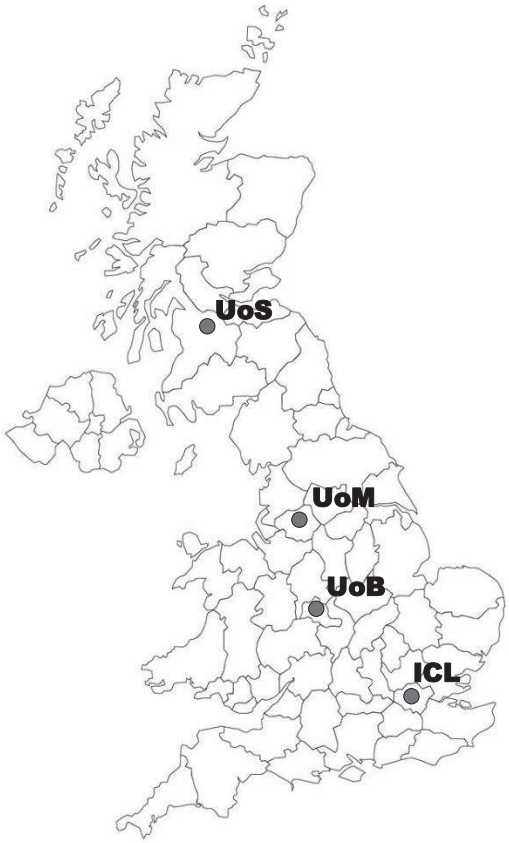

Figure 3.6: Location of PMUs

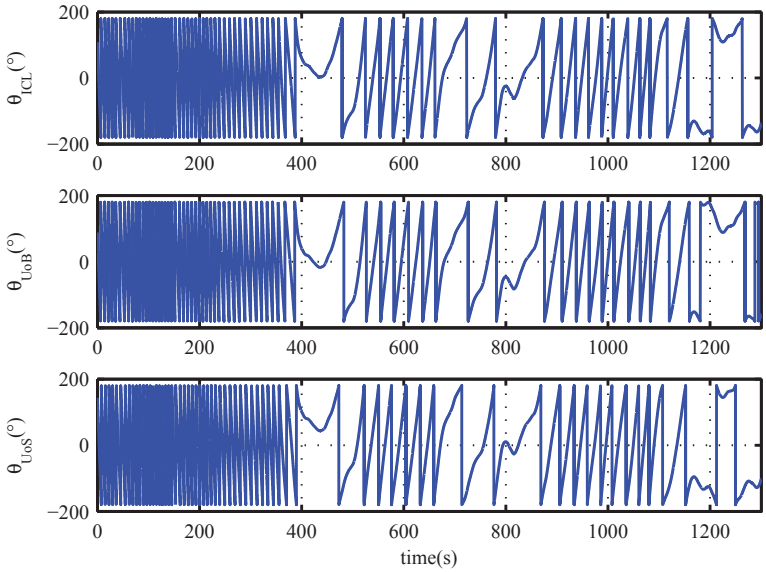

Figure 3.7: Voltage phase angle measurements for ICL, UoB and UoS

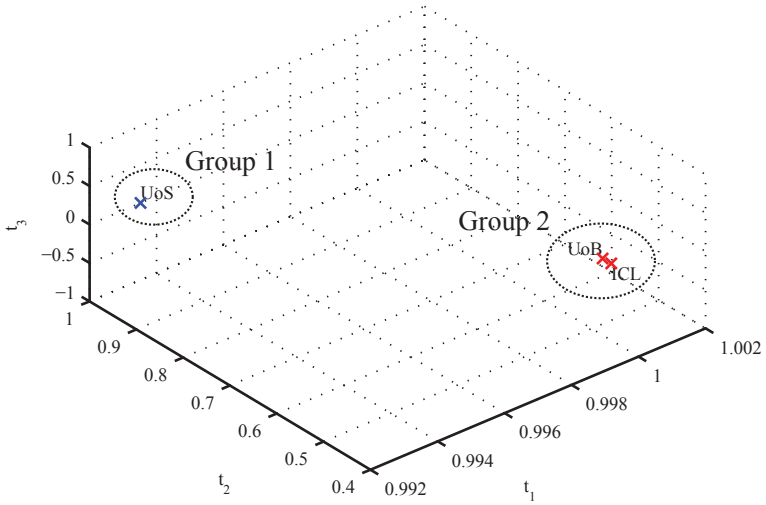

Figure 3.8: Coherency plot for actual WAMS data

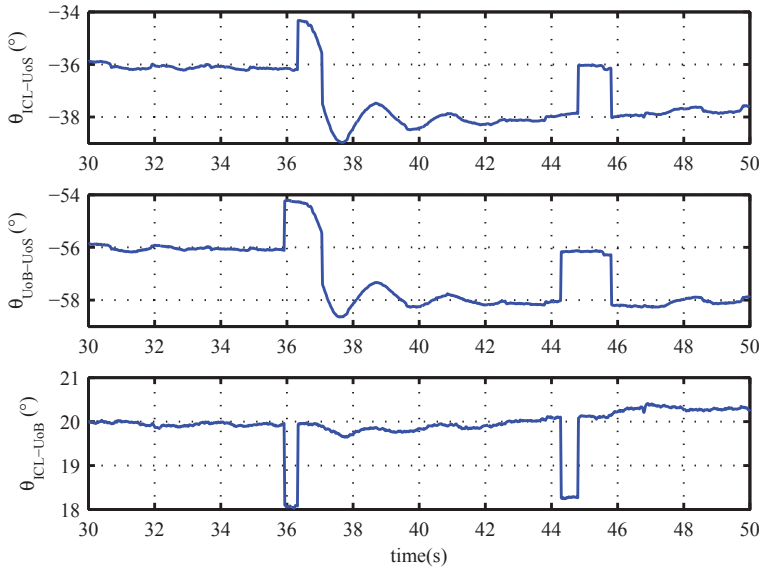

Figure 3.9: Phase angle differences for ICL-UoS, UoB-UoS and ICL-UoB

is observed from Fig. 3.9 that phase differences between ICL-UoS and UoB-UoS have a similar time-trend initiated by the mismatch in load-generation in the system. The phase difference between ICL and UoB shows a nearly constant angle of about 20° except for 36^{th} and 45^{th} second reflecting changes in the mismatch value, possibly due to generation control action in the system. Therefore, from these observations, the PMU measurements from ICL and UoB are confirmed to be coherent to each other. Hence, these two measurement points belong to the same coherent group. Meanwhile, PMU measurement from UoS is grouped into a different coherent group. The coherent group of generators from this observation validate the results of coherent groups obtained using proposed method as shown

in Fig. 3.8.

It is also important to verify this observation with the historical context of Scotland-England inter-area oscillations. Over the years, it is well understood and observed that there is an oscillation around 0.5 Hz between Scotland and England generations [44]. Thus, these two systems belong to different coherent groups. PMUs located at UoB and ICL are part of the English grid, while PMU located at UoS is part of Scottish grid. This observation is consistent with the result obtained using the proposed method on the PMU data at those locations. Hence, the ICA method works well to identify coherent groups on the practical data mixed with inherent noise obtained through University-based Wide-Area Measurement System.

Eventually, PMU is expected to be installed in all of transmission substations in the UK grid. Under that circumstance, it will be possible to obtain full bus and generator coherency groups which will be useful for National Grid, the grid operator in the UK, for any pro-active control decision.

3.5 Comparison and performance robustness

3.5.1 Comparison with other methods

In this section, the accuracy of coherent groups obtained using the ICA method is compared with the results obtained using the model-based direction cosine method [16] and the measurement-based PCA approach [32, 33]. The PCA approach will also be used to demonstrate the impact of noise towards the accuracy of the measurement-based coherency identification. Using the identical operating condition, the 16-machine 68-bus test system model is used for this evaluation.

3.5.1.1 Direction Cosine

In the direction cosine method, coherent generators are clustered by observing entries in the coherency matrix that have direction cosine close to unity. This is done by calculating direction cosines of row eigenvectors corresponding to generator angles. The use of direction cosines for the generator coherency identification of the system is well described in [16, 20] and briefly described here.

Consider a set of DAE equations represent the dynamic behaviour of power system.

$$\dot{\boldsymbol{x}} = \boldsymbol{f}(\boldsymbol{x}, \boldsymbol{y}) \tag{3.13a}$$

$$0 = \boldsymbol{g}(\boldsymbol{x}, \boldsymbol{y}) \tag{3.13b}$$

$\boldsymbol{x}$ and $\boldsymbol{y}$ are state and algebraic variables of the system, respectively. The state-space equation in (3.14) represents the linearization of (3.13) around initial operating points $\boldsymbol{x}_0$ and $\boldsymbol{y}_0$:

$$\begin{bmatrix} \triangle\dot{\boldsymbol{x}} \\ 0 \end{bmatrix} = \begin{bmatrix} \boldsymbol{J}_A & \boldsymbol{J}_B \\ \boldsymbol{J}_C & \boldsymbol{J}_D \end{bmatrix} . \begin{bmatrix} \triangle\boldsymbol{x} \\ \triangle\boldsymbol{y} \end{bmatrix} \tag{3.14}$$

The terms $\boldsymbol{J}_A$, $\boldsymbol{J}_B$, $\boldsymbol{J}_C$ and $\boldsymbol{J}_D$ are Jacobian matrices comprised of the partial derivative of functions in (3.13). Hence, the system state matrix is given by:

$$\boldsymbol{A} = \boldsymbol{J}_A - \boldsymbol{J}_B {\boldsymbol{J}_D}^{-1} \boldsymbol{J}_C \tag{3.15}$$

For any eigenvalue of $\boldsymbol{A}$:

$$\boldsymbol{A}\boldsymbol{v} = \boldsymbol{\lambda}\boldsymbol{v} \tag{3.16}$$

where $\boldsymbol{v}$ is the eigenvector of the matrix $\boldsymbol{A}$.

The first step to identify the coherency group of generators using the direction cosine method is to determine modes of the oscillation that form the basis of the coherency grouping. These modes are sorted from the lowest to the highest frequency, including the zero eigenvalue. Subsequently, the gap between frequencies is observed. There is a noticeable large gap between inter-area modes and the rest of electromechanical modes of the system. These inter-area modes are considered to form the basis of the coherency grouping. For p-machine n-bus system and r number of modes are considered for coherency grouping, the dimension of $\boldsymbol{v}$ in (3.16) will be $2\,(P \times R)$. A new vector of $\boldsymbol{w}$ with the dimension of $(P \times R)$ is constructed by considering rows corresponding to generator angle state variables. The direction cosine of two vectors, $\boldsymbol{w_{1i}}$ and $\boldsymbol{w_{2i}}$ is defined as:

$$dcv = \frac{\sum_{i=1}^{m} \boldsymbol{w_{1i}} \boldsymbol{w_{2i}}}{\sqrt{\sum_{i=1}^{p} \boldsymbol{w_{1i}^2} \sum_{i=1}^{p} \boldsymbol{w_{2i}^2}}} \tag{3.17}$$

Generators belonging to the same coherent group will have the angle of $\boldsymbol{w}$ close to each other. When normalised by the denominator in (3.17), the direction cosine *dcv* for each generator will be closed to unity.

3.5.1.2 Principal Component Analysis (PCA)

The PCA technique has been used in the literature to identify the coherent group of generators in the system. It utilises measured data gathered from the system to highlight clusters of generators displaying common features after a disturbance. It is described in detail in [32, 33] and briefly explained here.

The PCA decomposes the data matrix $\boldsymbol{X}$ into matrix $\boldsymbol{W'}$ and $\boldsymbol{T}$ respectively. Row elements of matrix $\boldsymbol{W'}$ signify time trends of the oscillation presented in the system while the matrix $\boldsymbol{T}$ represents the weight of these time trends in measured signals. However, time trends in $\boldsymbol{W'}$ contain multi-mode components. These time trends in $\boldsymbol{W'}$ must be composed of dominant mono-frequency time trends for accurate weightings of $\boldsymbol{T}$. Thus, the PCA approach requires additional information of dynamic characteristics of the system. This is realised by using the combination of Hilbert Transform and Empirical Mode Decomposition (HT-EMD) to identify dominant modes of the oscillation by determining instantaneous attributes of intrinsic mode function (IMF) components through sifting process. For each i^{th} signals, HT-EMD gives n IMF functions such that:

$$x_i\left(t\right) = \sum_{n}^{j=1} c_j\left(t\right) + r\left(t\right) \tag{3.18}$$

These functions of $c_j\left(t\right)$ are nearly orthogonal and have zero local means. The term $r\left(t\right)$ represents the residue after the extraction of IMFs from the signal. Once the frequency f_n, phase ϕ and damping ζ are obtained from the IMFs, the dominant mode of principal components are represented using:

$$c_j(t) = e^{-\zeta 2\pi f_n t}\cos((2\pi f_n\sqrt{1-\zeta^2}) + \phi) \tag{3.19}$$

However, only the first few k IMFs that represent dominant modes of oscillations presented in the original dynamic data are considered for further analysis. Consequently, the PCA description is truncated to these k principal components as

follows:

$$\boldsymbol{X} = \boldsymbol{TW'} = \boldsymbol{T}(\boldsymbol{RM'}) = \boldsymbol{T_n M'} = \boldsymbol{T_n} \begin{bmatrix} \boldsymbol{c}_1 \\ \vdots \\ \boldsymbol{c}_k \end{bmatrix} \tag{3.20}$$

$\boldsymbol{T_n}$ represents the new weighting for time trends of $\boldsymbol{M'}$. The plot of elements in the $\boldsymbol{T_n}$ matrix gives the coherency plot of the system. These elements in the $\boldsymbol{T_n}$ matrix that have relatively similar coordinates form a cluster. This formation of the cluster helps in identifying the coherent group of generators in the system.

3.5.1.3 Comparison

Generators speed signals of the 16-machine 68-bus system model sampled at every 10 ms for 20 s are used to construct the data matrix for measurement-based approaches (PCA and ICA). Ten percent increment of mechanical torque for 80 ms disturbance is considered for this study. Fig. 3.10a shows the result obtained using ICA method while Fig. 3.10b illustrates the result obtained using the PCA approach. On the other hand, Table 3.2 represents the coherency matrix obtained using the direction cosine method.

Table 3.2: Generators coherency matrix using direction cosine

	G1	G2	G3	G4	G5	G6	G7	G8	G9	G10	G11	G12	G13	G14	G15	G16
G1	**1.000**	**0.982**	**0.982**	**0.984**	**0.980**	**0.981**	**0.982**	**0.999**	**0.989**	0.935	0.915	0.869	0.848	0.700	0.648	0.709
G2	**0.982**	**1.000**	**1.000**	**1.000**	**0.999**	**1.000**	**1.000**	**0.987**	**0.999**	0.852	0.824	0.764	0.738	0.633	0.590	0.613
G3	**0.982**	**1.000**	**1.000**	**1.000**	**0.999**	**1.000**	**1.000**	**0.987**	**0.999**	0.852	0.824	0.764	0.738	0.633	0.590	0.613
G4	**0.984**	**1.000**	**1.000**	**1.000**	**0.999**	**1.000**	**1.000**	**0.989**	**0.999**	0.857	0.830	0.770	0.745	0.635	0.593	0.618
G5	**0.980**	**0.999**	**0.999**	**0.999**	**1.000**	**1.000**	**0.999**	**0.985**	**0.998**	0.846	0.818	0.757	0.731	0.626	0.586	0.605
G6	**0.981**	**1.000**	**1.000**	**0.999**	**1.000**	**1.000**	**1.000**	**0.987**	**0.999**	0.850	0.822	0.762	0.736	0.631	0.589	0.611
G7	**0.982**	**1.000**	**1.000**	**1.000**	**0.999**	**1.000**	**1.000**	**0.987**	**0.999**	0.853	0.825	0.764	0.739	0.632	0.590	0.613
G8	**0.999**	**0.987**	**0.987**	**0.989**	**0.985**	**0.987**	**0.987**	**1.000**	**0.993**	0.923	0.902	0.853	0.831	0.694	0.639	0.696
G9	**0.989**	**0.999**	**0.999**	**0.999**	**0.998**	**0.999**	**0.999**	**0.993**	**1.000**	0.873	0.846	0.788	0.763	0.653	0.601	0.637
G10	0.935	0.852	0.852	0.857	0.846	0.850	0.853	0.923	0.873	**1.000**	**0.998**	**0.981**	**0.968**	0.766	0.701	0.836
G11	0.915	0.824	0.824	0.830	0.818	0.822	0.825	0.902	0.846	**0.998**	**1.000**	**0.990**	**0.980**	0.747	0.707	0.840
G12	0.869	0.764	0.764	0.770	0.757	0.762	0.764	0.853	0.788	**0.981**	**0.990**	**1.000**	**0.998**	0.685	0.678	0.797
G13	0.848	0.738	0.738	0.745	0.731	0.736	0.739	0.831	0.763	**0.968**	**0.980**	**0.998**	**1.000**	0.653	0.668	0.771
G14	0.700	0.633	0.633	0.635	0.626	0.631	0.632	0.694	0.653	0.766	0.747	0.685	0.653	**1.000**	0.594	0.742
G15	0.648	0.590	0.590	0.593	0.586	0.589	0.590	0.639	0.601	0.701	0.707	0.678	0.668	0.594	**1.000**	0.668
G16	0.709	0.613	0.613	0.618	0.605	0.611	0.613	0.696	0.637	0.836	0.840	0.797	0.771	0.742	0.668	**1.000**

From Fig. 3.10a, it is shown that the ICA method clustered the generators in the test system model into five coherent groups of generators. First nine generators (G1 to G9) form a group of coherent generators, while G10 to G13 form another group of generators. For other three generators, G14, G15, and G16 each form a

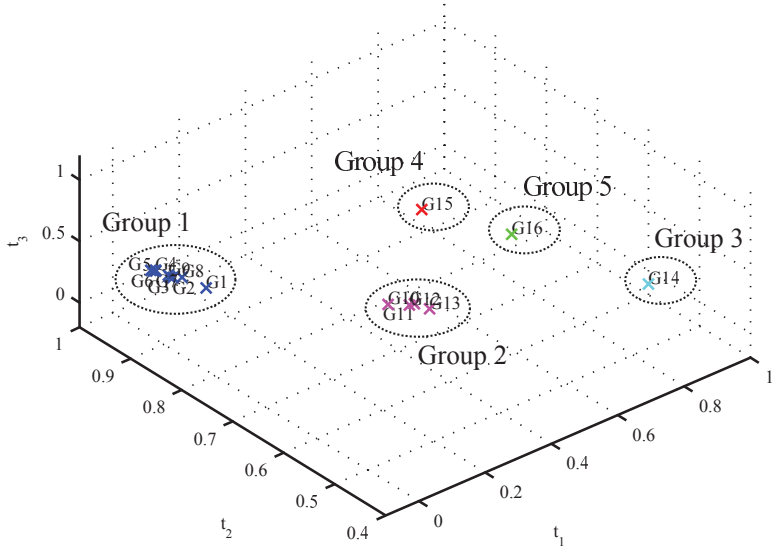

(a) ICA approach

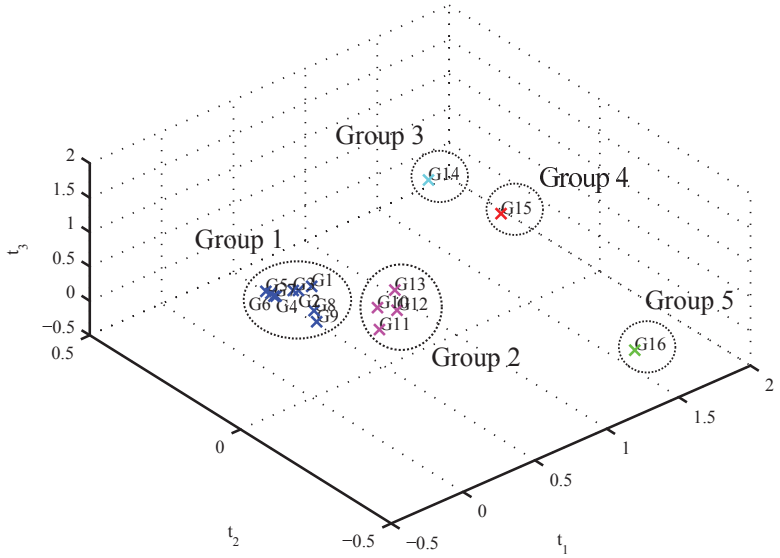

(b) PCA approach

Figure 3.10: Comparison of coherency identification techniques

single coherent group. Similar groups of coherent generators are observed in Fig. 3.10b where the PCA approach is applied on the generator speed data to identify coherent groups in the system. The coherency matrix obtained using the direction cosine method in Table 3.2 also clustered the system into five different groups of coherent generators. These five groups are in bold.

These results demonstrate that the proposed ICA method grouped the system into five coherent groups of generators. This implies that results obtained using the proposed method match with coherent groups of generators obtained in the measurement-based PCA technique and the model-based direction cosine method.

3.5.2 Performance under noise

The performance of any data-driven method is very much affected by the presence of noise in measured data. Therefore, it is sensible to evaluate the performance of ICA and PCA with noise present in the data. Same measured data are utilised for this study with the addition of white Gaussian noise with Signal-to-Noise Ratio (SNR) of 25. Both PCA and ICA are applied on the measured data to identify coherent groups of generators after the disturbance.

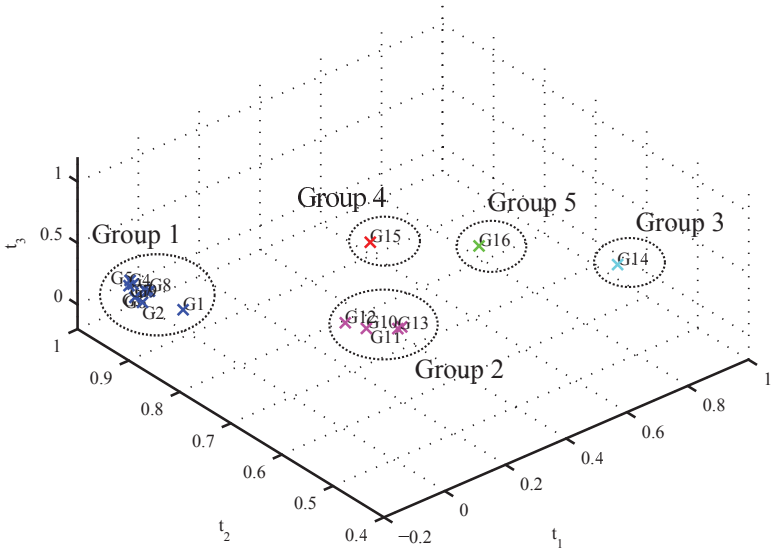

(a) ICA approach

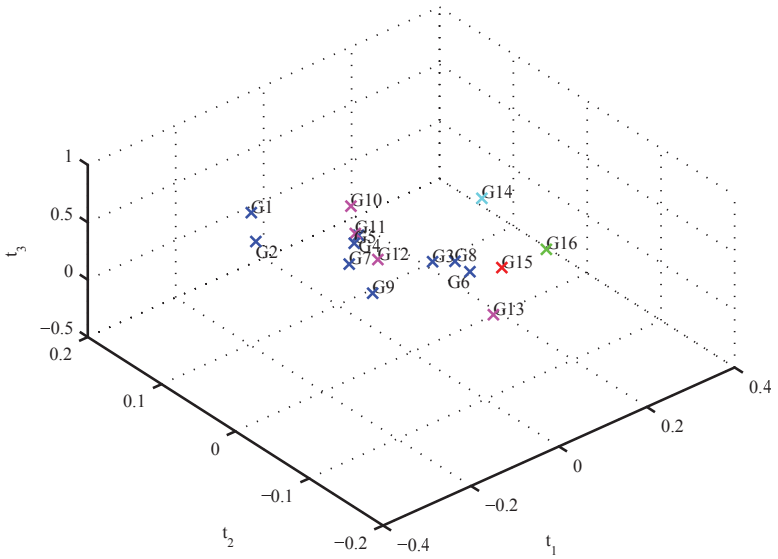

(b) PCA approach

Figure 3.11: Performance using measurements data with the presence of noise

Fig. 3.11a shows the coherency plot obtained with the ICA method, while Fig. 3.11b shows the coherency plot obtained with the PCA method. The results indicate that the PCA method shows limitation in identifying the same coherent groups of generators with the presence of noise in the measured data. Since the choice of SNR=25 is arbitrary, the test is repeated using different values of SNR. It is observed with SNR=50, the PCA method produces visibly better coherent clusters than it does with SNR=25. The visibility of the coherent clusters produced by the ICA is not affected by the level of noise in the data. This demonstrates that the noise in measured signals has significant influence in the results of measurement-based coherency identification technique. Nevertheless, it can be noticed that the coherency plot of ICA approach proposed in this paper are able to cluster the generators into their respective coherent groups even with the presence of noise in measured data. However, the direction cosine method is not a data-driven method, thus it is not relevant for noise performance analysis.

The ratio between measured signals and low frequency components in the system helps in identifying coherent groups of generators in the system. The ICA approach finds a set of ICs from measured signals that results in the preferential extraction of mono-frequency components. However, this is not the case with the PCA approach. As noise can be considered as a frequency process, the PCA approach is unable to identify the accurate coherent groups of generators in the system.

The proposed method consists of a spectral-based analysis, which analyses the power spectra translated from a time-trend of the signal. On the other hand, the PCA approach reported in [32, 33] consists of a time-domain-based analysis, which analyses the time-trend of the signal. The analysis in spectral-domain has an advantage over the analysis in time-domain. It gives improved performances in the presence of the high signal-to-noise ratio if the spectral content of the wanted signal occupies a narrow band of frequency compared to noise. This is an important characteristic to be considered when dealing with measured data with noise.

The proposed method can be thought of as an extension or improvement of spectral PCA [45]. The disadvantage of spectral PCA over spectral ICA is that more than one peak may appear in the spectrum-like principle component (PC). Different PCs may also contain same peaks, or peaks at the same position but with different signs [35]. Therefore, spectral ICA is preferred in the application of

the coherency identification in the power system discussed in this chapter. The performance of the proposed coherency identification technique using ICA method is consistent and robust even in the presence of noise in measured signals. These attributes are important for a measurement-based coherency identification tool as the presence of the noise in measured data is inevitable.

3.5.3 Response to fault

This section reports the performance of the proposed method in response to a fault in the system. Two fault cases: Case 1 and Case 2 have been considered in this study to demonstrate the robustness of the proposed method over a wide range of scenario in the system.

In Case 1, a three-phase fault occurred at Bus #1, cleared in 0.05 s and line 1-2 cleared in a further 0.05 s is considered as disturbance. The line 8-9 is out-of-service. The system operating condition considered in this case is identical with the case discussed in [16]. The proposed method is applied on measured data of bus voltage angles for all generators following fault inception in the system. Fig. 3.12 shows the coherency plot obtained from the application of the proposed method on measured data. The result shows that the system is segregated into two coherent groups of generators following the fault inception, namely as Group #1 and Group #2. Group #1 consists of Generator #1 to #9 (G1 to G9), while Group #2 consists of Generator #10 to #16 (G10 to G16). It is interesting to compare coherent groups of generators obtained using the proposed method with time trends of generator rotor angles in the system illustrated in Fig. 3.13 The figure also indicates that the system is separated into two coherent groups. One group consists of Generator #1 to #9, while the other group consists of Generator #10 to #16. In addition, the result obtained using the proposed method is consistent with the result reported in [16] using an identical system operating condition.

In Case #2, a temporary three-phase fault inception at Bus #31, cleared after 480 ms is considered as disturbance. The proposed method is applied on measured data of bus voltage angles at all generators, and the coherency plot of the system is plotted and displayed in Fig. 3.14. The result shows that the system is segregated into two coherent groups, where Group #1 consists of Generator #10 (G10), while Group #2 consists of all other generators in the system (G1 to G9

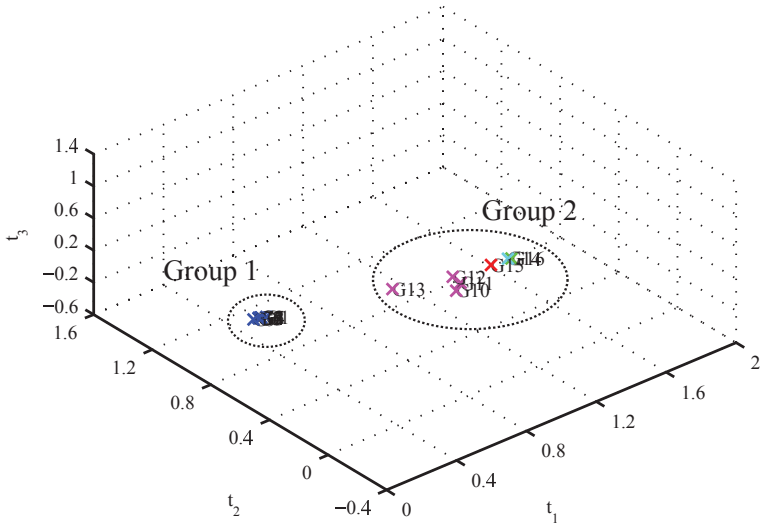

Figure 3.12: Coherency plot of the system for Case 1

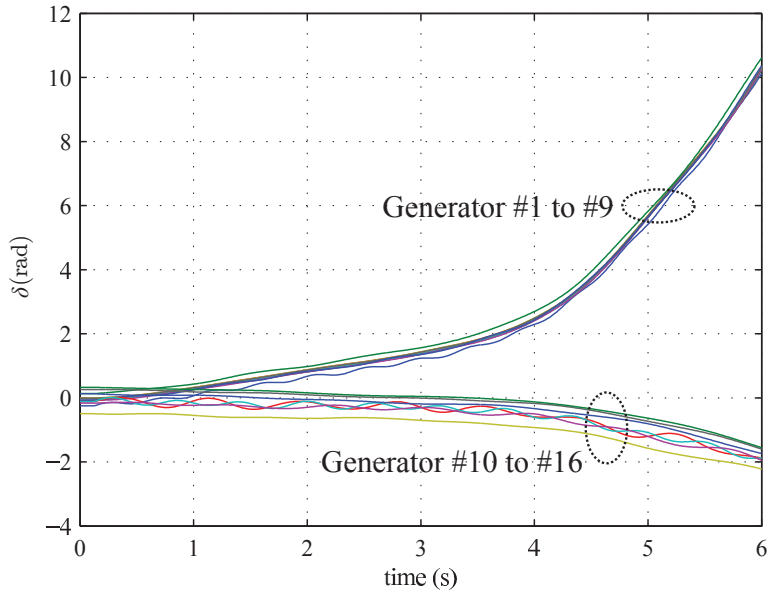

Figure 3.13: Generator rotor angles for Case 1

and G11 to G16). The result implies that Generator #10 oscillates against the rest of generators in the system. This is because the location of the fault considered in this case is close to Generator #10. The fault that is close to a generator may cause the generator to oscillate against the rest of the system [46]. The time trend of generator rotor angles following the fault in the system shown in Fig. 3.15 is consistent with the result obtained using the proposed method as in Fig. 3.14. The rotor angle response of Generator #10 diverges from the rest of generators in the system following the fault considered in this study. Results obtained using the proposed method in the case of faults discussed in this subsection imply that

the proposed method is robust over a wide range of scenarios in the system.

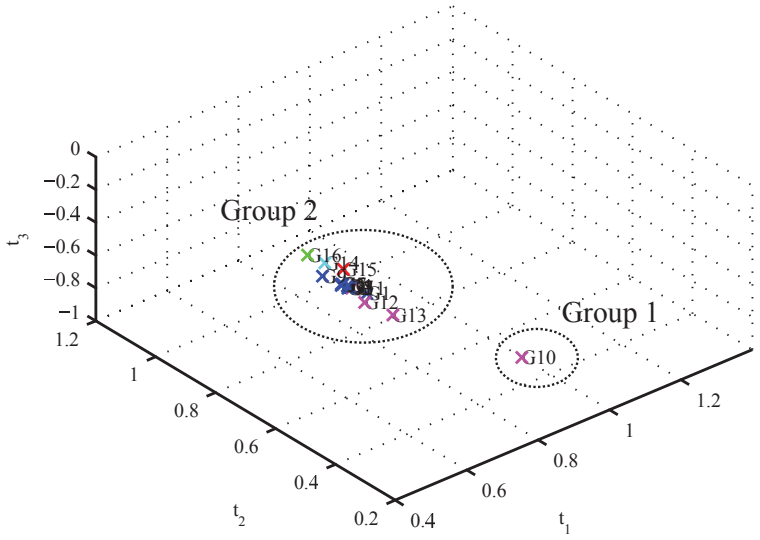

Figure 3.14: Coherency plot of the system for Case 2

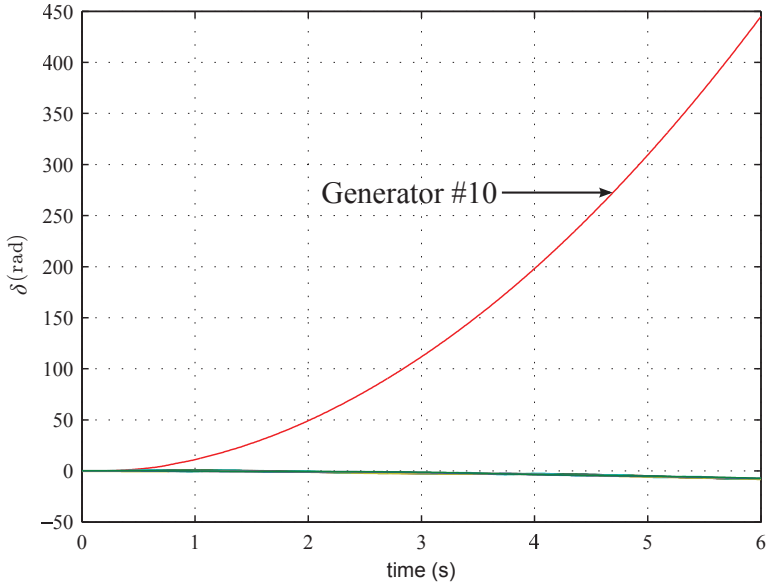

Figure 3.15: Generators rotor angle for Case 2

3.6 Chapter summary

A measurement-based coherency identification technique in the interconnected power system has been proposed. The approach is based on the application of independent component analysis (ICA) technique on wide-area generator speeds

and bus voltage angle signals to extract the coherency property of the system. This technique clusters generators and buses displaying common features in measured signals into their coherent areas by extracting the mixing ratio of ICs from measured signals. The accuracy of the proposed method is validated by comparing results obtained from the proposed method with results generated from the direction cosine method and the coherency identification technique using PCA. It is also found that the presence of noise in measured signals influences the accuracy of results obtained from the coherency identification technique using PCA. However, the method proposed in this chapter identifies coherent groups of generators even with the presence of noise in the measured data accurately. The proposed method also works well with actual data gathered through UK University-based WAMS. The method is simple and does not require detailed system modelling information.

Chapter 4

Dynamic model parameter estimation

This chapter presents a new approach in estimating important parameters of the power system transient stability model such as the direct axis transient reactance x'_d, quadrature axis speed voltage E_q and generator inertia H. It uses a variation of unscented Kalman filter (UKF) on the phasor measurement unit (PMU) data. An accurate estimation of these parameters is very important for assessing the stability and tuning the adaptive protection system on power swing relays. The chapter begins with an overview of the dynamic parameter estimation in the power system and the motivation behind this research. This is followed by a section that reports recent and ongoing research efforts in the dynamic model parameter estimation. Consequently, the approach used to utilize UKF for the dynamic model parameter estimation using PMU measurements is presented. Next, the proposed approach is applied to measured data simulated from 16-machine 68-bus system models. Results obtained using the technique are analysed and discussed. Subsequently, the robustness of the method is further validated in the presence of noise that is likely to be in the PMU data in reality. The results obtained using proposed method are validated and compared with the actual parameters. The results presented in this chapter have been published by IEEE Transaction on Power Systems in an article titled, "*Estimating Dynamic Model Parameters for Adaptive Protection and Control in Power System*".

4.1 Overview

In the aftermath of several recent power blackouts, the technical investigation identified that the inadequacy of control and subsequent undesirable operations of the protection system after a disturbance triggered cascading events that ultimately led to the wide-area blackout. This is because the existing control and protection logic is designed based on model-based simulation studies over a fixed number of operating scenarios. Thus, the variation of network operating scenarios and load demands requires control and protection settings to be recalculated and retuned accordingly. Furthermore, there is always some risks in the model-based system design. In practice, the dynamic behaviour of the complex power network with hundreds of synchronous generators, thousands of loads and transformers can never be very closely represented through model-based simulations. The famous WECC blackout in 1996 substantiated this fact, where measured responses in the period prior to the blackout did not match with simulated results using the planning model [1].

Amongst various other suggestions, one important recommendation to reduce the probability of blackouts is implementing an adaptive protection, mainly on the out-of-step relay system. The out-of-step relay determines the stability of the evolving electromechanical swing after a disturbance and provides the appropriate tripping or/and blocking decision to bring the power system to a viable steady state. This is realised by observing the apparent impedance trajectories at vulnerable locations after a disturbance. The characteristic of an out-of-step relay is mostly determined by three parameters: transient reactance of direct axis x'_d, speed voltage of quadrature axis E_q and the inertia constant of the generator H [11]. The value of x'_d influences the sensitivity and speed of the relay operation while the values of E_q and H influence the speed of the impedance trajectory seen by the relay. Therefore, it is clear that an accurate and secure action of the out-of-step protection unit, these parameters need to be precise. The generator manufacturers' data can be representative. Moreover, increasing the addition of renewable generation interfaced with power electronics at the transmission level influences the apparent impedance seen by the out-of-step relay during electromechanical oscillations. All these parametric uncertainties and variations demand regular updates of relay settings to suit to the prevalent operating situation. Thus, the continuous estimations of x'_d, E_q and H are evidently required to accomplish this objective.

The advent of the PMU technology provides high resolution time-synchronized measurement data across the power system network. Hence, it is possible to have a fast estimation tool that is able to estimate dynamic parameters in real time. However, PMU measurements are influenced by transient, process and measurement noise in practice. This affects the performance of any measurement-based dynamic parameter estimation tools. The existing literature does not appear to address these issues comprehensively. The algorithm proposed in this chapter is demonstrated to address these issues properly. Dynamic parameters of the system are estimated using a moment-matching recursive estimation using augmented unscented Kalman filter (UKF). The UKF method is simple, accurate, fast and robust in filtering out the effect of noise on the accuracy of estimated parameters.

4.2 State of the Art

The objective of the dynamic model parameter estimation is to provide an accurate representation of the dynamic behaviour of the system for simulation studies. Conventionally, short-circuit tests on unloaded generators represented the standard measure of transient performance and various commonly accepted approximations formed the basis of model parameter derivations. However, due to their limitations on providing q-axis transient and sub-transient constant, several alternative tests, such as enhanced sudden short circuit test, stator decrement test and standstill frequency response test have been proposed to obtain better representations of the dynamic model [47]. Although accurate, these approaches are not economically feasible because the generator under investigation must be offline.

Online methods have been proposed to address the pitfall of the staged test approach to identify dynamic model parameters. The approaches underlying these methods are diverse, e.g., trajectory sensitivity [48], extended Kalman filter (EKF) [49], non-linear least square technique [50], Newton Raphson [51] and Euler [52]. Despite having advantages over offline methods, these techniques have some limitations. These techniques assume the availability of an accurate rotor angle and speed; field voltage and current; terminal voltage and current; and active and reactive power measurement. In practice, it is not always possible to have all these measurements time-stamped.

The method of dynamic model parameter estimation driven based on PMU data has been proposed in the literature. PMU provides the data across the network with time synchronous stamping. The maximum likelihood estimation (MLE) approach is reported in [53] to estimate dynamic model parameters of the system. The method requires *a-priori* additional information of the state variable to estimate those parameters accurately. Another effort integrates hybrid dynamic simulation, trajectory sensitivity, parameter correlation analysis and a minimum variance criterion to solve the estimation problem [54]. It is a non-recursive and computationally exhaustive. Another approach, inter-area model estimation (IME), is reported in [55] and [56] to estimate dynamic parameters. The proposed method extrapolates the system impedance and inertia using inter-area oscillation components in voltage variables after a disturbance. Besides being non-recursive, the complexity of the method increases exponentially with the number of generators in the system.

Many research groups exploit variants of EKF [57, 58]. EKF works on the assumption that all non-linear transformations are quasi-linear. Hence, EKF simply linearises all non-linear transformations and substitutes Jacobian matrices for linear transformation. Although the EKF maintains an elegant and computationally efficient recursive update, it has some limitations. It works on the linearisation of the non-linear dynamic process which may produce highly unstable filters if the assumption of the local linearity is violated. The high complexity and non-linearity of power system are susceptible to these problems. Furthermore, calculations of Jacobian matrices are often very difficult. Also, the observability of parameters from the measurement point using EKF are limited as reported in [57]. The method shows limitation in estimating the generator inertia constant from measured data. It requires complementary information from the staged test method in order to estimate the generator inertia constant accurately. The iterative EKF approach proposed in [58] eliminates the requirement of stage-test complementary information as required in [57]. Besides being computationally expensive, the iterative EKF-based prediction suffers from the linearisation error. The robustness and accuracy associated with EKF driven methods in [57] and [58] are not thoroughly investigated. The presence of noise in measured signals influences the accuracy of the dynamic model parameter estimation technique. Therefore, it is important to guarantee that the dynamic model parameter estimation technique is robust in the presence of noise in measured signals.

In this chapter, dynamic model parameters of synchronous generators are estimated by processing the PMU measurements using UKF; a moment-matching filter that is significantly better than EKF. UKF is developed in [59, 60] to address the issues in EKF. It calculates the statistic of random variables that undergo a nonlinear transformation. This method works on the assumption that *it is easier to approximate a probability distribution than it is to approximate an arbitrary nonlinear function or transformation* [60]. UKF has earlier been used in the power system for dynamic state estimation [61, 62] and parameter estimation using operational data [63]. It has potential to be reformulated to solve dynamic parameter estimation problems [64]. However, the method proposed in this chapter employs a better sigma point distribution and filtering approach compared to [64], which reflects in a better accuracy of the estimated parameter and consumes less computing power. UKF offers a flexibility to allow information beyond mean and covariance to be incorporated in the estimation [65]. Hence, UKF is able to estimate accurate dynamic model parameters even with the presence of noise in measured data. Moreover, the UKF is completely data driven and recursive thus offering a real opportunity for a fast estimation in real time.

4.3 Dynamic model parameter estimation using UKF

Generally, power system dynamics are represented using a set of continuous-time nonlinear equations, given in (4.1).

$$\dot{\boldsymbol{x}}(t) = \bar{\boldsymbol{f}}[\boldsymbol{x}(t), \boldsymbol{u}(t), \boldsymbol{v}(t)] \tag{4.1a}$$

$$\boldsymbol{y}(t) = \boldsymbol{h}[\boldsymbol{x}(t), \boldsymbol{u}(t), \boldsymbol{v}(t)] + \boldsymbol{w}(t) \tag{4.1b}$$

where the $\boldsymbol{x}(t)$ vector represents the state variable, the $\boldsymbol{y}(t)$ vector represents the output variable, and $\boldsymbol{u}(t)$ is the input variables. In (4.1), $\bar{\boldsymbol{f}}\,[.]$ represents the continuous form of system differential function and $\boldsymbol{h}\,[.]$ represents the measurement algebraic function. Equations (4.1) are rewritten in discrete form with a time step

of $\triangle t$, given by (4.2),

$$\begin{aligned} \boldsymbol{x}_k &= \boldsymbol{x}_{k-1} + \bar{\boldsymbol{f}}[\boldsymbol{x}_{k-1}, \boldsymbol{u}_{k-1}, \boldsymbol{v}_{k-1}]\triangle t \\ &= \boldsymbol{f}[\boldsymbol{x}_{k-1}, \boldsymbol{u}_{k-1}, \boldsymbol{v}_{k-1}] \qquad (4.2a) \\ \boldsymbol{y}_k &= \boldsymbol{h}[\boldsymbol{x}_k, \boldsymbol{u}_k, \boldsymbol{v}_k] + \boldsymbol{w}_k \qquad (4.2b) \end{aligned}$$

The state $\boldsymbol{x}_k$ is considered as a random variable with an estimated mean $\hat{\boldsymbol{x}}_k$ and an estimated covariance $\boldsymbol{P}_{x_k}$. The process noise $\boldsymbol{v}_k$ in (4.2) is assumed to be non-additive, while the measurement noise $\boldsymbol{w}_k$ is assumed to be additive. The covariance matrix for $\boldsymbol{v}_k$ and $\boldsymbol{w}_k$ are denoted by $\boldsymbol{Q}$ and $\boldsymbol{R}$, respectively. Both are assumed to be constant. In the equations, $\boldsymbol{f}\,[.]$ represents the discrete forms of system differential function, while $\boldsymbol{h}\,[.]$ represents the measurement algebraic function. Assume that (4.2) is parameterised by the unknown vector $\boldsymbol{\psi}_k$. The state $\boldsymbol{x}_k$ and the set of model parameters $\boldsymbol{\psi}_k$ need to be estimated simultaneously. If $\boldsymbol{\psi}$ is also treated as a state, then it may be augmented with $\boldsymbol{x}_k$ to give an augmented state vector $\boldsymbol{x}_k^a$, i.e. $\boldsymbol{x}_k^a = [\boldsymbol{x}_k{}^\top, \boldsymbol{\psi}_k^\top]^\top$. The state-space model in (4.2) is reformulated as:

$$\begin{aligned} \boldsymbol{x}_k^a &= \boldsymbol{f}_a[\boldsymbol{x}_{k-1}^a, \boldsymbol{u}_{k-1}, \boldsymbol{v}_{k-1}] \qquad (4.3a) \\ \boldsymbol{y}_k &= \boldsymbol{h}[\boldsymbol{x}_k^a, \boldsymbol{u}_k, \boldsymbol{v}_k] + \boldsymbol{w}_k \qquad (4.3b) \end{aligned}$$

where $\boldsymbol{f}_a\,[.]$ represents the discrete form of augmented system differential function, while $\boldsymbol{h}\,[.]$ represents the measurement algebraic function. Using the same approach in (4.3), the process noise $\boldsymbol{v}_k$ may also be concatenated with $\boldsymbol{x}_k^a$, resulting higher-dimensional state random variables $\boldsymbol{X}_k = [\boldsymbol{x}_k^{a\top}, \boldsymbol{v}_k{}^\top]^\top$ with an estimated mean $\hat{\boldsymbol{X}}_k$ and covariance $\boldsymbol{P}_{X_k}$. Hence, the state random variable is redefined as the augmentation of the original state $\boldsymbol{x}_k$, the set of unknown model parameter $\boldsymbol{\psi}_k$ and the process noise $\boldsymbol{v}_k$ given in (4.4);

$$\boldsymbol{X}_k = \begin{bmatrix} \boldsymbol{x}_k^a \\ \boldsymbol{v}_k \end{bmatrix} = \begin{bmatrix} \boldsymbol{x}_k \\ \boldsymbol{\psi}_k \\ \boldsymbol{v}_k \end{bmatrix} \qquad (4.4)$$

In a similar manner, the corresponding augmented state covariance is built up from individual covariance matrices of $\boldsymbol{x}_k$, $\boldsymbol{\psi}_k$ and $\boldsymbol{v}_k$ given in (4.5):

$$\boldsymbol{P}_{X_k} = \begin{bmatrix} \boldsymbol{P}_{\boldsymbol{x}_k} & 0 & 0 \\ 0 & \boldsymbol{Q}_{\boldsymbol{\psi}_k} & 0 \\ 0 & 0 & \boldsymbol{Q}_{\boldsymbol{v}_k} \end{bmatrix} \tag{4.5}$$

Hence, the state-space model in (4.3) is rewritten as follows,

$$\boldsymbol{X}_k = \boldsymbol{f}_{aa}[\boldsymbol{X}_{k-1}, \boldsymbol{u}_{k-1}] \tag{4.6a}$$

$$\boldsymbol{y}_k = \boldsymbol{h}[\boldsymbol{X}_k, \boldsymbol{u}_k] + \boldsymbol{w}_k \tag{4.6b}$$

Consequently, given that the augmented system differential equation $\boldsymbol{f}_{aa}[.]$, measured signals from PMU, the measurement algebraic function $\boldsymbol{h}[.]$ and all noise covariances are available, the unknown parameter vector $\boldsymbol{\psi}_k$ is estimated using the recursive algorithm by finding the real-time estimates of the mean and covariance of the augmented state $\boldsymbol{X}_k$.

The genesis of the idea that leads to the formulation of the UKF method proposed in this chapter is inspired from the work presented in [66] and [67]. The work reported in [66] formulates the UKF method to estimate the state and the set of unknown parameters of the system by augmenting the state and the set of unknown parameter into a higher order of state vector. However, the process noise covariance has not been augmented in the state vector. The work presented in [67] provides an insight of the advantage in augmenting the state and the process noise covariance into a higher order of state vector to improve the accuracy of estimations. The discussion of idea in [66] and [67] leads to the development of the novel feature in the UKF formulation for dynamic model parameter estimation presented in this chapter. The augmentation of the state, the set of unknown model parameters, and the process noise covariance into a higher order of state vector as presented in (4.4) is one of novel contributions of this thesis. The sigma point distribution in the UKF algorithm applied in this chapter is also considered as one of novel contributions in this study. This is because the sigma point distribution in the UKF algorithm employed in this thesis has never been applied in any application of the UKF algorithm in the power system prior to the work reported in this thesis. The distribution of sigma points used in this study is discussed in the following subsection.

4.3.1 Unscented Kalman Filter (UKF)

The idea of UKF is the propagation of the statistical distribution of the state through non-linear equations. This is realised by obtaining a set of vectors called sigma points, which capture the mean and covariance of the state $\boldsymbol{X}$ distribution. A set of sigma points, denoted as $\boldsymbol{\chi}_i$, is selected in such a way that the mean and covariance of these points are $\hat{\boldsymbol{X}}$ and $\boldsymbol{P}_{\boldsymbol{X}}$. Consequently, these points are transformed into a set of transformed points by applying $\boldsymbol{\chi}_i$ into a non-linear measurement algebraic function $\boldsymbol{h}[.]$. This process is described as follows:

$$\boldsymbol{\gamma}_i = \boldsymbol{h}(\boldsymbol{\chi}_i) \tag{4.7}$$

Next, the mean $\hat{\boldsymbol{y}}$ and covariance $\boldsymbol{P}_y$ of transformed points are calculated. The mean $\hat{\boldsymbol{y}}$ is the weighted average of transformed points while the covariance $\boldsymbol{P}_y$ is the weighted outer product of transformed points. For l numbers of sigma points, $\hat{\boldsymbol{y}}$ and $\boldsymbol{P}_y$ are calculated as follows:

$$\hat{\boldsymbol{y}} = \sum_{i=0}^{l} W_i \boldsymbol{\gamma}_i \tag{4.8a}$$

$$\boldsymbol{P}_y = \sum_{i=0}^{l} W_i (\boldsymbol{\gamma}_i - \hat{\boldsymbol{y}})(\boldsymbol{\gamma}_i - \hat{\boldsymbol{y}})^\top \tag{4.8b}$$

To provide an unbiased estimate, the weight W_i used to calculate $\hat{\boldsymbol{y}}$ and $\boldsymbol{P}_y$ must be set such that:

$$\sum_{i=0}^{l} W_i = 1 \tag{4.9}$$

In this chapter, for L number of state, a set of $l = 2L + 1$ points is used to distribute the sigma points. The set of points described in (4.10) satisfied the

condition described above:

$$\boldsymbol{\chi}_0 = \hat{\boldsymbol{X}} \tag{4.10a}$$

$$W_0 = 1 - \frac{L}{3} \tag{4.10b}$$

$$\boldsymbol{\chi}_i = \hat{\boldsymbol{X}} + \left[\sqrt{\frac{L}{1-W_0}\boldsymbol{P}_{\boldsymbol{X}}}\right]_i \tag{4.10c}$$

$$W_i = \frac{1-W_0}{2L} \tag{4.10d}$$

$$\boldsymbol{\chi}_{i+L} = \hat{\boldsymbol{X}} - \left[\sqrt{\frac{L}{1-W_0}\boldsymbol{P}_{\boldsymbol{X}}}\right]_{i+L} \tag{4.10e}$$

$$W_{i+L} = \frac{1-W_0}{2L} \tag{4.10f}$$

The set of sigma points described in (4.10) is able to exploit any additional known information about the error distribution associated with an estimate and maintain the mean $\hat{\boldsymbol{X}}$ and covariance $\boldsymbol{P}_{\boldsymbol{X}}$. This set of sigma points provides approximations accurate to the third-order moment of the Gaussian probability density function (pdf), regardless of the form of the non-linear transformation function used in the estimation [65]. The weight associated with the new sigma point, W_0 provides a parameter for controlling some aspect of the higher moments of the distribution of sigma points without affecting the mean of the covariance. In this chapter, the value of W_0 is set such that the error of the fourth-order moment of the Gaussian pdf is minimized [65]. Consequently, each sigma points is passed through the model of state evolution to obtain the predicted-state sigma points given as:

$$\boldsymbol{\chi}_k^- = \boldsymbol{f}\left(\boldsymbol{\chi}_{k-1}, \boldsymbol{u}_{k-1}\right) \tag{4.11}$$

Subsequently, the weighted mean and covariance of the predicted sigma points $\boldsymbol{\chi}_k^-$ defined as $\hat{\boldsymbol{X}}_k^-$ and $\boldsymbol{P}_{\boldsymbol{X}_k}^-$, respectively, are calculated using (4.12):

$$\hat{\boldsymbol{X}}_k^- = \sum_{i=0}^{2L} W_i(\boldsymbol{\chi}_{i,k}^-) \tag{4.12a}$$

$$\boldsymbol{P}_{\boldsymbol{X}_k}^- = \sum_{i=0}^{2L} W_i \left(\boldsymbol{\chi}_{i,k}^- - \hat{\boldsymbol{X}}_k^-\right)\left(\boldsymbol{\chi}_{i,k}^- - \hat{\boldsymbol{X}}_k^-\right)^\top \tag{4.12b}$$

Subsequently, the predicted sigma points $\boldsymbol{\chi}_k^-$ are instantiated through the measurement equation to generate the predicted-measurement sigma points $\boldsymbol{\gamma}_k^-$ as follows:

$$\boldsymbol{\gamma}_k^- = \boldsymbol{h}\left(\boldsymbol{\chi}_k^-, \boldsymbol{u}_k\right) \tag{4.13}$$

Consequently, the weighted mean of the predicted measurement $\hat{\boldsymbol{y}}_k^-$, the corresponding covariance matrix $\boldsymbol{P}_{\boldsymbol{y}_k}^-$ and the cross-correlation matrix $\boldsymbol{P}_{\boldsymbol{x}_k\boldsymbol{y}_k}^-$ are computed as shown in (4.14). The matrix $\boldsymbol{P}_{\boldsymbol{x}_k\boldsymbol{y}_k}^-$ represents the cross-correlation between the difference of the predicted-state sigma points $\boldsymbol{\chi}_{i,k}^-$ with the corresponding predicted-state $\hat{\boldsymbol{X}}_k^-$, and the difference of predicted-measurement sigma points $\boldsymbol{\gamma}_{i,k}^-$ with the corresponding predicted-measurement $\hat{\boldsymbol{y}}_k^-$:

$$\hat{\boldsymbol{y}}_k^- = \sum_{i=0}^{2L} W_i(\boldsymbol{\gamma}_{i,k}^-) \tag{4.14a}$$

$$\boldsymbol{P}_{\boldsymbol{y}_k}^- = \sum_{i=0}^{2L} W_i\left(\boldsymbol{\gamma}_{i,k}^- - \hat{\boldsymbol{y}}_k^-\right)\left(\boldsymbol{\gamma}_{i,k}^- - \hat{\boldsymbol{y}}_k^-\right)^\top + \boldsymbol{R} \tag{4.14b}$$

$$\boldsymbol{P}_{\boldsymbol{x}_k\boldsymbol{y}_k}^- = \sum_{i=0}^{2L} W_i\left(\boldsymbol{\chi}_{i,k}^- - \hat{\boldsymbol{X}}_k^-\right)\left(\boldsymbol{\gamma}_{i,k}^- - \hat{\boldsymbol{y}}_k^-\right)^\top \tag{4.14c}$$

Finally, the Kalman gain matrix $\boldsymbol{K}_k$ is calculated to find the mean $\hat{\boldsymbol{X}}_k$ and covariance matrix $\boldsymbol{P}_{X_k}$ as given in (4.15):

$$\boldsymbol{K}_k = \boldsymbol{P}_{\boldsymbol{x}_k\boldsymbol{y}_k}^-(\boldsymbol{P}_{\boldsymbol{y}_k}^-)^{-1} \tag{4.15a}$$

$$\hat{\boldsymbol{X}}_k = \hat{\boldsymbol{X}}_k^- + \boldsymbol{K}_k\left(\boldsymbol{y}_k - \hat{\boldsymbol{y}}_k^-\right) \tag{4.15b}$$

$$\boldsymbol{P}_{X_k} = \boldsymbol{P}_{\boldsymbol{X}_k}^- - \boldsymbol{K}_k\boldsymbol{P}_{\boldsymbol{y}_k}^-\boldsymbol{K}_k^\top \tag{4.15c}$$

4.3.2 Implementation for dynamic model parameter estimation

The power system first swing dynamics are represented as follows:

$$\frac{d\delta(t)}{dt} = (\omega(t) - \omega_0)\,\omega_s \tag{4.16a}$$

$$\frac{d\omega(t)}{dt} = \frac{1}{2H}\left(P_m - P_g(t) - D\left(\omega(t) - \omega_0\right)\right) \tag{4.16b}$$

where $\delta(t)$, $\omega(t)$, ω_0 and ω_s are rotor angle, rotor speed, synchronous speed and base speed, respectively. This study focuses on the estimation of parameters that influence settings of an out-of-step protection. These settings are mainly influenced by E_q, x'_d and H. The damping coefficient is relevant but less important compared to E_q, x'_d and H in the out-of-step protection application. It is often neglected in literature related to the out-of-step protection system [2, 5, 11]. Thus, only these three parameters are considered in this study in order to maximise the speed and to maintain the accuracy of the proposed method for the adaptive protection and control application. Therefore, neglecting the damping coefficient D, the discrete form of (4.16) is given by:

$$\delta_k = \delta_{k-1} + (\omega_{k-1} - \omega_0)\,\omega_s \triangle t \tag{4.17a}$$

$$\begin{aligned}\omega_k &= \omega_{k-1} + \frac{\triangle t}{2H_{k-1}}\left(P_m - P_{g_{k-1}}\right) \\ &= \omega_{k-1} + G_{k-1}\left(P_m - P_{g_{k-1}}\right)\end{aligned} \tag{4.17b}$$

Since $\triangle t$ and H_k are constant, ω_k is simplified by substituting the term $\frac{\triangle t}{2H_k}$ with G_k to reduce the nonlinearity of the equation. Consequently, the state vector of the system given in (4.17) is defined as $\boldsymbol{x}_k = [\delta_k \quad \omega_k]^\top$ and is parameterized by inertia constant H, transient impedance x'_d and generator internal voltage E_q. These parameters and variable are unknown and represented by the vector $\boldsymbol{\psi}_k = \begin{bmatrix}E_{q_k} & x'_{d_k} & G_k\end{bmatrix}^\top$. As described in (4.3), the state $\boldsymbol{x}_k$ and the unknown parameter vector ψ_k are simultaneously estimated by augmenting these two vectors into a higher-dimensional state variables $\boldsymbol{x}^a_k = \begin{bmatrix}\delta_k & \omega_k & E_{q_k} & x'_{d_k} & G_k\end{bmatrix}^\top$. Hence, to accommodate this change, the state evolution equation in (4.17) is reformulated as:

$$\delta_k = \delta_{k-1} + (\omega_{k-1} - \omega_0)\,\omega_s \triangle t \tag{4.18a}$$

$$\omega_k = \omega_{k-1} + G_{k-1}\left(P_m - P_{g_{k-1}}\right) \tag{4.18b}$$

$$E_{q_k} = E_{q_{k-1}} \tag{4.18c}$$

$$x'_{d_k} = x'_{d_{k-1}} \tag{4.18d}$$

$$G_k = G_{k-1} \tag{4.18e}$$

In (4.18), the mechanical input power P_m is assumed to be known. It is approximated to the electrical power measured at the generator terminal bus prior to a disturbance in the system. The dynamic behaviour of one generator unit can be analysed independently from the dynamic behaviour of the rest of the network.

This is realised by separating the signals at the terminal bus into two groups: inputs and measurements. It is assumed that PMU provides time-tagged voltage magnitude V_g, phasor angle θ_g, active power P_g and reactive power Q_g measurements at the generator terminal bus to monitor the dynamic behaviour of the generators. Hence, V_g and P_g at the terminal bus are treated as the input signals, while θ_g and Q_g are treated as the measurements to decouple one generation unit from the rest of the system. The equations for the measurement quantities, θ_g and Q_g of a generation unit are:

$$\theta_{g_k} = \delta_k - \tan^{-1}\left(\frac{P_{g_k} x'_{dk}}{\sqrt{\left(E_{q_k} V_{g_k}\right)^2 - \left(P_{g_k} x'_{dk}\right)^2}}\right) \tag{4.19a}$$

$$Q_{g_k} = \frac{\sqrt{\left(E_{q_k} V_{g_k}\right)^2 - \left(P_{g_k} x'_{dk}\right)^2} - {V_{g_k}}^2}{x'_{dk}} \tag{4.19b}$$

In the presence of noise in the measured signals, dealing with V_g and P_g may cause a problem to the UKF algorithm. Hence, the actual values of V_g and P_g have to be redefined to include the effect of noise in the estimation algorithm. Consequently, the actual inputs (V_g and P_g) are equal to the differences of their measured values (V_g^u and P_g^u) and the associated noise (V_g^w and P_g^w). The associated noise V_g^w and P_g^w also drive the system modelled in the UKF algorithm. They are modelled as in [61] and given below.

$$V_{g_k} = {V_g^u}_k - {V_g^w}_k \tag{4.20a}$$

$$P_{g_k} = {P_g^u}_k - {P_g^w}_k \tag{4.20b}$$

Hence, ${V_g^u}_k$ and ${P_g^u}_k$ formed a pseudo input vector $\boldsymbol{u}_k$ while ${V_g^w}_k$ and ${P_g^w}_k$ formed a pseudo process noise vector $\boldsymbol{v}_k$. As derived in (4.4), the process noise $\boldsymbol{v}_k$ is concatenated with the state vector and the unknown parameter $\boldsymbol{\psi}_k$ vector to form an augmented state $\boldsymbol{X}_k = \begin{bmatrix}\delta_k & \omega_k & E_{q_k} & x'_{d_k} & G_k & {V_g^w}_k & {P_g^w}_k\end{bmatrix}^\top$. This formulation incorporates the process noise $\boldsymbol{v}_k$ into the predicted state vector with the same level of accuracy as the propagated estimation errors without the needs to calculate the Jacobian, Hessian or other numerical approximation [60]. Therefore, the UKF algorithm as described in the preceding subsection will be directly applied to estimate $\boldsymbol{X}_k$.

4.4 Application, results and analysis

The 16-machine 68-bus system model is considered as the test system. Bus data, line data and dynamic characteristics of the systems are available in [16, 41] and listed in Appendix A as well. Fig. 4.1 shows the single line diagram of the system. Nonlinear simulations of the test system model are performed in MATLAB Simulink. The synchronous generators in the test system are modelled as classical models. The mechanical power input to the generators is assumed to be constant. The disturbance considered for this study is a three-phase bolted fault at Bus #21. The fault is applied at $t = -0.9s$ and cleared by removing line 21-22 after 100 ms. The proposed method is applied on measured data 800 ms following the clearance of the fault to avoid the transient error of the PMU estimation during the transition period from pre-fault to post-fault condition [7]. For the parameter estimation, the proposed method is applied to the voltage magnitude V_g, voltage phase angle θ_g, active power P_g, and reactive power Q_g signal from all generators in the system.

The main aim of the proposed methodology is to provide a parameter estimation tool for an adaptive protection and control application, mainly for the adaptive out-of-step protection. Therefore, the scope is focused on the dynamic in the first swing time scale (0.5 to 0.8 Hz) [2]. In this time scale, the speed voltage E_q is relatively constant because of the large field circuit time constant (constant flux linkage situation). Transient reactance x'_d and inertia constant H will not be affected by the inclusion of the sophisticated electromagnetic dynamic model. Therefore, a classical model (speed voltage behind a transient reactance) is adequate for the purpose of this investigation. The choice of sampling frequency is important. In this chapter, 120 Hz is used as recommended for 60 Hz system in the recent IEEE Standard for Synchrophasor Measurements for Power System C37.118.1-2011 [8].

Fig. 4.2 illustrates measured signals from Generator #4 terminal bus. Fig. 4.2a-4.2d display the measured data of V_g, θ_g, P_g, and Q_g, respectively. All other generators are also measured. As described in Section 4.3, V_g and P_g are used as the input, while θ_g and Q_g are used as the measurements for the UKF. The proposed method is applied to the whole set of measured data and the parameters are estimated. The initial parameters for UKF algorithm used in this chapter are

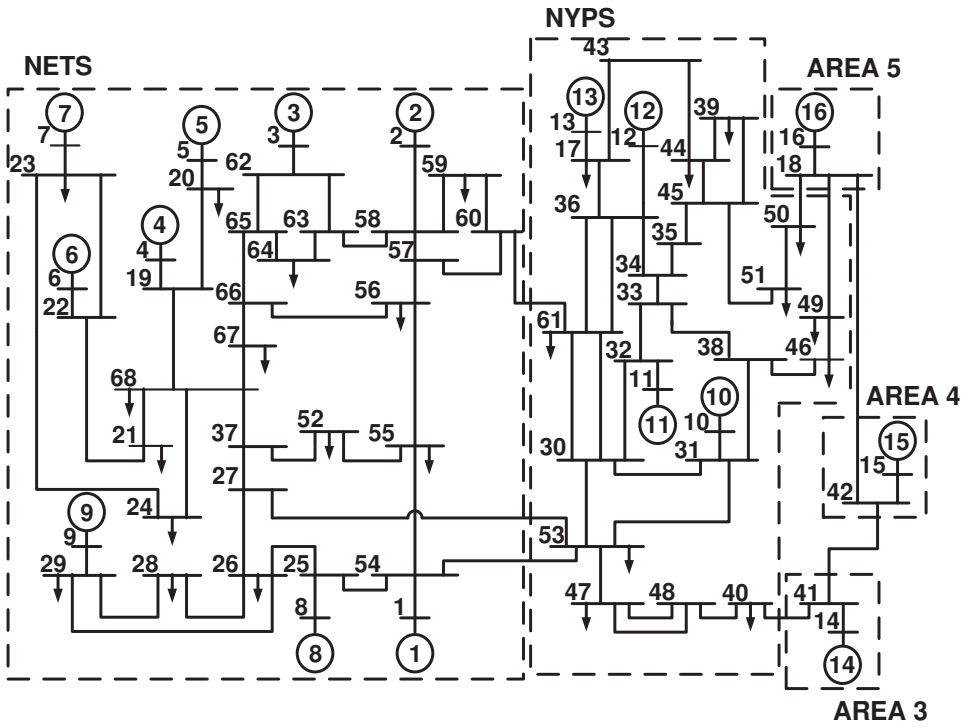

Figure 4.1: 16-machine 68-bus test system model

described as follows:

$$\begin{aligned}
\boldsymbol{X}_0 &= [\boldsymbol{x}_0 \;\; \boldsymbol{\psi}_0 \;\; \boldsymbol{v}_0]^\top \\
&= [\delta_0 \;\; \omega_0 \;\; E_{q_0} \;\; x'_{d_0} \;\; H_0 \;\; 0 \;\; 0]^\top \\
&= \left[\frac{\pi}{2} \;\; 1.0 \;\; 1.0 \;\; 0.5 \;\; 5.0 \;\; 0 \;\; 0\right]^\top && \text{(4.21a)} \\
\boldsymbol{P}_{\boldsymbol{x}_0} &= diag\,\{[1 \;\; 1]\} && \text{(4.21b)} \\
\boldsymbol{Q}_{\boldsymbol{\psi}_0} &= diag\,\{[1 \;\; 1 \;\; 1]\} && \text{(4.21c)} \\
\boldsymbol{Q}_{\boldsymbol{v}_0} &= diag\left\{\left[1 \times 10^{-4} \;\; 1 \times 10^{-3}\right]\right\} && \text{(4.21d)} \\
\boldsymbol{P}_{\boldsymbol{X}_0} &= diag\,\{[\boldsymbol{P}_{\boldsymbol{x}_0} \;\; \boldsymbol{Q}_{\boldsymbol{\psi}_0} \;\; \boldsymbol{Q}_{\boldsymbol{v}_0}]\} && \text{(4.21e)} \\
\boldsymbol{R} &= diag\left\{\left[1 \times 10^{-4} \;\; 1 \times 10^{-3}\right]\right\} && \text{(4.21f)}
\end{aligned}$$

The values of initial parameters influence the convergence rate of the proposed method. The closer the values of initialised parameters to the actual values of the parameters, the faster is the convergence of the proposed method in estimating the dynamic model parameters of the system. However, the work presented in this chapter assumes that the initial parameters are unknown. Therefore, the proposed method is initialised at the same values as shown in 4.21 for all generators to

provide an unbiased assumption in estimating the dynamic models parameters using UKF. The initial values for the covariance matrix of $\boldsymbol{P}_{\boldsymbol{x}_0}$ and $\boldsymbol{Q}_{\boldsymbol{\psi}_0}$ are not important. It will be updated throughout the UKF iteration process and its value will become zero if the algorithm has converged. On the hand, the values of $\boldsymbol{Q}_{\boldsymbol{v}_0}$ and $\boldsymbol{R}$ represent the process and measurement noise covariance matrix and their values are assumed to be known. Fig. 4.3 shows the results of the dynamic model parameter estimation for the 16-machine 68-bus test system model.

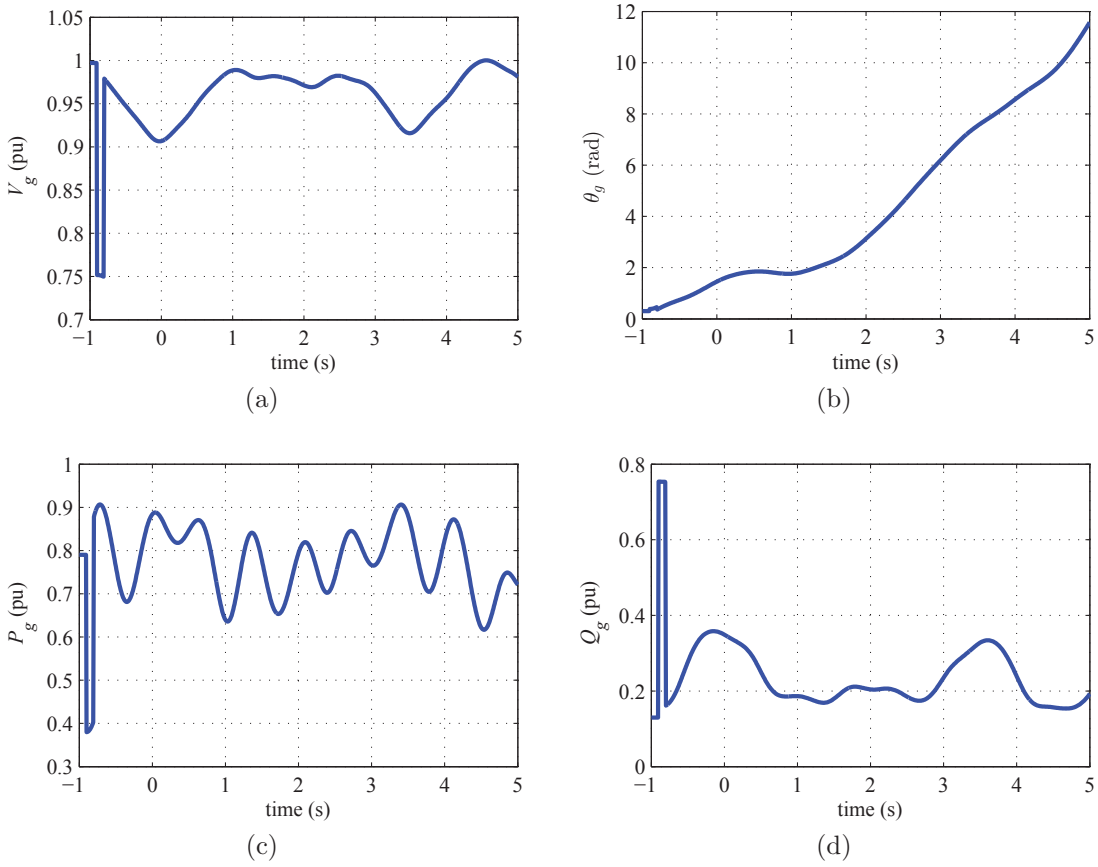

Figure 4.2: Generator #4 measured data

Fig. 4.3a, 4.3b and 4.3c display the convergence of E_q, x'_d and H, respectively. The dashed line indicates the convergence of estimated parameters obtained using the proposed method, while the solid line represents the actual parameters of the test system. In this application, the parameters are assumed to be unknown. The initial parameters were set arbitrarily. All the results in the figure converged to their actual value. E_q is initialised arbitrarily at 1.0 pu. After the first iteration, E_q increased before it became constant at 1.0660 pu after 1.0 s. On the other hand, the initial value of x'_d is set arbitrarily to 0.5 pu. After 1.0 s, x'_d has converged

to 0.3081 pu and finally converged to its actual value of 0.2995 pu after 4.5 s. Similar observation can be made for H, where the value is initially set at 5.0s and consequently converged at 4.1629 s after 1.0 s.

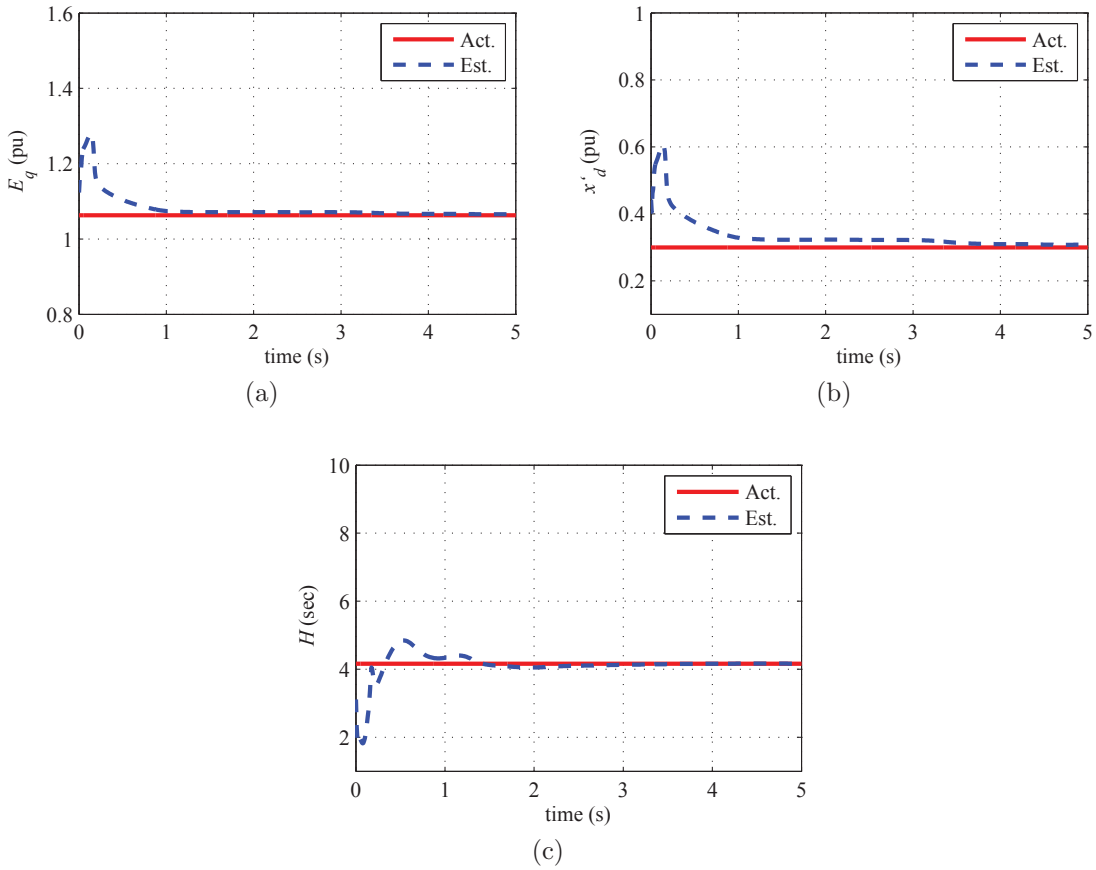

Figure 4.3: Genarator #4 parameter estimation

Fig. 4.4 shows the estimation of the rotor angle δ for Generator #4 and its corresponding error of estimation. In addition, Fig. 4.5 shows the estimation of rotor speed ω for Generator #4 and its corresponding error of estimation. From Fig. 4.4a, the estimated δ matches very well with the actual δ of the generator. However, there are discrepancies between the estimated δ with the actual δ before 1.0 s of the UKF convergence as observed in Fig. 4.4b. These discrepancies are expected to be in the analysis because the estimated parameters do not match with the actual parameters before 1.0 s of the UKF convergence as demonstrated in Fig. 4.3. On the other hand, as shown in Fig. 4.5b, the error between the estimated ω and the actual ω is small as compared to the error in the δ estimation. This is because the initial condition of ω estimation, which is arbitrarily set for all generators at 1.0 pu, is set close to the actual ω of the generator. Therefore, the

convergence of the estimated ω is relatively fast as compared to the convergence of the estimated δ of the generator.

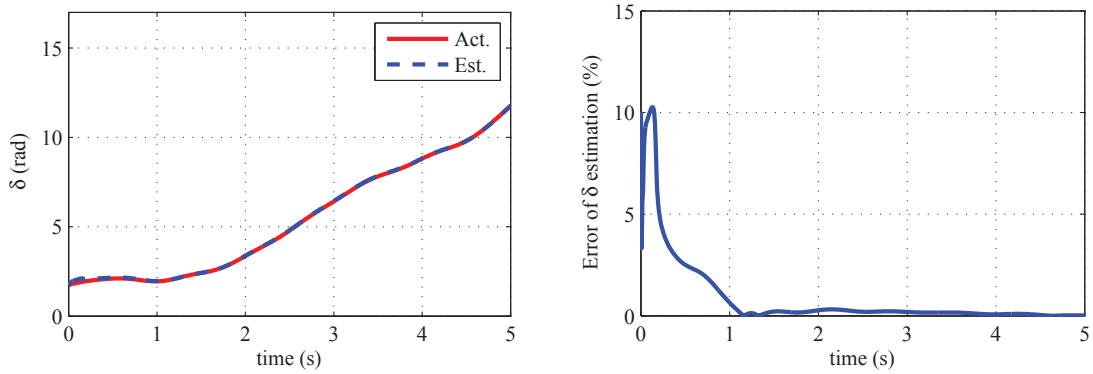

(a) (b)

Figure 4.4: Generator #4 a) δ estimation b) error of δ estimation

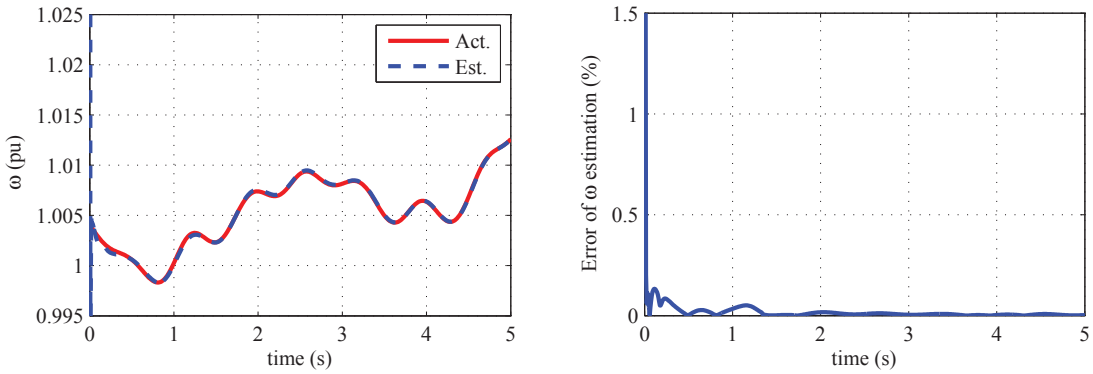

(a) (b)

Figure 4.5: Generator #4 a) ω estimation b) error of ω estimation

The discussions of the results for all other generators in the test system model are relatively similar with the discussions of the results for Generator #4. Table 4.1 summarises the results of the dynamic model parameter estimation for 16-machine 68-bus test system model. E_q, x'_d and H for all machines were initialised to 1.0 pu, 0.5 pu and 5.0 s, respectively. From the table it can be observed that the estimated parameters are very close to the actual value of the dynamic model parameters for all machines. The maximum percentage errors in estimation for E_q, x'_d and H are 0.29%, 3.26% and 0.21%, respectively. This indicates that the results obtained using dynamic model parameter estimation technique proposed in this chapter are accurate and consistent for all machines in a large interconnected power system context.

Table 4.1: Comparison between the actual and estimated parameters

i	${E_q}^{act}$ (pu)	${E_q}^{est}$ (pu)	${x'_d}^{act}$ (pu)	${x'_d}^{est}$ (pu)	H^{act} (s)	H^{est} (s)
1	1.1867	1.1871	0.2480	0.2485	3.4000	3.4030
2	1.1176	1.1194	0.4253	0.4296	4.9494	4.9540
3	1.1232	1.1250	0.3831	0.3868	4.9623	4.9673
4	1.0629	1.0660	0.2995	0.3081	4.1629	4.1627
5	1.1227	1.1224	0.3600	0.3595	4.7667	4.7769
6	1.1611	1.1607	0.3543	0.3534	4.9107	4.9303
7	1.1145	1.1144	0.2990	0.2987	4.3267	4.3434
8	1.0489	1.0485	0.3538	0.3519	3.9150	3.9221
9	1.0932	1.0930	0.4872	0.4867	4.0365	4.0427
10	1.0307	1.0305	0.4868	0.4846	2.9106	2.9133
11	1.0093	1.0093	0.2531	0.2536	2.0053	2.0068
12	1.1527	1.1523	0.5525	0.5515	5.1791	5.1827
13	1.0398	1.0405	0.3345	0.3454	4.0782	4.0786
14	1.0030	1.0029	0.2850	0.2837	3.0000	3.0004
15	1.0023	1.0022	0.2850	0.2781	3.0000	2.9974
16	1.0233	1.0231	0.3590	0.3572	4.4500	4.4460

For all generators the estimated parameters are declared 1.0 s following the starts of the UKF convergence. This value is set based on heuristic assumption by considering the maximum error of the estimated parameters and the speed of convergence for all generators. The maximum error of the estimated parameters for all the generators using this stopping criterion is equal to 3.26%. For the application of a recursive estimation method such as UKF, this assumption is viable for this study [68], considering the complexity of the test system model used in this study and the requirements (maximum error and speed of estimation) to declare the value of the estimated parameters. For a more complex problem, a comprehensive technique such as the backward error approach can be used to determine the stopping criterion for the method as reported in [68].

The proposed method is able to estimate the dynamic model parameters of the systems without prior knowledge of system model. The UKF method requires a time window of 1.0 s to estimate the parameters accurately. Therefore, the method requires 120 iterations to precisely estimate the parameters using the measured data sampled at every 8.33 ms. The computation speed of the UKF method recorded in MATLAB Simulink environment using Intel Xeon L5520 2.26 GHz quad-core processor with 12 GB DDR3 RAM platform is 281.2 μs per iteration. Hence, considering the time windows required for estimation and the

computation time of UKF, it only requires 1.0337 s for the proposed method to precisely estimate E_q, x'_d and H at real time. Typically, a power swing oscillates with the frequency of 0.5-0.8 Hz [2], which gives a time windows of 1.25-2.0 s to analyse the oscillation as it develops. Thus, the speed of estimation using the proposed method is sufficiently fast for adaptive out-of-step protection application which focuses only on the first few swings of the system.

4.5 Comparison and performance robustness

In this section, the accuracy of the dynamic model parameters estimated using the proposed method is compared with the results obtained using the EKF approach [57, 58]. The performances of the proposed method and the EKF method are also evaluated in the presence of noise in the measured signals. Using identical operating condition, the 16-machine 68-bus test system model is used for this evaluation.

4.5.1 Parameter estimation using EKF

The details of the EKF method for dynamic model parameter estimation are reported in [57, 58] and are briefly discussed here to extend the discussion of the idea presented in this chapter. The EKF is formulated as a two-step prediction-correction process. The prediction step is a time update using the discretized differential equations as follows:

$$\delta_k = \delta_{k-1} + (\omega_{k-1} - \omega_0)\,\omega_s \triangle t \tag{4.22a}$$

$$\omega_k = \omega_{k-1} + \frac{\triangle t}{2H}\left[P_m - \frac{E_{q_{k-1}} V_{g_{k-1}}}{x'_{d_{k-1}}} \sin\left(\delta_{k-1} - \theta_{g_{k-1}}\right)\right] \tag{4.22b}$$

$$E_{q_k} = E_{q_{k-1}} \tag{4.22c}$$

$$x'_{d_k} = x'_{d_{k-1}} \tag{4.22d}$$

$$H_k = H_{k-1} \tag{4.22e}$$

The discretized differential equations in (4.22) predict the state and measurement variables of the next time step using the estimated values of the state and measurement variables of the previous time step. E_q, x'_d and H are the unknown

parameters that need to be estimated. Apart from the state variables, the process also estimates the priori error covariance matrix corresponding to the state variables. Consequently, the estimated measurement is calculated using the following equations:

$$P_{g_k} = \frac{E_{q_k} V_{g_k}}{x'_{d_k}} \sin\left(\delta_k - \theta_{g_k}\right) \tag{4.23a}$$

$$Q_{g_k} = \frac{-{V_{g_k}}^2 + E_{q_k} V_{g_k} \cos\left(\delta_k - \theta_{g_k}\right)}{x'_{dk}} \tag{4.23b}$$

The next step involves the calculation of the Kalman gain, which corrects the error of the estimated state variables based on the discrepancy between the estimated and the actual measurement. The following set of equations summarized the prediction-correction process of EKF.

Prediction:

$$\boldsymbol{x}_k^- = f\left(\boldsymbol{x}_{k-1}, \boldsymbol{u}_{k-1}, 0\right) \tag{4.24a}$$

$$\boldsymbol{P}_k^- = \boldsymbol{A}_k \boldsymbol{P}_{k-1} {\boldsymbol{A}_k}^\top + \boldsymbol{W}_k \boldsymbol{Q}_{k-1} {\boldsymbol{W}_k}^\top \tag{4.24b}$$

Correction:

$$\boldsymbol{K}_k = \boldsymbol{P}_k^- {\boldsymbol{H}_k}^\top \left(\boldsymbol{H}_k \boldsymbol{P}_k^- {\boldsymbol{H}_k}^\top + \boldsymbol{V}_k \boldsymbol{R}_k {\boldsymbol{V}_k}^\top\right)^{-1} \tag{4.24c}$$

$$\boldsymbol{x}_k = \boldsymbol{x}_k^- + \boldsymbol{K}_k \left[\boldsymbol{y}_k - h\left(\boldsymbol{x}_k^-, \boldsymbol{u}_{k-1}, 0\right)\right] \tag{4.24d}$$

$$\boldsymbol{P}_k = \left(\boldsymbol{I} - \boldsymbol{K}_k \boldsymbol{H}_k\right) \boldsymbol{P}_k^- \tag{4.24e}$$

where,

$$\boldsymbol{A}_k = \frac{\partial \boldsymbol{f}\left(\boldsymbol{x}_{k-1}, \boldsymbol{u}_{k-1}, 0\right)}{\partial \boldsymbol{x}}, \; \boldsymbol{W}_k = \frac{\partial \boldsymbol{f}\left(\boldsymbol{x}_{k-1}, \boldsymbol{u}_{k-1}, 0\right)}{\partial \boldsymbol{w}},$$
$$\boldsymbol{H}_k = \frac{\partial \boldsymbol{h}\left(\boldsymbol{x}_{k-1}, \boldsymbol{u}_{k-1}, 0\right)}{\partial \boldsymbol{x}}, \quad \boldsymbol{V}_k = \frac{\partial \boldsymbol{h}\left(\boldsymbol{x}_{k-1}, \boldsymbol{u}_{k-1}, 0\right)}{\partial \boldsymbol{w}}$$

Using this process, the unknown parameters E_q, x'_d and H, along with other state variables will be updated at every time step. If the EKF process converged, E_q, x'_d and H estimates will approach their actual values.

4.5.2 Comparison

In order to evaluate the performance of the proposed method, the dynamic model parameters estimated using the proposed method are compared with the results obtained using EKF. For this evaluation, 16-machine 68-bus test system model is used to simulate the measurement of V_g, θ_g, P_g and Q_g for every generator sampled at 120 Hz. The disturbance considered for this evaluation is similar to the disturbance considered in Section 4.4. Using identical initialization of the parameters, the estimation of E_q, x'_d and H, for Generator #4 obtained using UKF and EKF is illustrated in Fig. 4.6.

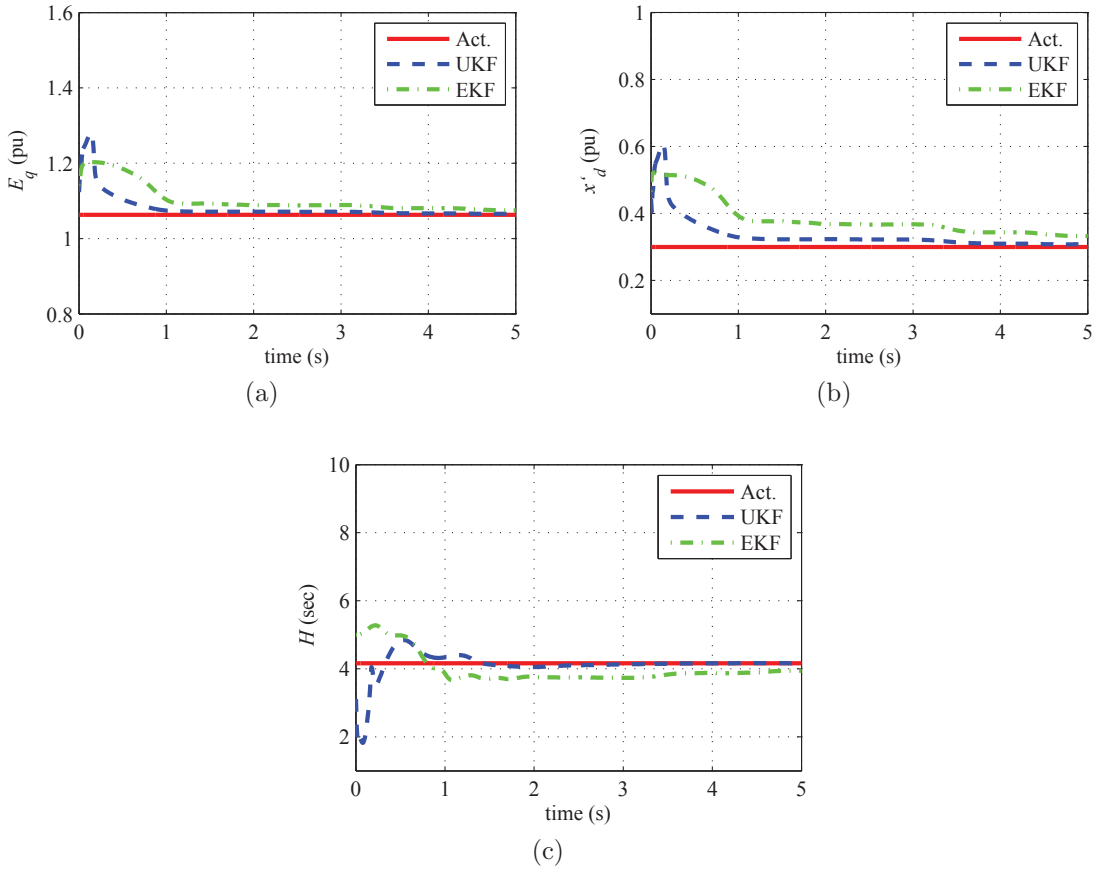

Figure 4.6: The comparison of UKF and EKF estimation for Generator #4

The results in Fig. 4.6 show that E_q, x'_d and H estimated using UKF and EKF converged to its actual value of 1.1250 pu, 0.3868 pu and 4.1627 s, respectively. This implies that both UKF and EKF are able to estimate the dynamic model parameters in the system. However, it is observed from the results that the proposed method shows better performance in estimating the parameters in

Generator #4, especially for the estimation of x'_d. The EKF requires about 3.5 s while the proposed method only requires about 1.0 s to converge to its actual value of x'_d. This is because the proposed method has a better approximation of the nonlinear process in each iteration compared to the EKF approach.

It is also necessary to compare the computational speed of UKF and EKF, formulated to estimate the dynamic model parameters. The computational speed of EKF is 497.6 μs per iteration while the computational speed of UKF is 281.2 μs per iteration to estimate E_q, x'_d and H. The difference in computational speed of EKF and UKF is related to the computational load at each iteration for both methods. The EKF algorithm requires the updating of Jacobian matrix at every step of computation to estimate E_q, x'_d and H. On the other hand, the UKF method does not need the calculation of the Jacobian matrix. This finding is consistent with the discussion reported in [69]. This implies that the EKF consumes more computing power compared to the proposed method in estimating the dynamic model parameters of the system.

4.5.3 Performance robustness

4.5.3.1 Performance under noise

It is well known that the presence of noise in the data influences the quality of any measurement-based method. This subsection evaluates the performance of the proposed technique in the presence of noise in the measured signals. For this evaluation, the measured data illustrated in Fig. 4.2 is added with white Gaussian noise and the proposed technique is applied on this data to estimate E_q, x'_d and H of the generator. The presence of noise affects the quality of the PMU measurements. It is assessed by the Total Vector Error (TVE) of the PMU measurements described as follows:

$$\text{TVE}\,(n) = 100 \times \sqrt{\frac{\left[\hat{X}_r\,(n) - X_r\,(n)\right]^2 + \left[\hat{X}_i(n) - X_i(n)\right]^2}{\left[X_r\,(n)\right]^2 + \left[X_i\,(n)\right]^2}} \tag{4.25}$$

According to [8, 15] PMU must maintain TVE less than 1% under steady-state condition and TVE less than 3% under dynamic condition. Since the scope of this thesis covers the steady state, as well as the dynamic aspect of the study system, the TVE of 3% is considered. The plots of the data are given in Fig. 4.7a-4.7d

represent V_g, θ_g, P_g, and Q_g for Generator #4. Fig. 4.8 displays the result obtained from the application of the UKF method using the measured signals with noise.

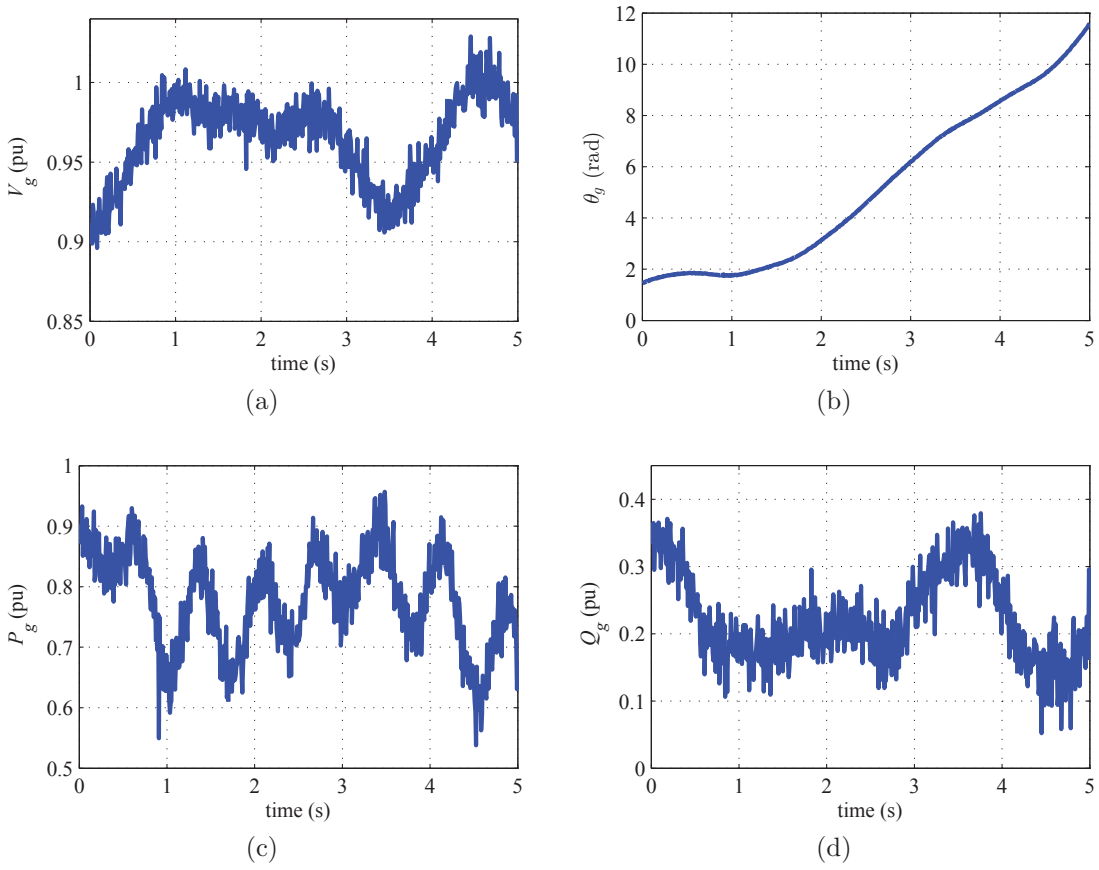

Figure 4.7: Generator #4 measured data with noise

The estimation of E_q, x'_d and H using the measured data with noise are illustrated in Fig. 4.8a-4.8c. The green lines represent the 99% confidence interval of the estimated parameters. The results clearly show that the UKF method has a fast convergence rate even with the presence of noise in the measured data. All parameters converged to the actual value in about 1.0 s. E_q, x'_d and H converged to 1.0627 pu, 0.2998 pu and 4.2278 s, respectively. It is also observed that the actual values of the parameters lie between the upper and lower bounds for the 99% confidence interval of the estimated parameters.

The proposed algorithm is applied to all machines in the test system model and the results are shown in Table 4.2. In Table 4.2, results obtained using the UKF method are validated by comparing the estimated results with the actual value of the dynamic model parameters. As depicted in the table, the estimated

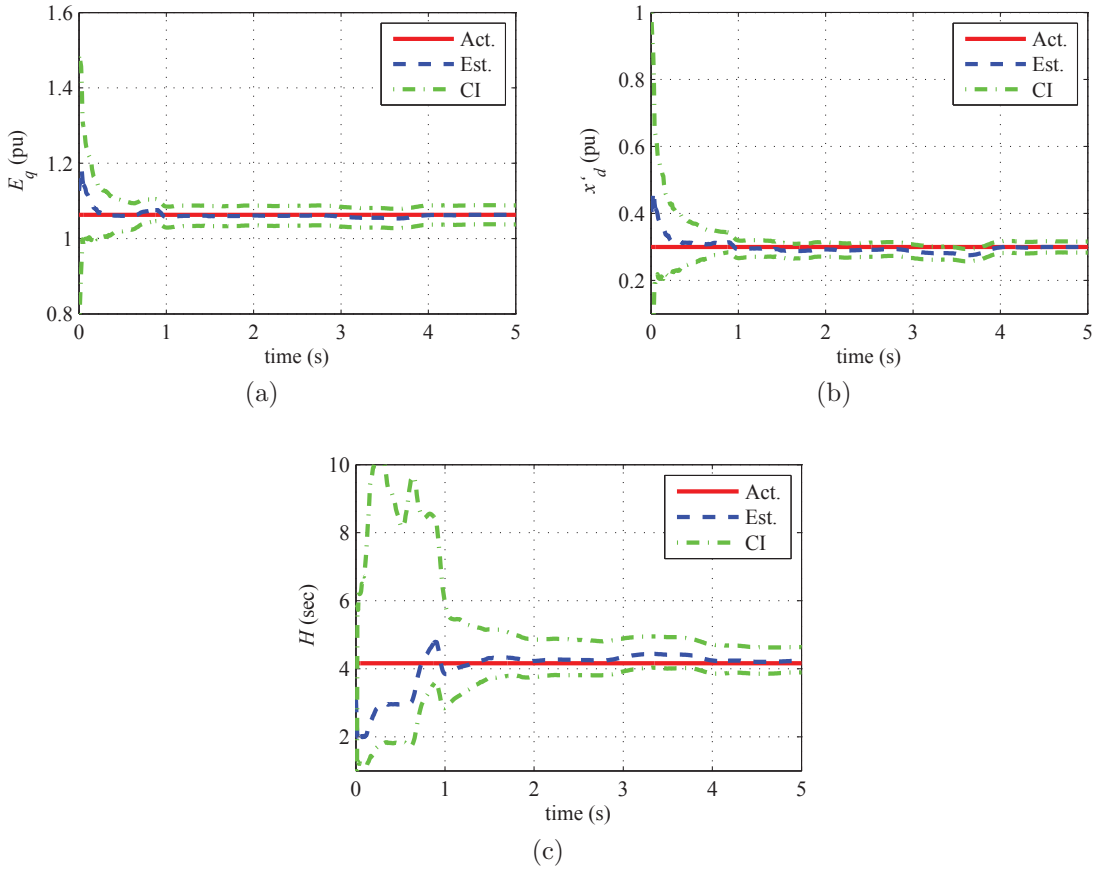

Figure 4.8: Generator #4 parameter estimation in the presence of noise

value of E_q, x'_d and H are very close with the actual value of the dynamic model parameters, even with the presence of noise in the measured signals.

4.5.3.2 Comparison with EKF in the presence of noise

Both UKF and EKF require measured signals from PMU to estimate E_q, x'_d and H of the system. It is worthwhile to assess the performance of UKF and EKF in the presence of noise in the measured signals. In this investigation, the UKF and EKF are applied to the measured signals with TVE of 3% illustrated in Fig. 4.7. The convergence of E_q, x'_d and H using both methods are plot in Fig. 4.9a-4.9c, respectively.

The results displayed in Fig. 4.9 show that both methods are able to estimate E_q accurately using the measured signals with noise. The EKF method requires about 5.0 s while the proposed method only requires about 0.2 s to estimate E_q accurately. The estimation of x'_d and H using the EKF approach shows

Table 4.2: Comparison between the actual and estimated parameters (measured data with noise)

i	${E_q}^{act}(pu)$	${E_q}^{est}(pu)$	${x'_d}^{act}(pu)$	${x'_d}^{est}(pu)$	H^{act} (sec)	$H^{est}(sec)$
1	1.1867	1.1803	0.2480	0.2354	3.4000	3.5498
2	1.1176	1.1207	0.4253	0.4335	4.9494	5.0670
3	1.1232	1.1158	0.3831	0.3668	4.9623	5.0914
4	1.0629	1.0627	0.2995	0.2998	4.1629	4.2278
5	1.1227	1.1234	0.3600	0.3558	4.7667	4.6444
6	1.1611	1.1669	0.3543	0.3714	4.9107	4.7569
7	1.1145	1.1117	0.2990	0.2997	4.3267	4.3902
8	1.0489	1.0529	0.3538	0.3659	3.9150	3.7245
9	1.0932	1.0858	0.4872	0.4633	4.0365	4.2310
10	1.0307	1.0345	0.4868	0.5073	2.9106	3.0081
11	1.0093	1.0091	0.2531	0.2556	2.0053	2.0931
12	1.1527	1.1485	0.5525	0.5456	5.1791	5.1894
13	1.0398	1.0430	0.3345	0.3618	4.0782	4.0552
14	1.0030	1.0034	0.2850	0.3025	3.0000	2.9742
15	1.0023	1.0024	0.2850	0.3056	3.0000	3.0075
16	1.0233	1.0218	0.3590	0.3559	4.4500	4.5790

that the presence of noise in the measured data influences the accuracy of the dynamic model parameter estimation technique. The EKF method shows limitation in estimating x'_d and H using the measured signals with noise. However, the proposed method is able to estimate x'_d and H even with the presence of noise in the measured data. This may be due to the fact that the approach proposed in this chapter accurately approximate the posterior mean and covariance up to the third order of the Taylor series expansion for any non-linear system while the EKF method only achieved first-order accuracy [65]. The results imply that the proposed method outperforms EKF in estimating the dynamic model parameter in the system, particularly in the presence of noise in the measured data. These attributes are important for any data-driven estimation tools as the presence of the noise in measured data is inevitable.

4.5.3.3 Performance in coloured noise

Coloured noise covers a wide range of intensities and bandwidths for a variety of flow fluctuation during power system operation [70]. Since it may be present in the measured data, hence influencing the accuracy of any data-driven method,

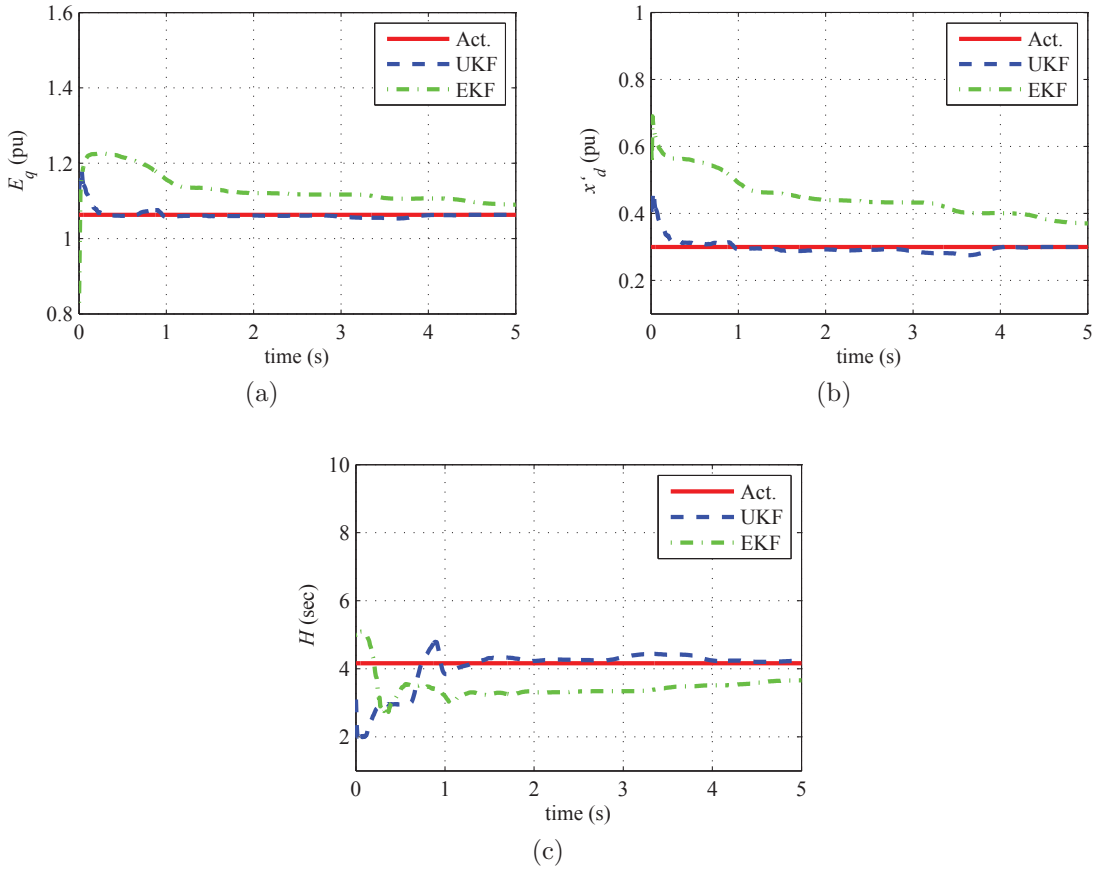

Figure 4.9: The comparison of UKF and EKF in the presence of noise

it is necessary to assess the operation of the proposed method in the presence of coloured noise in the measured signals. The coloured noise used for this evaluation is generated by filtering the white Gaussian noise used to produce signals in Fig. 4.7 through a low pass finite impulse response (FIR) filter of order 31 with normalized cut-off frequency of 0.5 [71]. The measured signals illustrated in Fig. 4.2 are added with the coloured noise and the UKF method is applied to estimate the dynamic model parameters of the system. Fig. 4.10 depicts the UKF estimation trace of E_q, x'_d and H in the presence of coloured noise in the measured data. For the purpose of comparison, the UKF estimation in the presence of white noise is also plotted in the same figure.

From the figure, it is observed that the UKF estimation of E_q, x'_d and H in the presence of white and coloured noise demonstrate good convergence to the actual value of parameters. The performance of the proposed method in the presence of coloured noise is similar to that of the proposed method in the presence of white Gaussian noise. Therefore, this implies that the proposed method is able

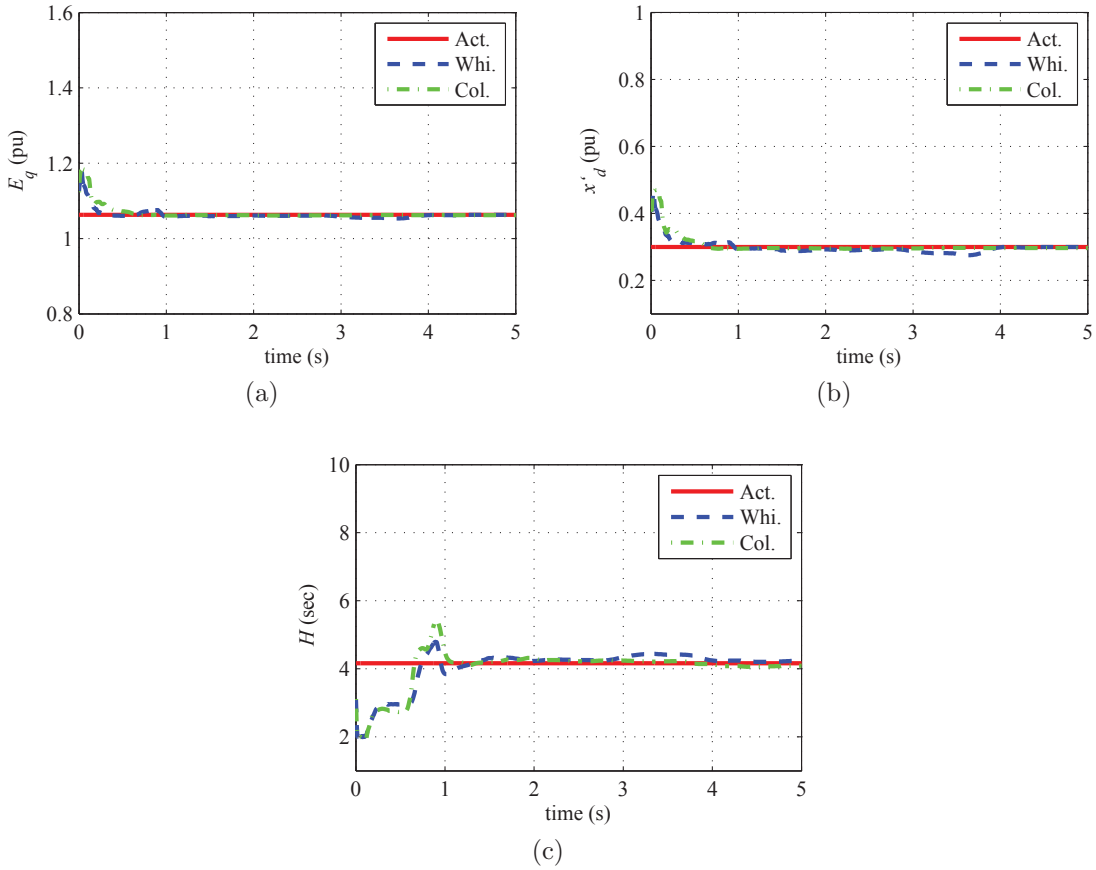

Figure 4.10: The UKF estimation in the presence of white and coloured noise

to estimate E_q, x'_d and H of the system in the presence of coloured noise in the measured data. This is an important feature for any data-driven method as the fluctuation of power flows is inevitable during power system operation.

4.6 Model validation

In this study, the results obtained in Table 4.1 and 4.2 are substituted into the 16-machine 68-bus test system model. Three cases with different types of disturbances were considered in this study. The disturbances considered in this analysis are as follows,

Case 1 - Fault at Bus #61, line 61-30 is removed to clear the fault after 50 ms,

Case 2 - Fault at Bus #67, line 67-68 is removed to clear the fault after 100 ms,

Case 3 - Fault at Bus #46, line 38-46 is removed to clear the fault after 100 ms.

Fig. 4.11 displays the response of the systems with this study.

For all cases, the blue, red, green, and magenta lines represent the response from the test system model using the actual parameters, the estimated parameters, the estimated parameters using measured data with noise, and the actual parameters with 30% error, respectively. The response of the generator represented by the magenta line is included in the graphs to demonstrate the impact of the inaccurate dynamic model parameters to the quality of the test system model. The quality of estimated parameters is evaluated by the accuracy and consistency of the dynamic model represented using the estimated parameters [57]. The dynamic model is accurate if it can adequately capture the relevant dynamics for a single event. A consistent dynamic model means that the dynamic model can replicate the generator's dynamic responses for multiple disturbance events. The results in Fig. 4.11 show that, for all cases, there are significant discrepancies between the responses of the test system model using the actual parameters with 30% error with the response of the test system model using the actual parameters. These discrepancies of the response from the dynamic model representation may lead to an inappropriate control decision of the protection system. There are small differences between the response of the dynamic model represented by the estimated parameters using the proposed method with the response of the dynamic model represented using the actual parameters. This is true for all cases considered in this study. This indicates that the result obtained using the proposed method is able to represent the dynamic response of the system accurately and consistently.

4.7 Chapter summary

A measurement-based dynamic model parameter estimation for power system has been proposed. The approach is based on the application of the augmented unscented Kalman filter (UKF) technique to estimate the dynamic model parameters from wide-area voltage magnitude, voltage angle, real power and reactive power signals. In the proposed method, the unknown states (rotor angle and speed), the unknown parameters (inertia constant, transient reactance and internal voltage)

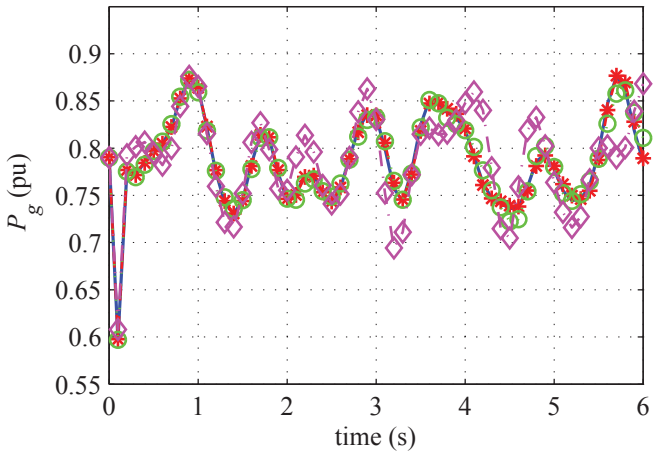

(a)

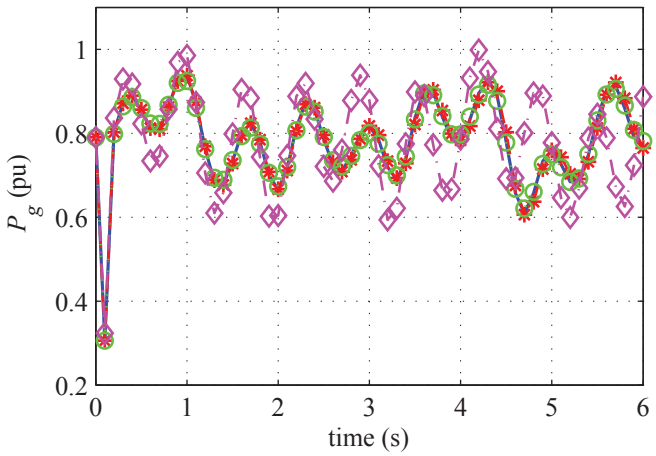

(b)

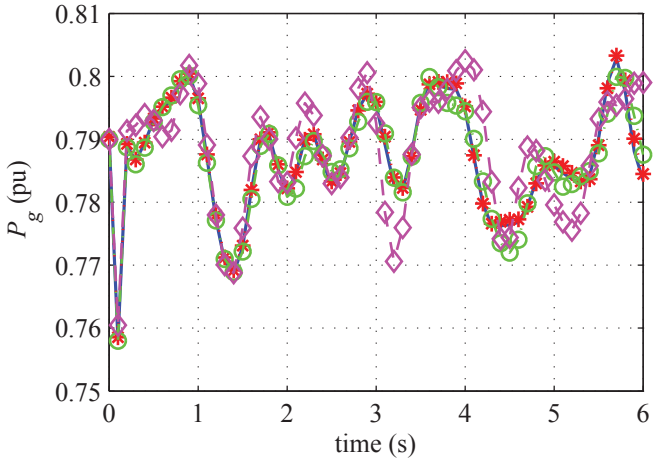

(c)

Figure 4.11: Generator #4 model validation a) Case 1 b) Case 2 c) Case 3

and the process noise covariance are augmented into a single higher-dimensional state vector. Subsequently, the proposed UKF method is used on the augmented state vector to estimate the dynamic model parameters of the system.

The accuracy of the estimation is validated by comparing the estimated results with the actual parameters of the system. The presence of noise always affects the performance of any data driven method. Nevertheless, the UKF method accurately estimates the dynamic model parameters even with the presence of noise in measured data. Results demonstrate that the proposed method outperforms EKF in estimating the dynamic model parameter in the system, particularly in the presence of noise in measured data. The method is simple, fast and does not require *a-priori* details of the system information. Finally, estimating the value of the dynamic mode parameters in real time is essential to ensure appropriate operation of power system protection. This will be discussed further in the following chapter.

Chapter 5

Adaptive protection against power swing

This chapter takes adaptive out-of-step relay for generator protection as an application example of using the coherency identification technique using ICA elaborated in Chapter 3 and the dynamic model parameters estimation method reported in Chapter 4. Following a severe contingency in the system, the generators may lose their synchronism with the system in the event of a power swing. An out-of-step protection scheme is engineered to detect this condition and provide appropriate control action to mitigate the impact of the disturbance. The following sections discuss the nature and the necessity for out-of-step generator protection, reviews basic transient stability concepts, describes the out-of-step impedance characteristics typical of large generators connected to high-voltage transmission systems, and presents various relaying schemes that are used for generator out-of-step protection. An adaptive out-of-step protection system for generator out-of-step protection is developed. The method is based on the application of extended equal area criterion (EEAC) which requires identification of coherent groups of generators and dynamic model parameters estimation of the system to represent the dynamic behaviour of a multi-machine system.

5.1 Introduction

Conventionally, power system protection relays operate in a predetermined and set manner. Typically, the relays are set biased towards dependability. These

protection systems act as dormant sentinels, protecting the network using local voltage and current measurements to detect abnormal operating conditions in the system. Experiences shows that rigid relay settings may mal-operate under abnormal stressed operating conditions. This is due to the fact that the implicit system assumptions incorporated in the relay settings are no longer suitable under stressed operating conditions. This conjecture is corroborated with the fact that a total of 14 impedance relays mal-operated in the 2003 USA/Canada Northeastern blackout [1]. It is obvious that unnecessary line tripping further magnified the impact of the disturbance to the system. Therefore, it is crucial to adapt the protection setting to suit the current operating condition of the system. It is understood that not every protection system is suitable for redesign to be adaptive. The scope of adaptive protection is proposed, mainly for non-instantaneous protection. Therefore, the protection scheme for the system stability enhancement such as an out-of-step relay is an ideal candidate for adaptive relaying. Recent research on adaptive out-of-step protection systems has been reported in the literature [72, 73, 74, 75]. Although the concept of adaptive relaying offers substantial rewards in improving the network reliability, protection engineers have been reluctant to implement the concept of adaptive relaying in practice. Therefore, it is necessary to find an option to compromise with the demand from industry as well as benefiting from the adaptive relaying philosophy.

5.2 Transient power swing: overview

It is essential to review the concept of transient power swing to form a concrete understanding on out-of-step phenomena in power systems. A slow-clearing protection system in response to a fault in the transmission network may lead to the transient instability to the system. When a fault on the transmission system is not cleared rapidly, especially one that occurred close to the generating plant, it extends the period of unbalance between the mechanical and electrical generator outputs. The transmission line protection system is engineered to operate faster than the period for a generator to remain synchronized with the system. However, protection system failures which resulted in slow-clearing transmission system faults may happen during system operation [1]. Therefore, generators need to be protected from damage that is caused by the delayed operation of the

protection system in the transmission network. It is generally accepted that loss-of-synchronism protection at the generator is necessary to avoid machine damage.

Fig. 5.1 illustrates a typical power substation with a generator and a short circuit on a transmission line near the substation. The high fault current experienced during short circuit is predominantly reactive in nature. During the fault, E_G drops close to zero, therefore there is almost no real power transferred to the system. However, the generator mechanical turbine power P_M remains relatively constant during the short circuit. The resulting unbalance between mechanical P_M and electrical power P_E manifests as generator acceleration, increasing its voltage phase angle δ_G, with respect to the system phase angle δ_S. The generator acceleration rate depends on its inertia and initial pre-fault condition. If the fault in the transmission system is not cleared swiftly enough, the generator phase angle will advance until the machine goes out of synchronism with the rest of the system.

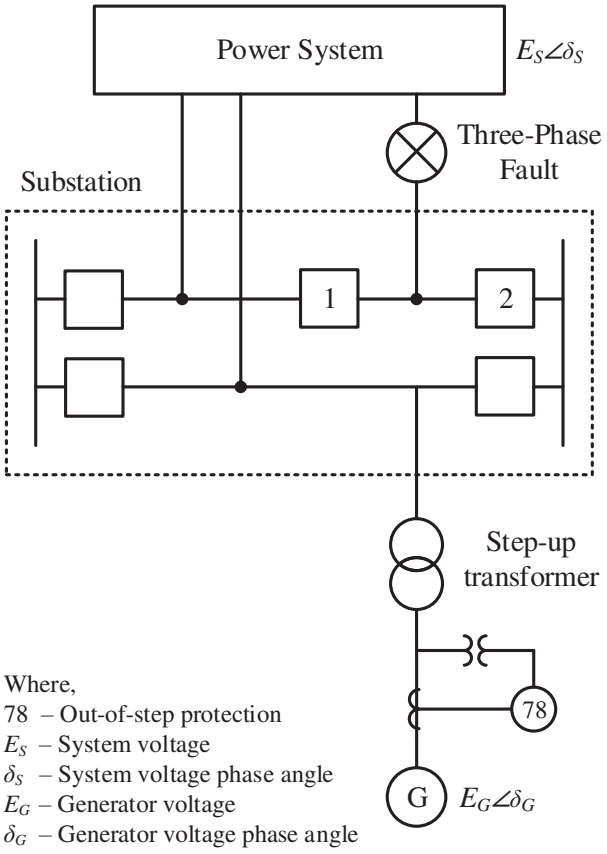

Figure 5.1: Typical generating substation single-line diagram

The maximum allowable time for the fault to persist on the system is called critical clearing time (CCT) and its corresponding angle separation between the

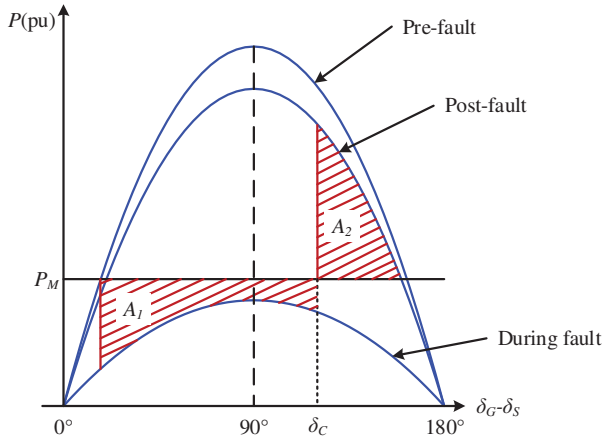

Figure 5.2: Power angle analysis

generator and the system is called critical switching angle (CCA). These two important terms can be determined using equal area criterion method as illustrated in Fig. 5.2. The half-cycle sinusoidal curves in the figure represent the power transfer equation of the system for two different operating conditions: pre-fault and post fault. The CCA δ_C is the angle when the area under the curve A_1 is equal to A_2. This is when the generator is at the point of losing its synchronism with the rest of the system. In the absence of detailed studies, many users establish the maximum instability angle at 120°. Because of the dynamic nature of the generator to recover during fault conditions, the 120° angle is larger than the 90° instability point for steady-state instability conditions. The time corresponds to δ_C is the CCT for the generator. If the fault clearing exceeds this angle, the generator will lose synchronism by "slipping a pole." A pole slipping condition causes high currents and voltages in the generator winding and high levels of transient shaft torques. Consequently, the generator must be tripped under this condition to avoid shaft torque damage.

Most power systems books and numerous papers describe the development of the concept of equal area criterion in detail. In the event of unstable power system oscillation, one equivalent generator rotates at a relatively different speed from the rest of the system. This condition is referred to as a loss-of-synchronism or an out-of-step condition. If such an event occurs in the system, it is necessary to separate these two asynchronous systems in a controlled manner using an out-of-step protection system (IEEE device number 78). It is also important that the distance relays on the transmission system do not operate under system oscillations

as the impedance locus might penetrate into the distance relay characteristic in the event of power swing.

5.3 Out-of-step characteristics

In practice, a general approach used to detect out-of-step phenomena following a disturbance is by monitoring the impedance trajectory variation at the generator terminal or HV terminals of the generator step up transformer using an impedance relay. The trajectory of the impedance swing depends on the dynamic behaviour of the system, level or loading of the generator, along with the type of disturbance that initiated the swing. Therefore, to extend the discussion on the out-of-step phenomena, consider a simple two sources system connected by a transmission line Z_L as displayed in Fig. 5.3. The sources are assumed to be represented by voltages of constant magnitude behind their transient impedances (Z_A and Z_B).

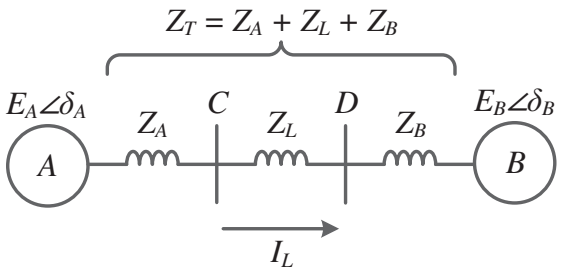

Figure 5.3: A two-source system

An impedance relay is installed at bus A. The apparent impedance seen by the relay at bus A is given by:

$$\begin{aligned} Z_C = \frac{V_C}{I} &= \frac{\tilde{E}_A - Z_A\tilde{I}}{\tilde{I}} \\ &= -Z_A + Z_T\left[\frac{E_A\angle\delta_A}{E_A\angle\delta_A - E_B\angle\delta_B}\right] \end{aligned} \tag{5.1}$$

Assume that δ_B is equal to zero so that E_A has a phase advance of δ_A over E_B and the ratio of the two source voltage magnitudes $\frac{E_A}{E_B} = 1$, (5.1) is simplified

as follows:

$$\begin{aligned} Z_C &= -Z_A + \frac{Z_T}{1\angle 0^\circ - 1\angle -\delta_A} \\ &= -Z_A + Z_T \left[\frac{1+\cos\delta_A + i\sin\delta_A}{2i\sin\delta_A}\right] \\ &= \left[\frac{Z_T}{2} - Z_A\right] - i\left[\frac{Z_T}{2}\cot\frac{\delta_A}{2}\right] \end{aligned} \tag{5.2}$$

Fig. 5.4 represent the impedance trajectory seen by the relay at C during power swings. For the impedance locus described in (5.1), the impedance locus is seen to be a straight line which is the perpendicular bisector of the total system impedance Z_T. The angle formed by lines from A and B to any point on the locus is equal to the corresponding angle δ_A. When δ_A is equal to zero, the current I is also equal to zero and consequently, the impedance seen by the relay under this condition is infinite. However, when δ_A is equal to 180°, the voltage at the electrical centre is zero. Hence, the impedance seen by the relay will see a three phase fault at the electrical centre. For this simplified case, the electrical centre is similar to the impedance centre of the line.

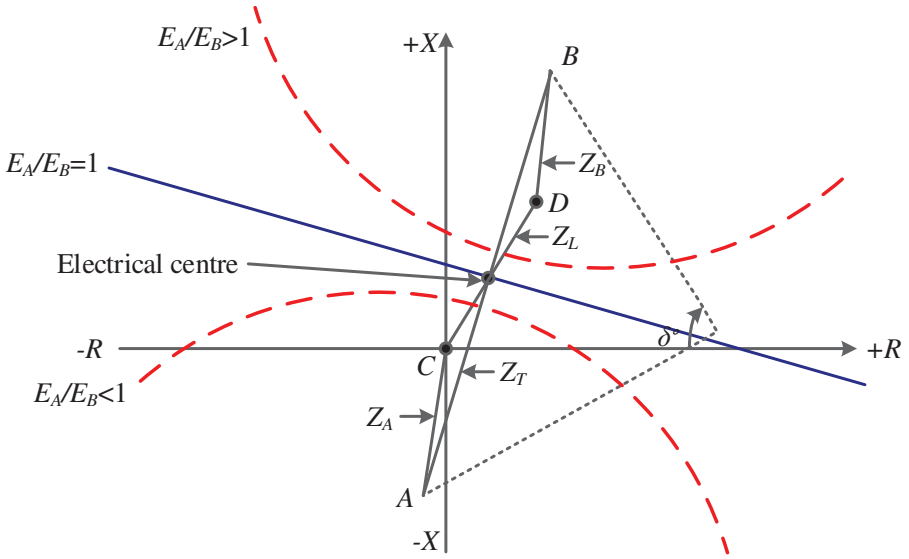

Figure 5.4: Typical out-of-step impedance trajectory

For more general cases where E_A is not equal to E_B, the impedance trajectories are circles with their centres on extensions of the impedance line AB. In the case when $\frac{E_A}{E_B} > 1$, the electrical centre is above the impedance centre of the

line, while for the case when $\frac{E_A}{E_B} < 1$, the electrical centre is below the impedance centre. Fig. 5.4 also illustrates the impedance trajectory for three different values of the ratio $\frac{E_A}{E_B}$.

The electrical centres of the system will vary corresponding to the change in the system impedances behind the line terminals and the internal generator voltages during operation. On the other hand, the rate of slip between systems depends on the accelerating torques, system inertias, and the level of generator output power before disturbance. Coherency identification techniques provide a means to determine the precise location of the electrical centre of the system in the event of a power swing. This information helps protection engineers to determine the appropriate location of out-of-step protection scheme to be applied in a system.

5.4 Generator out-of-step characteristic

Over the years, the application of high voltage and extra high voltage transmission systems, large conductor-cooled generators, fast response voltage regulators, and the expansion of transmission systems have strengthened the interconnection of power system transmission network. This network improvement changes the ratio between the generator impedance and the network system impedance. The generator and its corresponding step-up transformer impedances have relatively increased compared to the improved transmission network system impedances. As a result, the system impedance centre and electrical centre tend to occur within the generator or its corresponding step-up transformer rather than within the transmission network following a power swing in the system. Unfortunately, the protection schemes protecting the generator and the step-up transformer are usually designed based on differential relays, which will not detect power swings.

An out-of-step condition causes high currents and voltages in the affected generators with the frequency being a function of the rate of slip of its poles. If the slip frequency of the unit approaches a natural torsional frequency, the torques may be sufficient to break the generator's shaft. Hence, it is crucial to trip the generator as soon as possible, preferably during the first half slip cycle of a loss-of-synchronism, since shaft torque levels continually increase with each subsequent slip cycle. The pole slipping events may also cause abnormally high stator core end iron fluxes which consequently lead to overheating and shorting at the stator core

ends. Therefore, it is necessary to have an out-of-step relay that will detect and initiate appropriate control action to avoid these adverse effects on the affected generator and the rest of the system.

Transient stability studies during power system planning help in determining the impedance trajectory during a power swing in order to provide the best means of out-of-step detection. Conventional out-of-step schemes monitor the behaviour of the impedance trajectory to detect an unstable swing or when a generator slips a pole. One simple option exercised in practice is using a single impedance relay with the reach that covers the generator and step-up transformer. However, more sophisticated out-of-step detection schemes such as the single blinder scheme, double blinder scheme, or concentric circle scheme are preferred compared to the single blinder scheme [76]. These protection schemes provide better selectivity and sensitivity compared to the single impedance relay scheme. Recently, several variations of out-of-step detection methods have been proposed in the literature [72, 73, 74, 75]. However, there is no report on actual implementation of these methods. Therefore, the scope of this thesis focuses on the conventional out-of-step detection method as recommended in [77].

5.4.1 Single mho type relay scheme

For a system illustrated in Fig. 5.5, a single mho relay scheme monitors the apparent impedance at the HV terminal of the step-up transformer to look into the generator and its step-up transformer. The relay will immediately trip the generator when the apparent impedance monitored at the HV terminal encroaches into the mho offset characteristic. Thus, the mho offset characteristic of the relay has to be set such that it will initiate tripping only for an unstable swing.

Fig. 5.6 illustrates the principle of the single mho relay scheme detecting an out-of-step condition during a power swing. From the figure, the value of angle δ_C dictates the radius of the mho set characteristic, hence the sensitivity of the relay setting. Typically, δ_C is set at the point where the impedance locus enters the relay characteristics. The value of δ_C depends on the maximum permissible angular separation of the generator from the system without losing its synchronism which is usually around 120°. However, since the size of relay circle may expose the sensitivity of the relay, it is necessarily to perform detailed studies on the

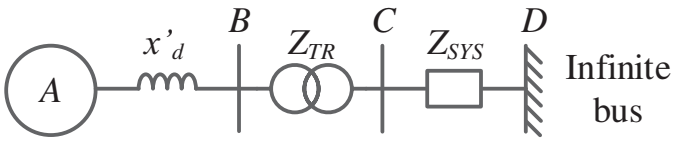

Figure 5.5: Single generator connected to infinite bus system

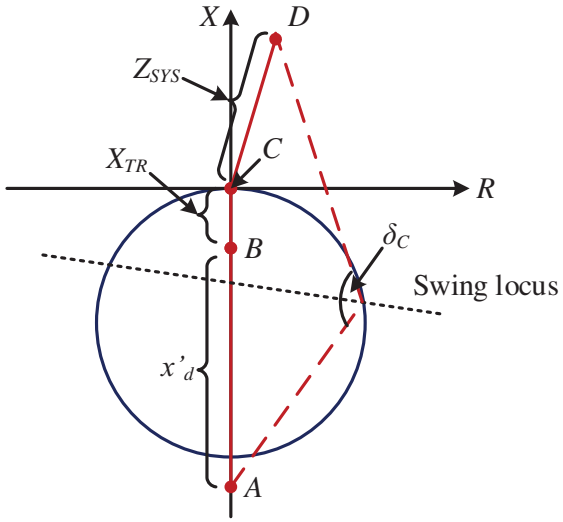

Figure 5.6: Single mho relay scheme

system to determine more accurate value of δ_C, hence appropriate setting of the relay, to ensure correct operation of the relay during a power swing.

It is also possible that this scheme may mal-operate during a loss-of-potential condition. Complementing the single mho relay scheme with a high speed over-current fault detector minimizes the probability of the relay mal-operation during a loss-of-potential condition.

5.4.2 Single blinder type relay scheme

A single blinder scheme uses two impedance elements called blinders that have opposite polarity and a supervisory offset mho relay to evaluate the stability of an evolving swing following a disturbance. The offset mho relay used in the scheme limits the operation area to the power swing that travels through or close to the generator and its step-up transformer. Fig. 5.7 illustrates a single blinder

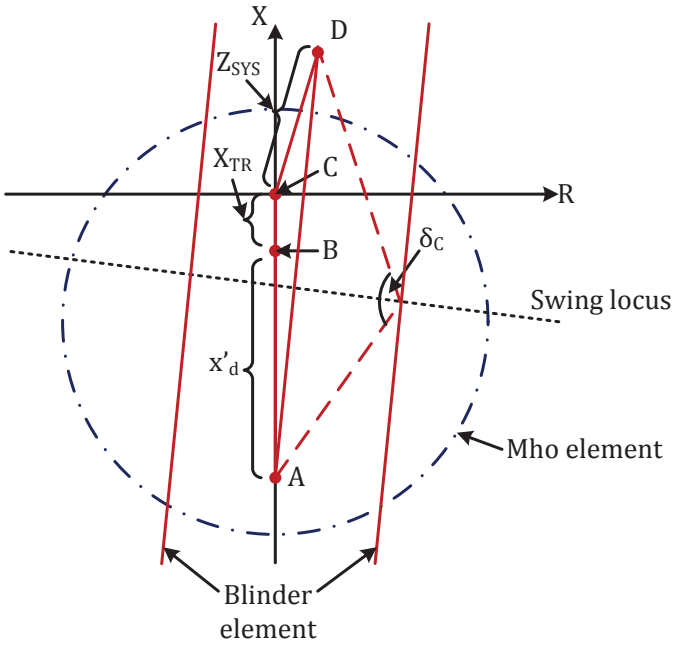

Figure 5.7: Single blinder scheme

scheme applied to the HV side of the generator step-up transformer in the system represented in Fig. 5.5. Also, it is possible to apply this detection scheme at the generator terminals looking into the system by adjusting the offset of the relay characteristic from the point of measurement.

Depending on the manufacturer, there are many options to apply single blinder scheme for out-of-step condition detection. One of the many options is to trip the generator when the apparent impedance trajectory is within the supervisory mho characteristic and crosses both blinders within a certain pre-determined period of time. Setting the single blinder scheme is relatively easy and it is extremely secure. It will only trip the generator during a swing that passes through 180°. This implies that there should be reversal of the power flow as viewed from the machine terminals, and the reversal should occur during a high current, in order for this relay to trip the affected generator. These two conditions imply that the generator is out-of-step with the rest of the system. Therefore, it cannot mal-operate during a stable swing. For these reasons, the single blinder scheme preferred over many of the other scheme.

The distance between two blinders, the timing to cross both blinders and the radius of the supervisory mho element dictates the sensitivity of this relay

scheme. Transient stability simulations studies are useful to determine the CCA and the corresponding CCT prior to the moment before the affected generator loses it synchronism with the system. This information is useful to assist the relay engineers to determine appropriate setting for this scheme. However, in the case where stability studies are not available, it is recommended to set the CCA for the blinder setting at 120° because at this angle, the swing is generally not recoverable.

5.4.3 Double blinder type relay scheme

The double blinder schemes operate in a similar manner to the scheme described in the previous subsection. Similar to the single blinder scheme, this scheme also used supervisory mho element to limit the reach of the relay system. Fig. 5.8 displays the double blinder scheme relay characteristic. The logic circuitry of this scheme recognizes an out-of-step condition if the swing impedance stays between the outer and inner element for longer than a certain pre-determined time. The logic circuitry will seal-in the out-of-step condition logic when the swing impedance enters the inner element. The impedance swing must travel from the inner to the outer element longer than a pre-set time. Depending on the logic scheme used, the trip will not be initiated until the reset of the supervisory mho element. In the case of a fault, the inner and outer element reset almost instantaneously. Therefore, the relay scheme will not issue any tripping signal in the event of fault.

Upon the detection of an out-of-step condition, the swing impedance has entered the relay inner characteristic. Consequently, the impedance swing may leave the inner and outer element in either direction and initiate the tripping signals. Therefore, a sophisticated transient stability analysis is crucial to determine the setting of this scheme so that the inner element of the relay should respond only to the swing from which the system cannot recover. However, the single blinder element scheme does not suffer from this limitation because its logic only requires the impedance swing to encroach the inner area from one direction and exit through the opposite. Therefore, a single blinder scheme may be a better option for the protection of a generator than the other conventional scheme such as mho, double blinder, or concentric circle scheme.

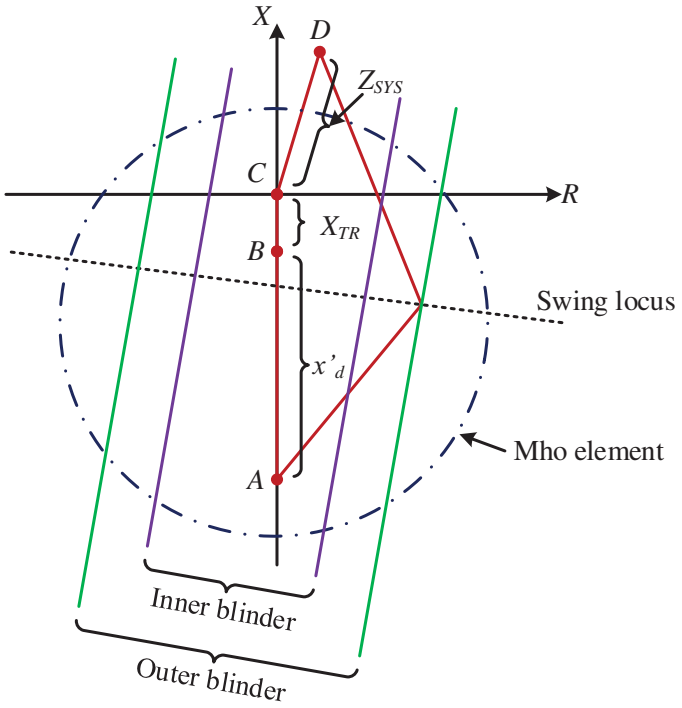

Figure 5.8: Double blinder schemes

5.4.4 Concentric circle schemes

The concentric circle scheme uses two mho relays and it works on the same principle as dual blinder scheme to detect an out-of-step condition in the system. It is crucial to ensure that the inner element responds only to the swing which the system cannot recover. Fig. 5.9 displays the characteristic of this scheme in various shapes used in practice.

5.5 Adaptive out-of-step protection scheme

There are a number of options to protect a generator against out-of-step condition. These methods are diverse such as the single-blinder, double blinder, and concentric schemes described previously. Basically, all these schemes operate on the same principle, which is monitoring the behaviour of the impedance swing following a disturbance in the system. It is necessary to perform an extensive transient stability study to determine the appropriate setting for an out-of-step protection scheme. However, in the absence of information from transient stability

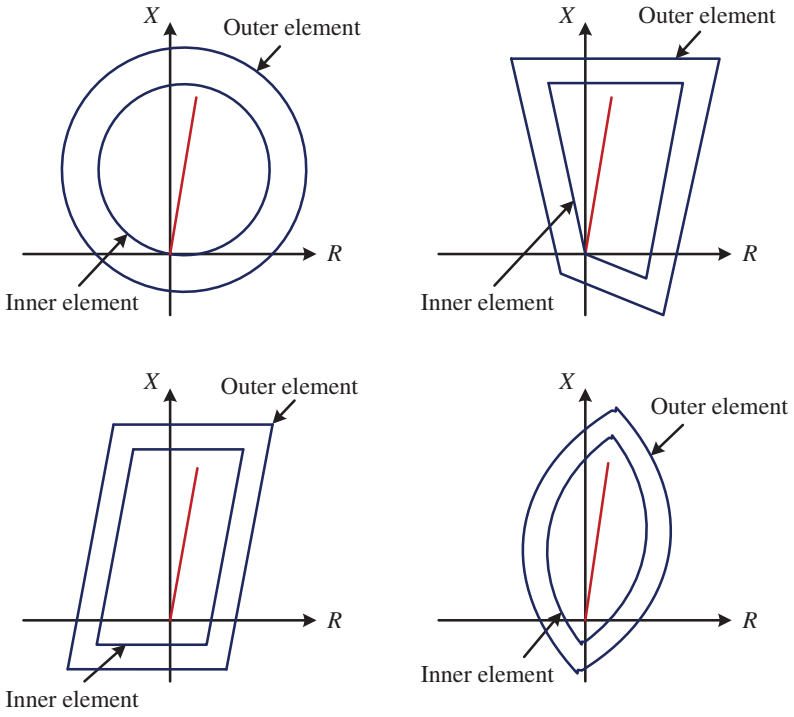

Figure 5.9: Concentric schemes

studies, the setting of an out-of-step protection scheme may be determined using a graphical procedure and conservative settings. This thesis focuses on adapting the setting of single blinder scheme to suit the prevailing operating conditions because it is the most preferred scheme implemented in practice [76]. This section presents a brief procedure to establish the setting of a single blinder scheme for generator out-of-step protection.

Fig. 5.10 depicts the impedance setting of a single blinder setting for generator out-of-step protection. The figure shows that to calculate the setting of the out-of-step relay requires several important parameters of the generator and the system such as generator transient reactance x'_d, unit transformer reactance X_{TR}, and system impedance Z_{SYS}. The supervisory mho element is set to reach 1.5 times the unit transformer impedance in the system direction and two times the generator transient reactance in the generator direction. The diameter D_{mho} and centre C_{mho} of the mho characteristic are calculated as follows [77]:

$$D_{mho} = 2 \times x'_d + 1.5 \times X_{TR} \tag{5.3}$$

$$C_{mho} = 1.5 \times X_{TR} - \frac{D_{mho}}{2} \tag{5.4}$$

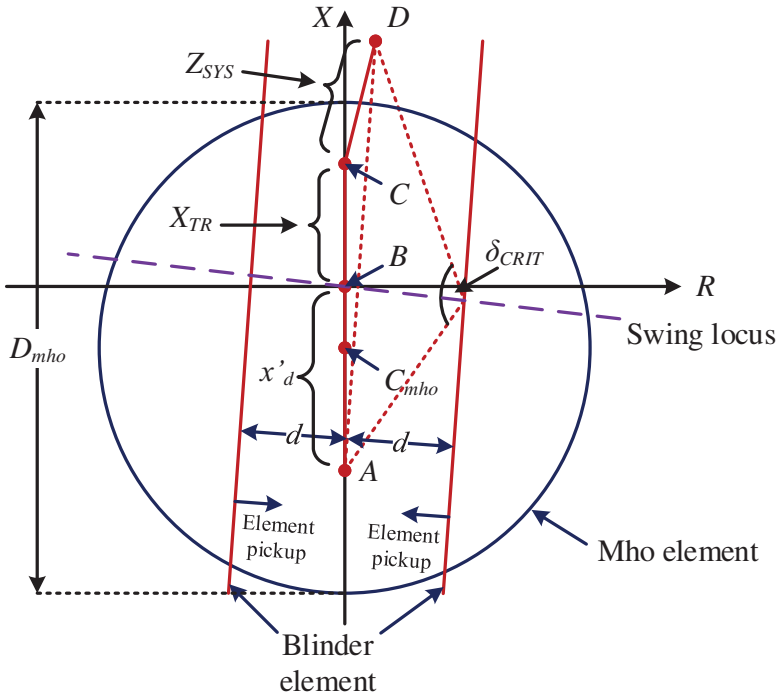

Figure 5.10: Procedure to set out-of-step relays

It is essential to determine the CCA δ_{CRIT} between the generator and the system in order to calculate the setting of the relay. The CCA occurs at the point when the generator begins to lose its synchronism with the system. This angle is obtained from transient stability studies of the system. General practice within the industry uses 120° angle because usually the system is not able to recover from the swing at this angle. Consequently, the setting of the blinder is calculated using the following equation [77]:

$$d = \frac{x'_d + X_{TR} + Z_{SYS}}{2} \times \tan\left(90° - \frac{\delta_{CRIT}}{2}\right) \tag{5.5}$$

The next step is to determine the time for the impedance swing to travel between the blinder elements. In order to implement the scheme that requires a minimum traverse time between the blinders, the time delay should be set to a value corresponding to the fastest travel time between the two blinders. However, setting the timer delay too short may jeopardize the sensitivity of the relay. An appropriate time delay is crucial to prevent relay mal-operation during transient event in power system operation.

5.5.1 Extended Equal Area Criterion

The calculation of an out-of-step relay setting is straightforward, provided that the CCT and the generator dynamic parameters are known. The procedure to approximate the CCT to determine the setting of out-of-step protection is the most exhaustive part of the process. In this chapter, the computational effort required is simplified by using the EEAC approach described in [78]. The implementation of EEAC involves the transformation of a multi-machine system into a two-machine system. Then, the two-machine system is further simplified into a single-machine infinite bus system. The swing equation of the i^{th} machine in a multi-machine system is formulated as follows [79]:

$$M_i \ddot{\delta}_i (t) = P_i^{mech} (t) - P_i^{elec} (t) \tag{5.6}$$

where M, δ, P^{mech} and P^{elec} represent the inertia coefficient, rotor angle, mechanical input power and electrical input power of the generator, respectively. The EEAC works on the assumption that the multi-machine system is divided into two coherent groups, say group A and B, following a disturbance in the system. The swing equation is reformulated to accommodate this assumption as follows:

$$\sum_{j \in A} M_j \ddot{\delta}_j (t) = \sum_{j \in A} P_j^{mech} (t) - \sum_{j \in A} P_j^{elec} (t) \tag{5.7a}$$

$$\sum_{k \in B} M_k \ddot{\delta}_k (t) = \sum_{k \in B} P_k^{mech} (t) - \sum_{k \in B} P_k^{elec} (t) \tag{5.8a}$$

Equations (5.7) are rewritten as:

$$M_A \ddot{\delta_A} (t) = P_A^{mech} (t) - P_A^{elec} (t) \tag{5.9a}$$

$$M_B \ddot{\delta_B} (t) = P_B^{mech} (t) - P_B^{elec} (t) \tag{5.10a}$$

where,

$$\delta_A(t) = \frac{\sum_{j\in A} M_j \delta_j(t)}{\sum_{j\in A} M_j}, \qquad \delta_B = \frac{\sum_{k\in B} M_k \delta_k(t)}{\sum_{k\in B} M_k}$$
$$M_A = \sum_{j\in A} M_j \quad , \qquad M_B = \sum_{k\in B} M_k$$
$$P_A^{mech}(t) = \sum_{j\in A} P_j^{mech}(t) \quad , \quad P_B^{mech}(t) = \sum_{k\in B} P_k^{mech}(t)$$
$$P_A^{elec}(t) = \sum_{j\in A} P_j^{elec}(t) \quad , \quad P_B^{elec}(t) = \sum_{k\in B} P_k^{elec}(t)$$

The equivalent single machine infinite bus system is obtained using the following equations:

$$M_{smib}\ddot{\delta}_{smib}(t) = P_{smib}^{mech}(t) - P_{smib}^{elec}(t) \tag{5.11}$$

Where,

$$M_{smib} = \frac{M_A M_B}{M_A + M_B}$$
$$\delta_{smib}(t) = \delta_A(t) - \delta_B(t)$$
$$P_{smib}^{mech}(t) = \frac{M_A P_B^{mech}(t) - M_B P_A^{mech}(t)}{M_A + M_B}$$
$$P_{smib}^{elec}(t) = \frac{M_A P_B^{elec}(t) - M_B P_A^{elec}(t)}{M_A + M_B}$$

With the single machine infinite bus system equivalent, a standard equal area criterion is used for stability analysis to determine the CCA and CCT of the system, which is crucial information to calculate the settings of out-of-step protection. However, to ensure the relay setting is adapted to the current operating condition, the real-time information of the coherent groups of generators and the dynamic model parameters in the system are required to analyse a large interconnected network using EEAC. The method reported in Chapter 3 facilitates an elegant solution to identify the coherent group of generators in the system. On the other hand, the dynamic model parameters estimation technique elaborated in Chapter 4 are able to estimate these parameters in real-time.

5.5.2 The adaptive out-of-step protection algorithm

The idea presented in this chapter is instigated from the work reported in [80] and [81]. The adaptive protection schemes in [80] and [81] determine several groups of settings based on criteria that influence the sensitivity of protection scheme. The work in [80] determines the groups of settings based on the level of biasness towards security or dependability of relay operations. On the other hand, the work reported in [81] determines the groups of settings based on the zone reach of relay operation. Consequently, in both methods, a group of settings is selected from these groups based on the current operating conditions. The groups of relay settings are determined using the offline methods using various heuristic assumptions of the system operating conditions. Even with the increased number of settings that suit with a number of system operating conditions, the relay may mal-operate if the abnormal system operating condition is not anticipated during off-line determination of groups of relay settings. The work presented in this thesis proposed a novel adaptive out-of-step protection scheme that calculates the settings of the relay online, based on the timely estimations of the dynamic characteristics of the system. The proposed method ensures appropriate protection and control actions of the protection scheme following a disturbance in the system that prevents a wide-area blackout of the system caused by protection relays mal-operation.

Fig. 5.11 shows the algorithms of the proposed method to recalculate and retune the setting of an out-of step protection system. An algorithm performing such functions automatically for an out-of-step protection system requires several input measurements, an equivalent power system model and protection system constraints to perform the calculation. The proposed algorithm displayed in the figure is initiated by a change in power system condition that is monitored from the oscillation in the measured data. Since the out-of-step event is classified as a wide-area stability problem [11], measurements across a wide geographical area will be required for a large power system network. As discussed in Chapter 2, WAMS technology is able to facilitate the measurements required for the proposed adaptive out-of-step protection system. The measured data obtained from the WAMS is gathered to a centralised supervisory control centre for analysis. The measurement quantities of voltage magnitude, voltage phasor, active and reactive power, from the grid supply points and the large generations in the system are required for the algorithm. In the control centre, the coherent groups of generators

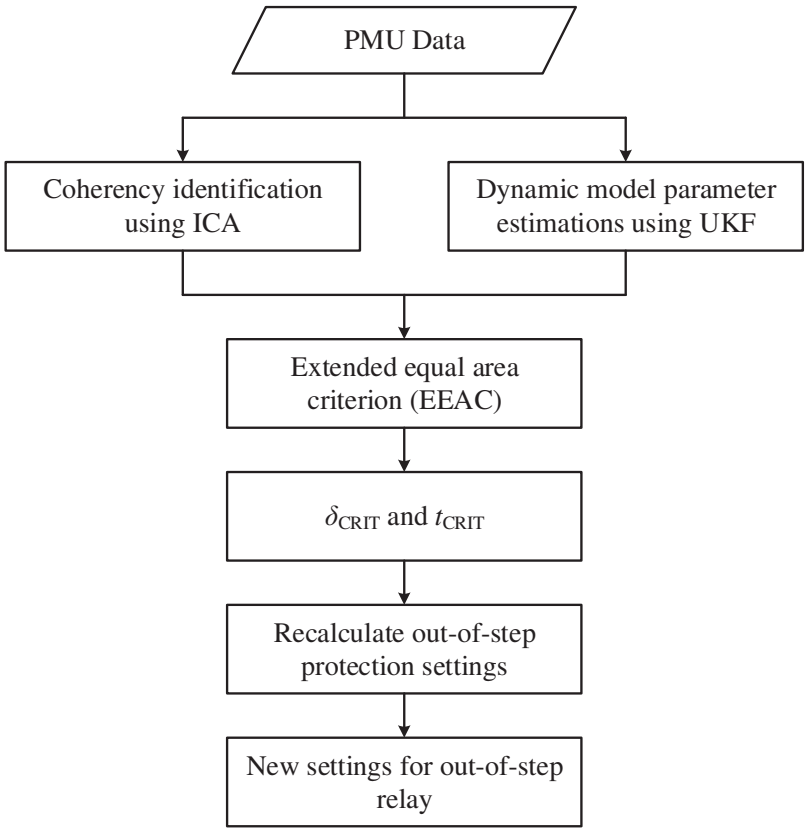

Figure 5.11: The algorithm for adaptive out-of-step protection scheme

are identified using the method proposed in Chapter 3 and the dynamic model parameters of the generators in the system are estimated using the method proposed in Chapter 4. The identified coherent groups and the estimated dynamic model parameters of generators represent the timely dynamic properties of the system. Since, the test system model considered in this study consists of a large number of generators, the EEAC method is used to determine the CCA and CCT of the system. This is realised by using an equivalent power systems model constructed using the dynamic properties obtained in the previous step. Subsequently the out-of-step relay settings are calculated using the value of CCA and CCT obtained from the EEAC method.

From the figure, the EEAC may be directly replaced by other transient stability analysis method such as the Single Machine Equivalent (SIME) [82], the closest unstable equilibrium point method [83], the controlling unstable equilibrium point [84],the potential energy boundary surface method (PEBS) [85] or the boundary of stability region-based controlling unstable equilibrium point method

(BCU) [86]. Although the application of EEAC for transient stability analysis is criticised due to its working assumptions, it provides a simple solution to determine the CCA and CCT of the system following a disturbance. It is acceptable to apply the EEAC method to assist generator out-of-step setting calculation as a generator losing its synchronism with the rest of the system is also equivalent to the two-machine system problem. Furthermore, according to the survey conducted in [87], the EEAC is widely implemented for transient stability studies in practice.

The proposed algorithm requires information of the coherent groups and the dynamic model parameters of the generators in the system. This information is obtained using the methods proposed and demonstrated in Chapter 3 and 4, respectively. The methods proposed in Chapter 3 and Chapter 4 require information from the oscillation in the measured data, which can be observed during the change in the system operating condition. Therefore, the proposed algorithm starts to execute when there is an oscillation in the measured data representing the change in the system operating condition. The proposed coherency identification technique requires at least a time windows 3-5 s of measurements to monitor the coherency properties of the system effectively [42]. On the other hand, the proposed dynamic model parameter estimations technique requires a time windows of approximately 1.0 s to be able to estimate the parameters accurately. In addition, the required measured data is gathered at a centralised supervisory control centre from PMU located at grid supply points or large generators via various level of PDC hierarchy. This process also introduces a time delay in the order of 30-100 ms [7]. Fig. 5.12 shows the time-line of the operation of the algorithm operation for adaptive out-of-step protection proposed in this thesis. From the figure, the proposed method is able to provide new settings to an out-of-step relay following a change in the system in approximately 5.2 s. However, the computation time for the proposed algorithm alone as recorded in MATLAB Simulink environment using Intel Xeon L5520 2.26 GHz quad-core processor with 12 GB DDR3 RAM platform is $33.6 + 31.2 + 4.7 = 69.6$ ms. This implies that the method proposed for adaptive out-of-step protection system computes new settings for an out-of-step relays almost instantaneously from the moment the data is available at the centralised control centre. The updated settings are adapted to the relay to protect the system from an out-of-step condition.

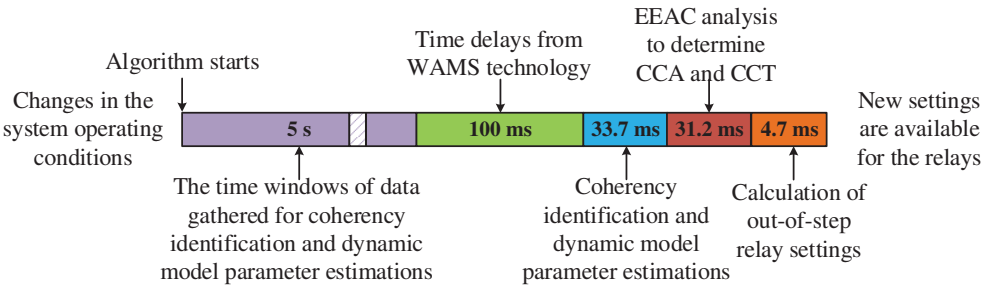

Figure 5.12: The time-line for adaptive out-of-step relay operations

5.6 Application, results and analysis

This section reports the determination of settings for an out-of-step generator protection system. The 16-machine 68-bus test system model is also considered in this investigation. The bus data, line data and dynamic characteristics of the systems are available in [16, 41] and listed in Appendix A as well. Fig. 5.13 displays the single line diagram of the 16-machine 68-bus test system model. Nonlinear simulations of the test system model are performed in MATLAB Simulink. The synchronous generators in the test system are modelled as classical models. The mechanical power inputs to the generators are assumed to be constant. This study demonstrates the procedure to determine the setting of the mho element, the blinder and the time delay for the impedance swing to cross both blinders for generator out-of-step protection. A three phase temporary fault at Bus #31 is considered as disturbance in this study. For demonstration purposes, this section focuses on the settings determination and performance evaluation of out-of-step relay for Generator #10. The settings for out-of-step relay for other generators in the system can be calculated in the similar manner.

In this section, the results of the three representative cases with different fault clearing times are discussed and analysed. The study starts with a fault clearing time of 200 ms with iterative increments of 10 ms until the generator is going out-of-step from the rest of the system. The fault clearing time considered for each representative case to determine the setting of out-of-step protection for Generator #10 are listed as follows:

1. Case 1 - Fault cleared after 200 ms
2. Case 2 - Fault cleared after 330 ms

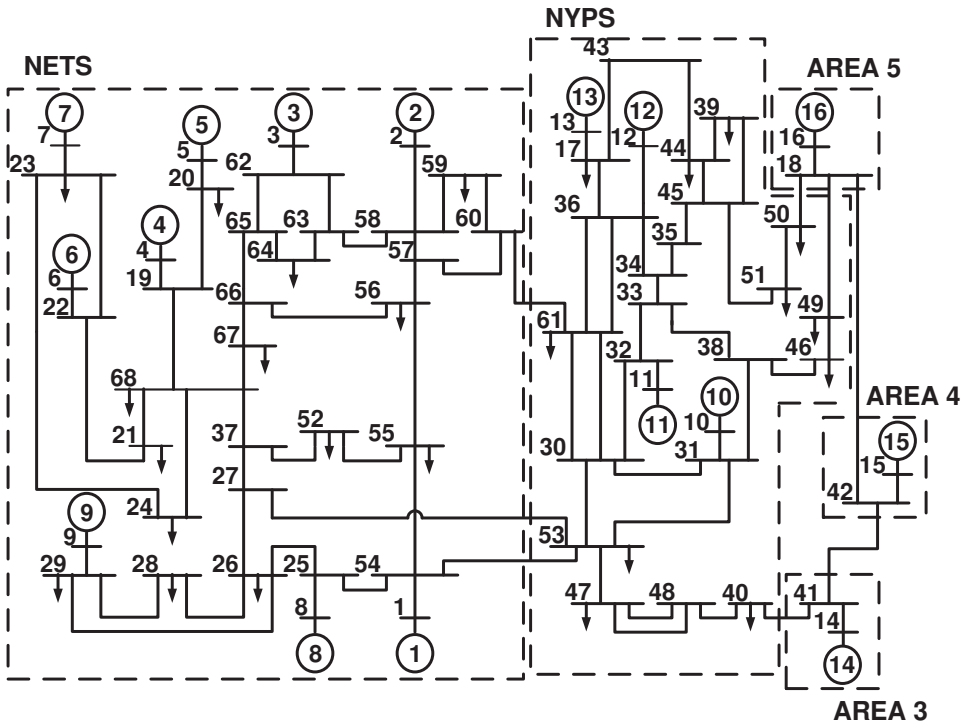

Figure 5.13: 16-machine 68-bus test system model

3. Case 3 - Fault cleared after 340 ms

Transient stability studies are able to provide information that represents the system operating condition during transient period. However, for out-of-step protection setting determination purposes, the most important information is the rotor angle response of the generators and the impedance trajectory plot at the point of interest in the system. Fig. 5.14 exemplifies the rotor angle for Generator #10 for all representative cases considered, each with a different fault clearing time. From the figure, it is observed that Generator #10 remains in synchronism when the fault is cleared 200 ms following the fault initiation at Bus #31. In Case 2, the generator still remains in synchronism with the system with a fault clearing time of 330 ms. However, the system loses it synchronism when the fault is cleared 340 ms after the fault inception in the system. This implies that the CCT for the generator to remain in synchronism with the system is approximated equal to 330 ms. Also, it is observed from the figure that the CCA is approximately 120° at time of 596 ms. The approximated CCA is used to determine the setting of the blinder element using (5.5). The time for the swing impedance locus to travel from the CCA to 180° is approximately 198 ms. Therefore, the travelling time within the blinder should be set at 198ms $\times$ 2 = 396ms. The setting of the supervisory

mho element is calculated using (5.3). Table 5.1 summarises the pre-determined settings used for in this chapter.

Table 5.1: The pre-determined out-of-step relay settings

d (pu)	D_{mho} (pu)	C_{mho} (pu)	Time to cross both blinders (ms)
0.0244	0.1201	-0.0211	396

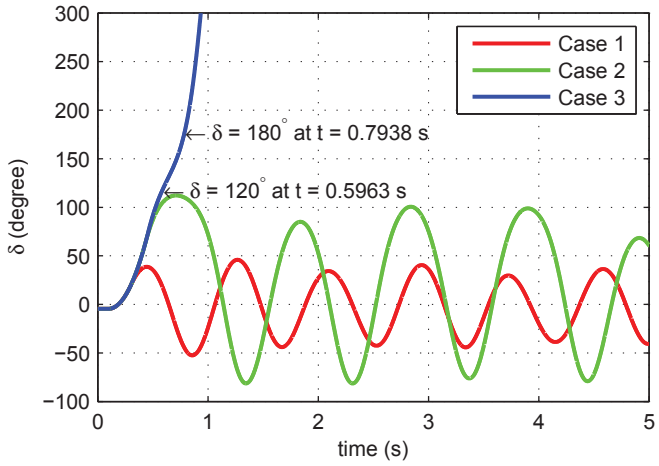

Figure 5.14: Rotor angle for Generator #10 for all three cases

Fig. 5.15 shows the out-of-step protection setting for Generator #10 and the swing impedance trajectory for all three cases. In the figure, the red, blue, and black lines represent the swing impedance seen by the relay, the line impedance covered by the relay and the settings of the relay (supervisory mho and blinder elements), respectively. From Fig. 5.15a, it is observed that the swing impedance encroaches the supervisory mho elements. However, the swing impedance does not crossing any blinder element of the relay. Therefore, the out-of-step relay will not trip the generator under this condition because it does not cross the blinder element of the relay. Fig. 5.15b shows the swing impedance for Case 2. The figure shows that the swing impedance penetrated the supervisory mho element and crossed the blinder on the right-hand side of the figure, and consequently starts the timer for the blinder elements of the relay. However, the swing impedance goes to the opposite direction after $t = 760$ ms, hence does not cross the blinder on the left-hand side of the figure. Therefore, the out-of-step relay does not recognize this condition as an out-of-step condition. Fig. 5.15b demonstrates that the swing impedance crosses the relay blinder element at t equals to 595 ms and consequently crosses the other blinder element at t equals to 994 ms. Therefore, the travelling

time for the swing impedance to cross the relay element is equals to 399 ms which exceeds the time delay setting of the relay. Consequently, the relay recognized this event as an out-of-step condition and issues tripping signal to isolate the generator from the system. It is clear that from the first two cases, the impedance trajectory does not cross the line of impedance of the system whereas the swing impedance crosses both blinder elements in the third case. Therefore, the relay only recognized the third case as an out-of-step condition. The outcome of the out-of-step protection decision is consistent with the rotor angle responses illustrated in Fig. 5.14.

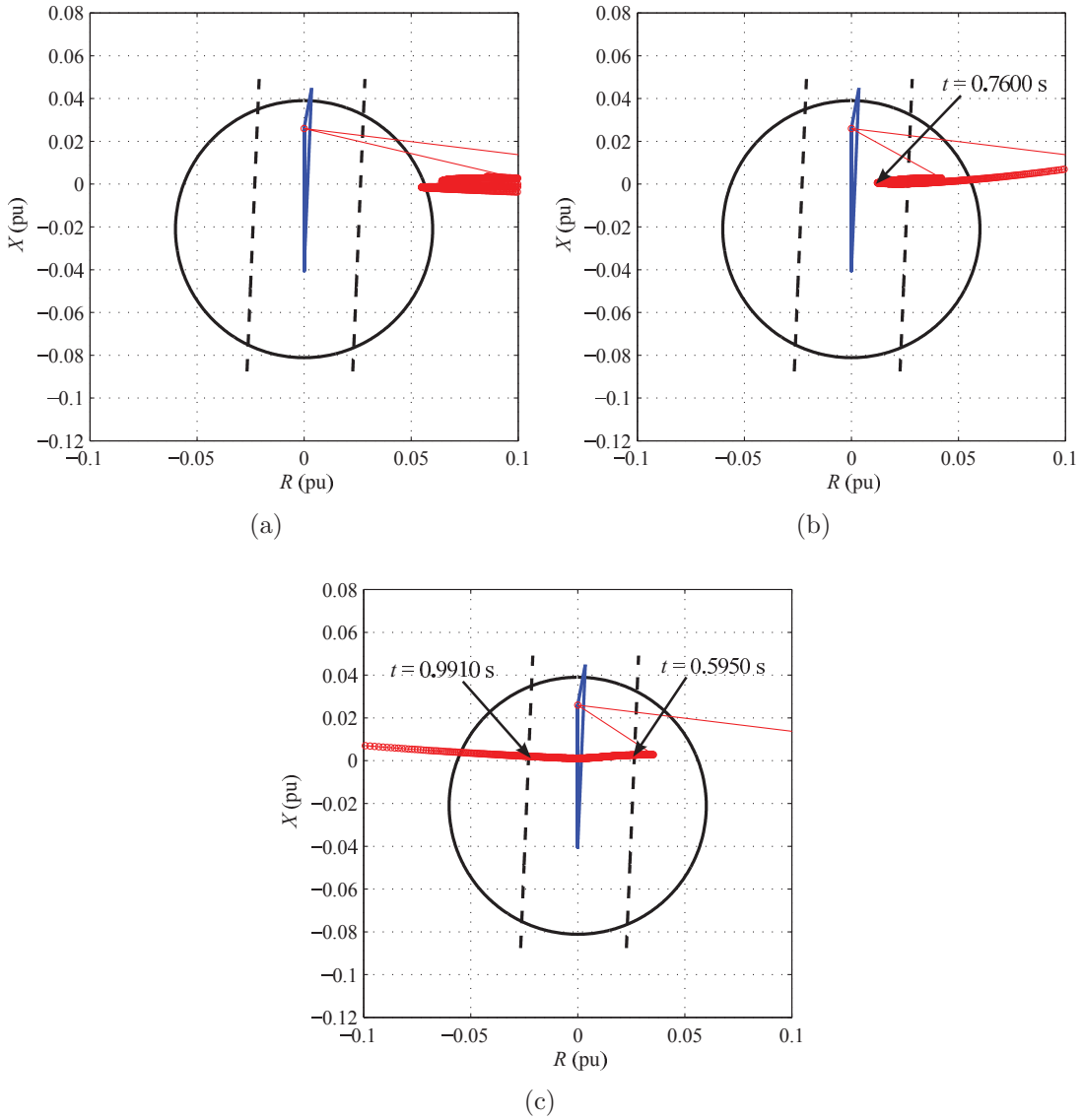

Figure 5.15: Impedance trajectories for a) Case 1 b) Case 2 c) Case 3

It is shown that the sensitivity and reach of the generator out-of-step relays

are influenced by the dynamic model parameters seen by the relay sensor. The generator out-of-step relay setting determined in this section operates in a fixed manner. Therefore, changes in these parameters may cause the out-of-step relay to mal-operate and further exacerbate the impact of disturbance in the system. Adapting the out-of-step protection setting according to these changes maintain the reliability and security of the relay operation.

5.7 Performance evaluation

This section evaluates the performance of the out-of-step protection obtained in the previous section. In practice with time the values of the generator dynamic model parameters will differ from the values supplied by the manufacturer. Inaccurate representation of dynamic model parameters is likely to have a significant impact on the system dynamic and frequency stability [1]. Furthermore, in the case of applying a relay for out-of-step protection for multiple units, the relay settings need to be updated regularly. This is due to the combined impedances and inertia constant seen by the relay depending on the number of generator being on-line and the network strength at that particular time [88]. The results of the three representative cases, namely Case A, B and C, each with different system operating conditions are presented and analysed. In this study, it is assumed that the total number of generator units in Generator #10 is equal to three. During normal operating condition, only two out of three generators are connected to the system. Here, the changes in the generator operating condition is set arbitrarily only to demonstrate the influence of the generator dynamic parameters to the out-of-step relay operation. A three phase temporary fault at Bus #31 is considered as disturbance for this investigation. In order to study the generator behaviour under out-of-step conditions, for each case, the fault clearing time is chosen such that the generator will lose its synchronism with the rest of the system. In the R-X diagrams discussed in this section, the red, blue, black, and magenta lines represent the swing impedance seen by the relay, the line impedance covered by the relay, the pre-determined settings of the relay, and the adaptive settings of the relay, respectively.

5.7.1 Case A

In Case A, a three phase fault cleared 450 ms after the fault inception is considered as the disturbance in the system. It is assumed that all three generators are online which are represented by the 50% increase of the inertia constant and the 50% reduction of combined transient reactance in Generator #10 seen by the relay. Fig. 5.16 displays the rotor angle for all generators in the system for this case following the disturbance. The figure shows that the Generator #10 loses its synchronism with the rest of the system following the fault at Bus #31. In this condition, it is necessary to isolate the generator from the system to prevent severe damage to the affected generator shaft.

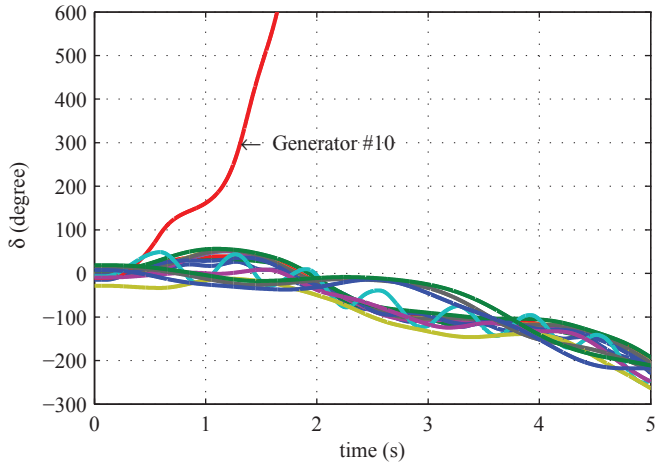

Figure 5.16: Rotor angle for all generator for Case A

Fig. 5.17 depicts the swing impedance trajectory on two different out-of-step protection settings. The setting illustrated in Fig. 5.17a represents the setting calculated based on the dynamic model parameters of Generator #10 operating at normal operation. In Fig. 5.17b, the setting of the out-of-step relay is recalculated using the adaptive out-of-step protection scheme described in Fig. 5.11. The minimum time required for the swing impedance to cross both blinders for the pre-determined out-of-step relay setting and the adaptive out-of-step relay setting are 396 ms and 437 ms, respectively. Table 5.2 summarises the pre-determined settings and the adaptive settings of the out-of-step relay used for in Case A.

The result shows that the swing impedance crosses both blinder elements of pre-determined relay seting in 639 ms while the swing impedance shown in Fig. 5.17b crosses both blinder elements of the adaptive relay setting in 528 ms. The

Table 5.2: The out-of-step relay settings for Case A

Types of setting	d (pu)	D_{mho} (pu)	C_{mho} (pu)	Time to cross both blinders (ms)
Pre-determined	0.0244	0.1201	-0.0211	396
Adaptive	0.0205	0.0931	-0.0075	437

time for the swing impedance to traverse both blinders exceeds the time delay setting for both relays. This implies that, both out-of-step relay settings are able to recognize the out-of-step condition in the system in this operating condition.

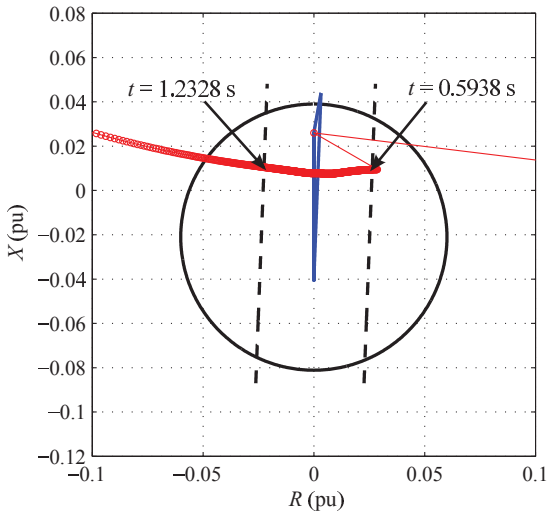

(a)

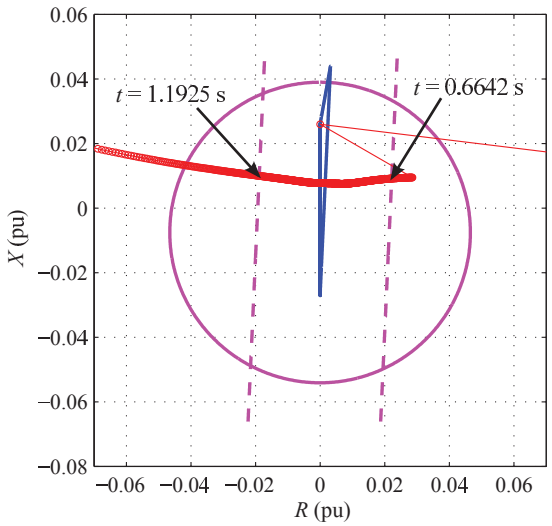

(b)

Figure 5.17: Relay settings for Case A a) Pre-determined b) Adaptive

5.7.2 Case B

A three phase fault cleared 190 ms after fault inception is considered as the disturbance in the system in Case B. In this case, it is assumed only one out of three generators is online. Therefore, there is a 50% decrease of the inertia constant and a 50% increase of the combined transient reactance in Generator #10 seen by the out-of-step relay element. Fig. 5.18 exhibits the generator rotor angle in the system following the disturbance considered for this case. The figure demonstrates that Generator #10 loses its synchronism during the first swing following the disturbance in the system. It is vital to separate the generator from the system to avoid severe damage to the generator and the system.

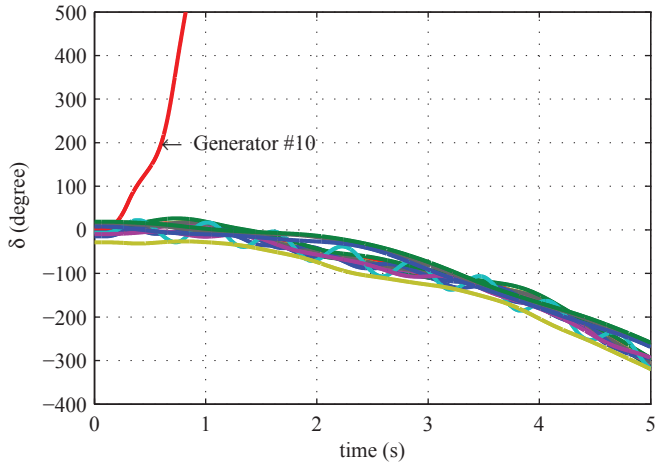

Figure 5.18: Rotor angle for all generator for Case B

Fig. 5.19 represents the swing impedance trajectory on two different relay settings. The out-of-step protection setting in Fig. 5.19a signifies the pre-determined out-of-step relay settings calculated based on the dynamic model parameters of Generator #10 operating at normal operating condition. In contrast, the settings of the adaptive out-of-step relay displayed in Fig. 5.19b are calculated using the approach elaborated in Fig. 5.11. The minimum time required for the swing impedance to cross both blinders for the pre-determined relay setting and the adaptive relay setting are 396 ms and 326 ms, respectively. Table 5.3 summarises the pre-determined settings and the adaptive settings of the out-of-step relay used for in Case B.

It is observed from Fig. 5.19a that the swing impedance crosses both blinder elements of relay setting in 188 ms. This indicates that the time for the swing

Table 5.3: The out-of-step relay settings for Case B

Types of setting	d (pu)	D_{mho} (pu)	C_{mho} (pu)	Time to cross both blinders (ms)
Pre-determined	0.0244	0.1201	-0.0211	396
Adaptive	0.0430	0.2031	-0.0616	326

impedance to traverse both blinders does not exceed the time delay for the pre-determined out-of-step relay settings. The relay recognized the swing impedance behaviour as a fault and should be handled by other protection schemes. This situation causes the out-of-step relay to miss-operate and cause severe damage to the generator. On the contrary, the adaptive out-of-step protection setting does not miss-operate in this condition as displayed in Fig. 5.19b. The result demonstrates that the swing impedance traverses both blinder elements of the relay in 348 ms which exceed the time delay of 326 ms set for the relay. This outcome implies that the adaptive relay setting recognized the changes in the system operating condition and adapted its settings to suit to the current operating condition that resulted in the appropriate control decision to mitigate the impact of the disturbance in the system.

5.7.3 Case C

During power system operations, it is possible for a recoverable stable swing to enter the relay characteristic following a fault in the system. A stable swing is determined as recoverable if the rotor angle separation between two or more group of generators is less than 120° [89]. The case discussed in this subsection investigates the performance of the out-of-step relay in an abnormal operating condition, where impedance swing corresponding to a recoverable stable swing enter the out-of-step relay characteristic causing the relay to mal-operate.

In this case, a three-phase fault cleared 566 ms after the fault inception is considered as the disturbance in the system. It is assumed all three generators are online. Therefore, there is a 50% increase of the inertia constant and a 50% decrease of the combined transient reactance in Generator #10 seen by the out-of-step relay element. In addition, the generator is assumed to operate at 50% of its internal voltage under normal operating condition. Although this condition is not a widespread problem, protection engineers have reported that this possibility exist for some types of generator's voltage regulators [90]. Similarly, with other cases

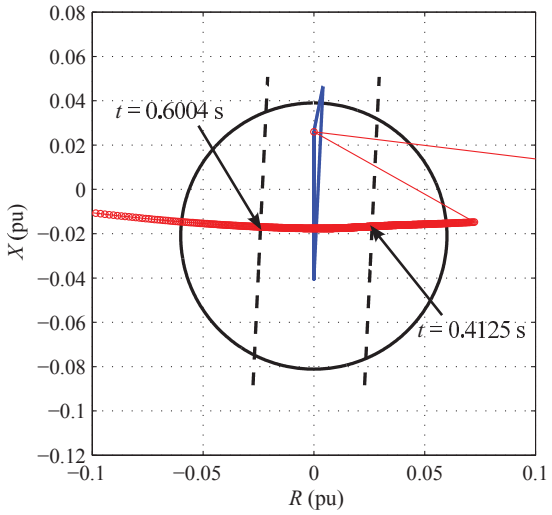

(a)

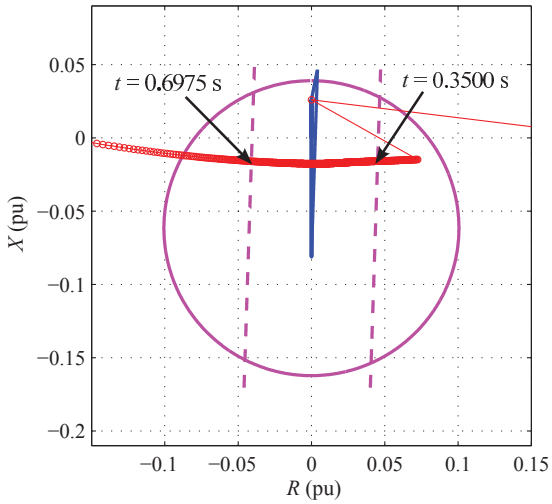

(b)

Figure 5.19: Relay settings for Case B a) Pre-determined b) Adaptive

discussed in this chapter, the performance of the out-of-step relay at Generator #10 is analysed.

Fig. 5.20 exhibits the generator rotor angle in the system following the disturbance. The figure demonstrates that Generator #10 maintains its synchronism with the rest of the system following the disturbance. The rotor angle responses of all the generators indicate that the system is likely to recover from the disturbance because the rotor angle separation between Generator #10 and the rest of the system does not exceed 120°. Consequently, an out-of-step relay scheme applied at a generator must not operate for recoverable swings because losing a generator due to relay mal-operation may turn a recoverable event into a major system outage

[89].

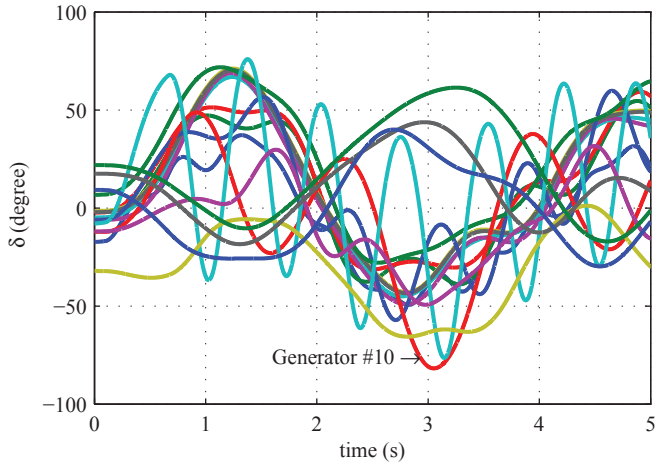

Figure 5.20: Rotor angle for all generator for Case C

Fig. 5.21 represents the swing impedance trajectories for two different out-of-step relay settings. The out-of-step protection settings in Fig. 5.21a signify the pre-determined out-of-step relay settings calculated during relay commissioning. In contrast, the adaptive out-of-step relay settings displayed in Fig. 5.21b are calculated based on the current operating condition of Generator #10. Table 5.4 summarises the pre-determined and adaptive settings of the out-of-step relay used in this exercise.

Table 5.4: The out-of-step relay settings for Case C

Types of setting	d (pu)	D_{mho} (pu)	C_{mho} (pu)	Time to cross both blinders (ms)
Pre-determined	0.0244	0.1201	-0.0211	396
Adaptive	0.0205	0.0931	-0.0075	382

It is observed from Fig. 5.21a that the swing impedance crosses both blinder elements of relay settings in 401 ms. This indicates that the time for the swing impedance to traverse both blinders exceeds the time delay of 396 ms set in the pre-determined out-of-step relay settings. Therefore, the relay recognizes the swing impedance behaviour as an out-of-step condition and initiates a trip signal to isolate Generator #10 from the system. However, it has been discussed earlier that the system is recoverable, following the disturbance considered in this study. Therefore, the out-of-step relays at Generator #10 must not operate under this condition because it will exacerbate the impact of disturbance to the system [89].

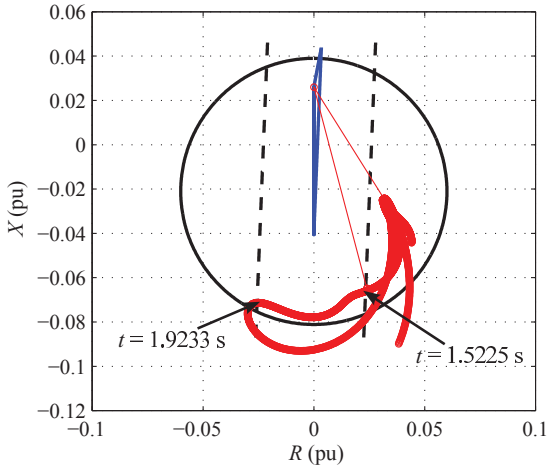

(a)

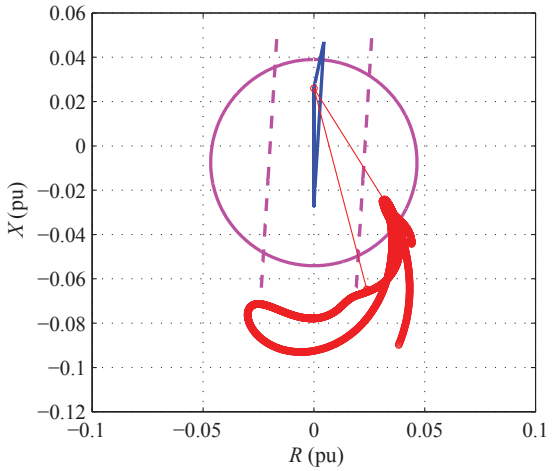

(b)

Figure 5.21: Relay settings for Case C a) Pre-determined b) Adaptive

On the contrary, the impedance trajectory displayed in Fig. 5.21, which are calculated using the adaptive out-of-step protection scheme proposed in this thesis, does not mal-operate in this condition. The result shows that the swing impedance trajectory did not traverse across the supervisory blinding zone of the relay. Therefore, the adaptive settings of the out-of-step relay do not initiate a trip signal to isolate the generator from the system. The result implies that the proposed method adapts its settings to suit the current operating situation, which provides appropriate protection and control actions that prevents relay mal-operation. Therefore, by ensuring appropriate protection and control action for the system, the proposed adaptive out-of-step protection system prevents a false trip of a generator, which caused by relay mal-operation.

False tripping of a generator during a stressed operating condition may increase the stress level in other parts of the system. This may trigger cascading tripping event of various protections in the network. Consequently, cascading events occurring in the network increase the level of stress to the system and eventually cause the catastrophic wide-area blackout. The blackout report published by IEEE Power and Energy Society [1] corroborated this fact. Therefore, preventing generator out-of-step relay mal-operation that unnecessarily isolates the generator from the system helps prevent an unnecessarily wide-area blackout in the system.

5.8 Chapter summary

An adaptive out-of-step protection for generators in a power system has been proposed. The approach is based on the extended equal area criterion (EEAC) method to determine the critical clearing angle (CCA) and time (CCT) of the system. This information is crucial in determining the setting of an out-of-step protection system. To ensure the relay setting adapts with the current operating condition, the coherent groups of generators are identified using the independent component analysis (ICA) technique reported in Chapter 3 and the dynamic model parameters of the system are estimated using unscented Kalman filter (UKF) approach proposed in Chapter 4. The coherent groups of generators in the system are identified in near real time and the dynamic model parameters in the system are estimated recursively to obtain an accurate and timely dynamic model representation of the system. Consequently, the setting of out-of-step protection is recalculated based on the estimated dynamic models to adapt with the changes during power system operation.

The procedure to calculate the settings of a single blinder scheme is also discussed. The dependability and security are validated by comparing the outcome of the relay with the response of the rotor angle in the system. The changes in the generator operating condition in the system have significant impact on the effectiveness of out-of-step relay operation for generator protection. Nevertheless, the method proposed in this chapter accurately detects the out-of-step condition even with the changes in system operating condition. The method is simple and does not require any prior information of the system.

Chapter 6

Conclusions and future recommendations

Interconnected power systems have suffered from catastrophic blackouts over the decades with obvious socio-economic consequences. The frequency of occurrence of large blackouts has increased in the last decade leading to setting up various task forces, advisory groups, research programmes and network operating standard across the world. This led to various solutions and standards. One important solution proposed in the literature is an adaptive out-of-step protection system. Conventional out-of-step protection operates in a fixed and pre-determined manner. Therefore, it is by design not to be able to adjust its setting to suit to the prevailing system operating condition. Past experience demonstrates that fixed and pre-determined relay settings may become suboptimal under extreme operating conditions. Therefore, it is obvious that the relay settings need to be retuned and recalculated to ensure secure operation during power swings. The novel work presented in this thesis aimed to provide vital dynamic information in real-time to recalculate and retune the relay setting of generator out-of-step protection to suit the prevailing system operating condition.

This chapter summarises the conclusions drawn from previous chapters, and also recommends some possible future work in the related research areas.

6.1 Conclusions

This thesis reports a measurement-based coherency identification method in interconnected power system operation. In this work, the measurements of wide-area generator speed and bus voltage angle are analysed with the independent component analysis (ICA) to extract the coherency properties of the system. The proposed method clusters the group of generators and buses presenting the common features in the measured signals into their coherent areas by extracting the mixing ratio of independent components from the signals. Although the ICA is able to isolate multiple sources of oscillation in measured data accurately, the algorithm suffers from order inconsistency of the ICs from one convergence to another. This limitations of ICA affects the consistency of the coherency plot for the system, hence the performance of the proposed coherency identification technique. The novel contribution of the method proposed for coherency identification is to deal with this issue by sorting the order of the ICs according to their dominance. The accuracy of the ICA method in identifying coherent groups of generators and buses in the system is compared with the results achieved with the direction cosine and PCA method. In this investigation, it is also found out that the presence of the noise in the measured signals influences the accuracy of the results obtained from coherency identification technique using PCA. Nevertheless, the proposed method identifies the coherent groups of generators precisely even with the presence of the noise in the measured signals. Furthermore, it is demonstrated that the proposed method works well with the practical data gathered through UK University-based WAMS. The implementation of the proposed method is simple and does not require detailed system modelling information.

A study on estimation of measurement-based dynamic model parameters for power system has been investigated. The proposed method is based on the application of an augmented unscented Kalman filter (UKF) approach to estimate the dynamic model parameters using wide-area voltage magnitude, voltage angle, active power, and reactive power measurements. The proposed approach augments the state (rotor angle and speed), the set of unknown model parameters (inertia constant, transient reactance and generator speed voltage), and the process noise covariance into a single higher order state vector. The formulation of the higher order state vector in the UKF algorithm for the dynamic model parameters estimation technique is one of the novel contributions in this thesis. The sigma point distribution in UKF algorithm, applied in this research, has never been applied in

the power system application prior to the work reported in this thesis. Hence, it is considered as one of the novel contributions in this research. The dynamic parameters of the system are estimated by applying the UKF method on the augmented state vector. The accuracy of the estimated parameters obtained in this study is compared with the results achieved using the extended Kalman filter (EKF) method and the actual value of the dynamic model parameters of the system. The accuracy of any data-driven method is always influenced by the presence of noise in the measured data. However, the dynamic model parameters estimated using the proposed method is accurate even with the presence of reasonable level of noise in the measured signals. The outcomes of this study indicate that the UKF method outperforms EKF in estimating the dynamic model parameter in the system, particularly in the presence of noise in the measured data.

It is demonstrated that the change in the system operating condition affects the performance of out-of-step relay. The result shows that the changes in the generator operating condition cause the pre-determined out-of-step relay setting to mal-operate during power swing. This thesis reports an adaptive generator out-of-step protection scheme that adapts to the current system operating condition. Novel contribution of the adaptive out-of-step protection system proposed in this thesis has been made in formulating the algorithm to calculate the setting of an out-of-step protection relay online based on the timely estimations of the dynamic characteristics of the system. The proposed algorithm is initiated by the oscillation in the measured data corresponding to the change in the system operating condition. This is realised by continuously monitoring the measured signals in the system. The algorithm identifies the coherent group of generators using the method proposed in Chapter 3, and estimates the dynamic model parameters of the generators using the method proposed in Chapter 4. The algorithm uses the timely dynamic characteristics obtained in the previous step to analyse the stability of the system in order to determine the critical clearing angle (CCA) and critical clearing time (CCT) of the system. This information (CCA and CCT) is vital for the calculation of the out-of-step relay settings. Calculating the relay settings using the timely information of the CCA and CCT of the system provides an out-of step relay settings that suit to the prevalent system operating condition. The results show that, unlike the pre-determined setting of the conventional out-of-step relays, the adaptive relay settings calculated using the proposed method are able to recognise an out-of-step condition even with changes in the system operating condition. This implies that the proposed method is able

to provide appropriate protection and control actions that suit to the prevalent system operating condition thus eliminating the likelihood of mal-operation of the relay. Technical reports from various blackout experiences suggest that relay mal-operations are often cause of cascaded tripping in the system. Conclusively, the adaptive out-of-step relay proposed in this thesis can prevent wide-area power blackouts.

6.2 Future recommendations

Various research efforts reported in adaptive protection schemes have been reported in the literature. Most of the reported methods are event-based which focusing on the direct stability assessment of an evolving swing to provide appropriate control actions in order to prevent mal-operation of a relay following a disturbance in the system. However, protection engineers have been reluctant to implement the concept of adaptive relaying in practice. This is due to fact that most of the methods reported in the literature eliminate the needs for relay settings during operation. This compromises the security and dependability of relay operation [81, 80]. Therefore, it is necessary to find an alternative to meet the demand from industry as well as benefiting from the adaptive relaying philosophy. The proposed method calculates new settings for the out-of-step relay that suits to the prevalent system condition. This provides an interesting alternative for protection engineers to implement the concept of adaptive relaying in the system. The proposed method is able to calculate new settings for an out-of-step protection relay in approximately 5.2 s from the moment there is a change in the system operating condition. In addition, it is worth noting that the proposed method alone is very fast, able to calculate new settings for an out-of-step relay in 69.9 ms from the moment the measured data is available at the centralised control centre. This difference comes from the time delay from WAMS, and the time windows of measurement required to monitor the oscillation in the system effectively. Furthermore, the adaptive protection architecture (APA) reported in [91] is able to facilitate the application of the adaptive distance protection system as reported in [91]. Hence, it has a potential to facilitate the implementation of the adaptive out-of-step relay proposed in this thesis. The time response for the APA architecture as proposed in [92] is up to several minutes following a disturbance in the

system. Therefore, the time response of the proposed adaptive out-of-step protection system is within the time response of the APA. The advantages offered by the adaptive philosophy adopted in out-of-step relay easily outweigh the performance of conventional out-of-step relay in practice, particularly in preventing a wide-area blackout. Since the APA is able to support the implementation of the proposed adaptive out-of-step protection system, it is easy for the protection engineers to apply the proposed method in a practical power system.

This thesis concludes on the application of the generator out-of-step protection in the system. In this condition, the electrical centre of the system is within the generator transient reactance and the step up transformer reactance due to the fault initiation that is closed to the generator. However, depending on the location and the duration of fault, the electrical centre will occur within the transmission network. This situation is likely to cause the distance relay that is close to the electrical centre to mal-operate and further contribute to the impact of the disturbance in the system. Therefore, it is necessary to determine the location of electrical centre following the system contingency in order to implement power swing blocking scheme effectively. It is also possible to have multiple electrical centres for a large interconnected power system. The coherency identification technique using ICA can be used to detect the location of the electrical centres during power swing. The links between the two different coherent areas indicate the location of electrical centres in the system. Tracking the electrical centre of the system presents an important topic in the area of the adaptive out-of-step protection to be pursued in the near future.

Another promising topic is the integration of renewable sources (wind and solar) and storage devices into the network. Maximum utilisation of these resources requires fast and accurate control and protection scheme for continuous coordination and optimisation with the system. This integration allows additional power system control and optimization schemes which coordinate the operation of the renewable sources with the bulk power system. The integration of storage devices into the network requires optimization continuous store and retrieve function to mitigate the effect of renewable energy variability and maximizing the amount of energy generated from the renewable sources. Therefore, it is obvious that the integration of renewable sources will increase the complexity of the dynamic system representation, which will affect the performance of the control and protection operation. The dynamic model parameters estimation technique using UKF can be

used as a monitoring scheme that will provide a more accurate and more frequent real-time model of the system, which will clear the path for new approaches for control, operation and protection of the power system.

Bibliography

[1] P. Kundur, C. Taylor, and P. Pourbeik, "Blackout experiences and lessons, best practices for system dynamic performance, and the role of new technologies," *IEEE Power Engineering Society Special Publication 07TP190*, 2007.

[2] P. M. Anderson, *Power System Protection*. New York: McGraw-Hill, 1999.

[3] M. McDonald and D. Tziouvaras, "Power swing and out-of-step considerations on transmission lines," *A report to the Power System Relaying Committee of the IEEE Power Engineering Society*, 2005.

[4] S. Mei, X. Zhang, and M. Cao, *Power Grid Complexity*. Berlin: Springer Verlag, 2011.

[5] S. H. Horowitz and A. G. Phadke, *Power System Relaying*. West Sussex: John Wiley & Sons, 2013.

[6] A. G. Phadke and J. S. Thorp, *Computer Relaying for Power Systems*. West Sussex: John Wiley & Sons, 2009.

[7] A. G. Phadke and J. S. Thorp, *Synchronized Phasor Measurements and Their Applications*. New York: Springer Verlag, 2008.

[8] "IEEE Standard for Synchrophasor Measurements for Power Systems," *IEEE Standard C37.118.1-2011 (Revision of IEEE Standard C37.118-2005)*, pp. 1–61, December 2011.

[9] A. Phadke and S. Horowitz, "Adaptive relaying," *IEEE Computer Applications in Power*, vol. 3, no. 3, pp. 47–51, July 1990.

[10] A. Phadke, J. Thorp, and S. Horowitz, "Study of adaptive transmission system protection and control," *Final Report, Oak Ridge National Laboratory*, 1988.

[11] P. Kundur, *Power System Stability and Control*. New York: McGraw-Hill, 1994.

[12] P. W. Sauer and A. Pai, *Power System Dynamics and Stability*. New Jersey: Prentice Hall, 1998.

[13] K. R. Padiyar, *Power System Dynamics: Stability and Control*. Kent: Anshan, 2004.

[14] A. Phadke and B. Kasztenny, "Synchronized phasor and frequency measurement under transient conditions," *IEEE Transactions on Power Delivery*, vol. 24, no. 1, pp. 89–95, January 2009.

[15] "IEEE Guide for Synchronization, Calibration, Testing, and Installation of Phasor Measurement Units (PMUs) for Power System Protection and Control," *IEEE Standard C37.242-2013*, pp. 1–107, March 2013.

[16] G. Rogers, *Power System Oscillations*. New York: Kluwer Academic, 2000.

[17] G. Troullinos and J. Dorsey, "Coherency and model reduction: state space point of view," *IEEE Transactions on Power Systems*, vol. 4, no. 3, pp. 988–995, August 1989.

[18] F. Wu and N. Narasimhamurthi, "Coherency identification for power system dynamic equivalents," *IEEE Transactions on Circuits and Systems*, vol. 30, no. 3, pp. 140–147, March 1983.

[19] R. Podmore, "Identification of coherent generators for dynamic equivalents," *IEEE Transactions on Power Apparatus and Systems*, vol. PAS-97, no. 4, pp. 1344–1354, July 1978.

[20] S. B. Yusof, G. J. Rogers, and R. T. H. Alden, "Slow coherency based network partitioning including load buses," *IEEE Transactions on Power Systems*, vol. 8, no. 3, pp. 1375–1382, August 1993.

[21] G. Ramaswamy, C. Evrard, G. C. Verghese, O. Fillatre, and B. Lesieutre, "Extensions, simplifications, and tests of synchronic modal equivalencing (SME)," *IEEE Transactions on Power Systems*, vol. 12, no. 2, pp. 896–905, May 1997.

[22] X. Wang, V. Vittal, and G. Heydt, "Tracing generator coherency indices using the continuation method: a novel approach," *IEEE Transactions on Power Systems*, vol. 20, no. 3, pp. 1510–1518, August 2005.

[23] M.-E.-A. Abd-EI-Rehim, I. Helal, and M. Omar, "Multi-machine power system dynamic equivalents using artificial intelligence (ANN)," in *Eleventh International Middle East Power Systems Conference, 2006 (MEPCON 2006)*. IEEE, December 2006, pp. 197–207.

[24] M. Davodi, H.-R. Modares, E. Reihani, M. Davodi, and A. Sarikhani, "Coherency approach by hybrid PSO, K-Means clustering method in power system," in *IEEE 2nd International Power and Energy Conference, 2008 (PECon 2008)*. IEEE, December 2008, pp. 1203–1207.

[25] M. Rios and O. Gomez, "Identification of coherent groups and PMU placement for inter-area monitoring based on graph theory," in *IEEE PES Conference on Innovative Smart Grid Technologies (ISGT Latin America), 2011*. IEEE, October 2011, pp. 1–7.

[26] G. Pyo, J. Park, and S. Moon, "A new method for dynamic reduction of power system using PAM algorithm," in *IEEE Power and Energy Society General Meeting, 2010*. IEEE, July 2010, pp. 1–7.

[27] H. Alsafih and R. Dunn, "Determination of coherent clusters in a multi-machine power system based on wide-area signal measurements," in *IEEE Power and Energy Society General Meeting, 2010*. IEEE, July 2010, pp. 1–8.

[28] T. Nababhushana, K. Veeramanju, and Shivanna, "Coherency identification using growing self organizing feature maps [power system stability]," in *Proceedings of International Conference on Energy Management and Power Delivery, 1998 (EMPD '98)*, vol. 1. IEEE, March 1998, pp. 113–116.

[29] K. Lo, Z. Qi, and D. Xiao, "Identification of coherent generators by spectrum analysis," *IEE Proceedings - Generation, Transmission and Distribution*, vol. 142, no. 4, pp. 367–371, July 1995.

[30] M. Jonsson, M. Begovic, and J. Daalder, "A new method suitable for real-time generator coherency determination," *IEEE Transactions on Power Systems*, vol. 19, no. 3, pp. 1473–1482, August 2004.

[31] N. Senroy, "Generator coherency using the Hilbert-Huang transform," *IEEE Transactions on Power Systems*, vol. 23, no. 4, pp. 1701–1708, November 2008.

[32] K. Anaparthi, B. Chaudhuri, N. Thornhill, and B. Pal, "Coherency identification in power systems through principal component analysis," *IEEE Transactions on Power Systems*, vol. 20, no. 3, pp. 1658–1660, August 2005.

[33] K. Anaparthi, "Measurement based identification and control of electromechanical oscillations in power systems," Ph.D. dissertation, Imperial College London, London, March 2006.

[34] J. Thambirajah, N. Thornhill, and B. Pal, "A multivariate approach towards interarea oscillation damping estimation under ambient conditions via independent component analysis and random decrement," *IEEE Transactions on Power Systems*, vol. 26, no. 1, pp. 315–322, February 2011.

[35] C. Xia, J. Howell, and N. Thornhill, "Detecting and isolating multiple plant-wide oscillations via spectral independent component analysis," *Automatica*, vol. 41, no. 12, pp. 2067–2075, December 2005.

[36] C. Xia and J. Howell, "Isolating multiple sources of plant-wide oscillations via independent component analysis," *Control Engineering Practice*, vol. 13, no. 8, pp. 1027–1035, August 2005.

[37] A. R. Messina, *Inter-Area Oscillations in Power Systems: A Nonlinear and Nonstationary Perspective*. New York: Springer Verlag, 2009.

[38] A. Hyvärinen and E. Oja, "A fast fixed-point algorithm for independent component analysis," *Neural Computation*, vol. 9, no. 7, pp. 1483–1492, October 1997.

[39] A. Hyvärinen, J. Karhunen, and E. Oja, *Independent Component Analysis*. New York: John Wiley & Sons, 2001.

[40] W. Li, H. Yue, S. Valle-Cervantes, and S. Qin, "Recursive PCA for adaptive process monitoring," *Journal of Process Control*, vol. 10, no. 5, pp. 471–486, October 2000.

[41] B. C. Pal and B. Chaudhuri, *Robust Control in Power Systems*. New York: Springer, 2005.

[42] P. Kundur, J. Paserba, V. Ajjarapu, G. Andersson, A. Bose, C. Canizares, N. Hatziargyriou, D. Hill, A. Stankovic, C. Taylor, T. Van Cutsem, and

V. Vittal, "Definition and classification of power system stability IEEE/CIGRE joint task force on stability terms and definitions," *IEEE Transactions on Power Systems*, vol. 19, no. 3, pp. 1387–1401, August 2004.

[43] V. Terzija, P. Regulski, L. Kunjumuhammed, B. Pal, G. Burt, I. Abdulhadi, T. Babnik, M. Osborne, and W. Hung, "Flexnet wide area monitoring system," in *IEEE Power and Energy Society General Meeting, 2011.* IEEE, July 2011, pp. 1–7.

[44] J. Paserba, "Analysis and control of power system oscillation," *CIGRE Special Publication 38.01.07*, 1996.

[45] N. Thornhill, S. Shah, B. Huang, and A. Vishnubhotla, "Spectral principal component analysis of dynamic process data," *Control Engineering Practice*, vol. 10, no. 8, pp. 833–846, August 2002.

[46] K. Tang and G. Venayagamoorthy, "Online coherency analysis of synchronous generators in a power system," in *IEEE PES Innovative Smart Grid Technologies Conference (ISGT), 2014.* IEEE, February 2014, pp. 1–5.

[47] "IEEE Guide for Synchronous Generator Modeling Practices and Applications in Power System Stability Analyses," *IEEE Standard 1110-2002 (Revision of IEEE Standard 1110-1991)*, pp. 1–72, December 2003.

[48] J. Sanchez-Gasca, C. Bridenbaugh, C. Bowler, and J. Edmonds, "Trajectory sensitivity based identification of synchronous generator and excitation system parameters," *IEEE Transactions on Power Systems*, vol. 3, no. 4, pp. 1814–1822, November 1988.

[49] J. Ma, B. Hogg, N. Zhiyuan, and Y. Yihan, "On-line decoupled identification of transient and sub-transient generator parameters," *IEEE Transactions on Power Systems*, vol. 9, no. 4, pp. 1908–1914, November 1994.

[50] M. Burth, G. Verghese, and M. Velez-Reyes, "Subset selection for improved parameter estimation in on-line identification of a synchronous generator," *IEEE Transactions on Power Systems*, vol. 14, no. 1, pp. 218–224, February 1999.

[51] M. Karrari and O. P. Malik, "Identification of physical parameters of a synchronous generator from online measurements," *IEEE Transactions on Energy Conversion*, vol. 19, no. 2, pp. 407–414, June 2004.

[52] P. Pourbeik, "Automated parameter derivation for power plant models from system disturbance data," in *IEEE Power and Energy Society General Meeting, 2009*. IEEE, July 2009, pp. 1–10.

[53] D. Meng, N. Zhou, S. Lu, and G. Lin, "An expectation-maximization method for calibrating synchronous machine models," in *IEEE Power and Energy Society General Meeting (PES), 2013*. IEEE, July 2013, pp. 1–5.

[54] C.-C. Tsai, W.-J. Lee, E. Nashawati, C.-C. Wu, and H.-W. Lan, "PMU based generator parameter identification to improve the system planning and operation," in *IEEE Power and Energy Society General Meeting, 2012*. IEEE, July 2012, pp. 1–8.

[55] J. Chow, A. Chakrabortty, L. Vanfretti, and M. Arcak, "Estimation of radial power system transfer path dynamic parameters using synchronized phasor data," *IEEE Transactions on Power Systems*, vol. 23, no. 2, pp. 564–571, May 2008.

[56] A. Chakrabortty, J. Chow, and A. Salazar, "A measurement-based framework for dynamic equivalencing of large power systems using wide-area phasor measurements," *IEEE Transactions on Smart Grid*, vol. 2, no. 1, pp. 68–81, March 2011.

[57] Z. Huang, P. Du, D. Kosterev, and S. Yang, "Generator dynamic model validation and parameter calibration using phasor measurements at the point of connection," *IEEE Transactions on Power Systems*, vol. 28, no. 2, pp. 1939–1949, May 2013.

[58] L. Fan and Y. Wehbe, "Extended kalman filtering based real-time dynamic state and parameter estimation using PMU data," *Electric Power Systems Research*, vol. 103, no. 0, pp. 168–177, October 2013.

[59] S. Julier, J. Uhlmann, and H. Durrant-Whyte, "A new approach for filtering nonlinear systems," in *Proceedings of the American Control Conference, 1995*, vol. 3, June 1995, pp. 1628–1632.

[60] S. J. Julier and J. K. Uhlmann, *Data Fusion in Nonlinear Systems*. Florida: CRC Press, 2001.

[61] A. Singh and B. Pal, "Decentralized dynamic state estimation in power systems using unscented transformation," *Power Systems, IEEE Transactions on*, vol. 29, no. 2, pp. 794–804, March 2014.

[62] E. Ghahremani and I. Kamwa, "Online state estimation of a synchronous generator using unscented Kalman filter from phasor measurements units," *IEEE Transactions on Energy Conversion*, vol. 26, no. 4, pp. 1099–1108, December 2011.

[63] G. Valverde, E. Kyriakides, G. Heydt, and V. Terzija, "Nonlinear estimation of synchronous machine parameters using operating data," *IEEE Transactions on Energy Conversion*, vol. 26, no. 3, pp. 831–839, September 2011.

[64] Y. Wehbe and L. Fan, "UKF based estimation of synchronous generator electromechanical parameters from phasor measurements," in *North American Power Symposium (NAPS), 2012*. IEEE, September 2012, pp. 1–6.

[65] S. Julier and J. Uhlmann, "Unscented filtering and nonlinear estimation," *Proceedings of the IEEE*, vol. 92, no. 3, pp. 401–422, March 2004.

[66] E. Wan and R. Van der Merwe, "The unscented kalman filter for nonlinear estimation," in *The IEEE Adaptive Systems for Signal Processing, Communications, and Control Symposium, 2000 (AS-SPCC)*. IEEE, October 2000, pp. 153–158.

[67] Y. Wu, D. Hu, M. Wu, and X. Hu, "Unscented kalman filtering for additive noise case: augmented versus nonaugmented," *IEEE Signal Processing Letters*, vol. 12, no. 5, pp. 357–360, May 2005.

[68] N. J. Higham, *Accuracy and stability of numerical algorithms*. Philadelphia: Siam, 2002.

[69] R. Kandepu, B. Foss, and L. Imsland, "Applying the unscented Kalman filter for nonlinear state estimation," *Journal of Process Control*, vol. 18, no. 7-8, pp. 753–768, August 2008.

[70] C. Nwankpa and S. Shahidehpour, "Colored noise modelling in the reliability evaluation of electric power systems," *Applied Mathematical Modelling*, vol. 14, no. 7, pp. 338–351, July 1990.

[71] S. V. Vaseghi, *Advanced Digital Signal Processing and Noise Reduction*. West Sussex: John Wiley & Sons, 2006.

[72] A. Abdelaziz, M. Irving, M. Mansour, A. El-Arabaty, and A. Nosseir, "Adaptive protection strategies for detecting power system out-of-step conditions using neural networks," *IEE Proceedings - Generation, Transmission and Distribution*, vol. 145, no. 4, pp. 387–394, July 1998.

[73] V. Centeno, A. Phadke, A. Edris, J. Benton, M. Gaudi, and G. Michel, "An adaptive out-of-step relay [for power system protection]," *IEEE Transactions on Power Delivery*, vol. 12, no. 1, pp. 61–71, January 1997.

[74] S. Paudyal, G. Ramakrishna, and M. Sachdev, "Application of equal area criterion conditions in the time domain for out-of-step protection," *IEEE Transactions on Power Delivery*, vol. 25, no. 2, pp. 600–609, April 2010.

[75] K. So, J. Heo, C. Kim, R. Aggarwal, and K. Song, "Out-of-step detection algorithm using frequency deviation of voltage," *IET Generation, Transmission Distribution*, vol. 1, no. 1, pp. 119–126, January 2007.

[76] C. Mozina and J. Gardell, "IEEE tutorial on the protection of synchronous generators (second edition)," *IEEE Power Engineering Society Special Publication of the IEEE Power System Relaying Committee*, 2011.

[77] "IEEE Guide for AC Generator Protection," *IEEE Standard C37.102-2006 (Revison of IEEE Standard C37.102-1995)*, pp. 1–177, February 2007.

[78] Y. Xue, T. Van Custem, and M. Ribbens-Pavella, "Extended equal area criterion justifications, generalizations, applications," *Power Systems, IEEE Transactions on*, vol. 4, no. 1, pp. 44–52, February 1989.

[79] M. Pavella, D. Ernst, and D. Ruiz-Vega, *Transient Stability of Power Systems: A Unified Approach to Assessment and Control*. Massachusetts: Kluwer Academic, 2000.

[80] E. Bernabeu, J. Thorp, and V. Centeno, "Methodology for a security/dependability adaptive protection scheme based on data mining," *IEEE Transactions on Power Delivery*, vol. 27, no. 1, pp. 104–111, Jan 2012.

[81] I. Abdulhadi, "Facilitating the validation of adaptive power system protection through formal scheme modelling and performance verification," Ph.D. dissertation, University of Strathclyde, Glasgow, August 2013.

[82] Y. Zhang *et al.*, "SIME: A hybrid approach to fast transient stability assessment and contingency selection," *International Journal of Electrical Power & Energy Systems*, vol. 19, no. 3, pp. 195–208, March 1997.

[83] H.-D. Chiang and J. Thorp, "The closest unstable equilibrium point method for power system dynamic security assessment," *IEEE Transactions on Circuits and Systems*, vol. 36, no. 9, pp. 1187–1200, September 1989.

[84] R. Treinen, V. Vittal, and W. Kliemann, "An improved technique to determine the controlling unstable equilibrium point in a power system," *IEEE Transactions on Circuits and Systems I: Fundamental Theory and Applications*, vol. 43, no. 4, pp. 313–323, April 1996.

[85] H.-D. Chiang, F. Wu, and P. Varaiya, "Foundations of the potential energy boundary surface method for power system transient stability analysis," *IEEE Transactions on Circuits and Systems*, vol. 35, no. 6, pp. 712–728, June 1988.

[86] H.-D. Chiang, F. Wu, and P. Varaiya, "A BCU method for direct analysis of power system transient stability," *IEEE Transactions on Power Systems*, vol. 9, no. 3, pp. 1194–1208, August 1994.

[87] V. Vittal, P. Sauer, S. Meliopoulos, and G. Stefopoulos, "Online transient stability assessment scoping study," *Power Systems Engineering Research Center (PSERC) Project Report*, 2005.

[88] C. Mozina and J. Gardell, "IEEE tutorial on the protection of synchronous generators," *IEEE Power Engineering Society Special Publication of the IEEE Power System Relaying Committee*, 1995.

[89] D. Reimert, *Protective Relaying for Power Generation Systems*. Florida: CRC Press, 2006.

[90] J. Berdy, "Out-of-step protection for generators," in *Georgia Institute of Technology Protective Relay Conference*. Georgia Tech, May 1976, pp. 1–26.

[91] I. Abdulhadi, F. Coffele, A. Dysko, C. Booth, and G. Burt, "Adaptive protection architecture for the smart grid," in *2nd IEEE PES International Conference and Exhibition on Innovative Smart Grid Technologies (ISGT Europe), 2011*. IEEE, December 2011, pp. 1–8.

Appendix A

16-machine 68-bus test system model data

All the data is specified in system base MVA = 100 MVA. The bus data, line data and dynamic characteristics of the systems are available in [16, 41].

Table A.1: Bus data

Bus no	V_b (pu)	θ_b (degree)	P_g (pu)	Q_g (pu)	P_L (pu)	Q_L (pu)	G (pu)	B (pu)
1.00	1.00	12.24	2.50	0.15	0.00	0.00	0.00	0.00
2.00	0.99	15.15	5.45	1.76	0.00	0.00	0.00	0.00
3.00	1.00	17.38	6.50	2.14	0.00	0.00	0.00	0.00
4.00	1.00	18.97	6.32	0.77	0.00	0.00	0.00	0.00
5.00	1.01	17.44	5.00	1.37	0.00	0.00	0.00	0.00
6.00	1.05	21.99	7.00	3.01	0.00	0.00	0.00	0.00
7.00	1.03	24.70	5.60	1.20	0.00	0.00	0.00	0.00
8.00	1.03	17.57	5.40	0.87	0.00	0.00	0.00	0.00
9.00	1.03	22.13	8.00	0.52	0.00	0.00	0.00	0.00
10.00	1.01	17.12	5.00	0.23	0.00	0.00	0.00	0.00
11.00	1.00	19.85	10.00	0.15	0.00	0.00	0.00	0.00
12.00	1.02	5.31	13.50	2.91	0.00	0.00	0.00	0.00
13.00	1.01	0.00	36.04	9.10	0.00	0.00	0.00	0.00
14.00	1.00	48.09	17.85	1.06	0.00	0.00	0.00	0.00
15.00	1.00	41.60	10.00	0.71	0.00	0.00	0.00	0.00
16.00	1.00	47.11	40.00	5.06	0.00	0.00	0.00	0.00
17.00	0.99	-6.84	0.00	0.00	60.00	3.00	0.00	0.00
18.00	0.99	40.16	0.00	0.00	24.70	1.23	0.00	0.00
19.00	0.99	13.80	0.00	0.00	0.00	0.00	0.00	0.00
20.00	0.99	12.32	0.00	0.00	6.80	1.03	0.00	0.00
21.00	0.99	11.54	0.00	0.00	2.74	1.15	0.00	0.00
22.00	1.01	16.59	0.00	0.00	0.00	0.00	0.00	0.00
23.00	1.01	16.29	0.00	0.00	2.48	0.85	0.00	0.00
24.00	0.99	8.85	0.00	0.00	3.09	-0.92	0.00	0.00
25.00	1.01	10.71	0.00	0.00	2.24	0.47	0.00	0.00

Bus no	V_b (pu)	θ_b (degree)	P_g (pu)	Q_g (pu)	P_L (pu)	Q_L (pu)	G (pu)	B (pu)
26.00	1.01	9.14	0.00	0.00	1.39	0.17	0.00	0.00
27.00	1.00	7.13	0.00	0.00	2.81	0.76	0.00	0.00
28.00	1.02	12.49	0.00	0.00	2.06	0.28	0.00	0.00
29.00	1.02	15.29	0.00	0.00	2.84	0.27	0.00	0.00
30.00	1.01	7.05	0.00	0.00	0.00	0.00	0.00	0.00
31.00	1.01	9.82	0.00	0.00	0.00	0.00	0.00	0.00
32.00	1.01	12.43	0.00	0.00	0.00	0.00	0.00	0.00
33.00	1.01	8.65	0.00	0.00	1.12	0.00	0.00	0.00
34.00	1.02	3.33	0.00	0.00	0.00	0.00	0.00	0.00
35.00	1.02	3.32	0.00	0.00	0.00	0.00	0.00	0.00
36.00	1.00	-0.41	0.00	0.00	1.02	-0.19	0.00	0.00
37.00	0.99	7.47	0.00	0.00	0.00	0.00	0.00	0.00
38.00	1.01	9.85	0.00	0.00	0.00	0.00	0.00	0.00
39.00	0.98	-8.22	0.00	0.00	2.67	0.13	0.00	0.00
40.00	1.03	16.66	0.00	0.00	0.66	0.24	0.00	0.00
41.00	1.00	46.55	0.00	0.00	10.00	2.50	0.00	0.00
42.00	1.00	40.74	0.00	0.00	11.50	2.50	0.00	0.00
43.00	0.99	-7.48	0.00	0.00	0.00	0.00	0.00	0.00
44.00	0.99	-7.51	0.00	0.00	2.68	0.05	0.00	0.00
45.00	1.01	3.32	0.00	0.00	2.08	0.21	0.00	0.00
46.00	0.99	10.77	0.00	0.00	1.51	0.28	0.00	0.00
47.00	1.03	8.36	0.00	0.00	2.03	0.33	0.00	0.00
48.00	1.03	10.38	0.00	0.00	2.41	0.02	0.00	0.00
49.00	0.98	14.11	0.00	0.00	1.64	0.29	0.00	0.00
50.00	1.01	20.55	0.00	0.00	1.00	-1.47	0.00	0.00
51.00	1.02	7.43	0.00	0.00	3.37	-1.22	0.00	0.00
52.00	0.98	6.54	0.00	0.00	1.58	0.30	0.00	0.00
53.00	1.01	7.62	0.00	0.00	2.53	1.19	0.00	0.00
54.00	1.00	9.64	0.00	0.00	0.00	0.00	0.00	0.00
55.00	0.98	6.27	0.00	0.00	3.22	0.02	0.00	0.00
56.00	0.95	5.03	0.00	0.00	5.00	1.84	0.00	0.00
57.00	0.95	6.11	0.00	0.00	0.00	0.00	0.00	0.00
58.00	0.96	6.87	0.00	0.00	0.00	0.00	0.00	0.00
59.00	0.96	4.35	0.00	0.00	2.34	0.84	0.00	0.00
60.00	0.96	3.75	0.00	0.00	5.22	1.77	0.00	0.00
61.00	0.99	3.27	0.00	0.00	1.04	1.25	0.00	0.00
62.00	0.97	9.65	0.00	0.00	0.00	0.00	0.00	0.00
63.00	0.96	8.70	0.00	0.00	0.00	0.00	0.00	0.00
64.00	0.95	8.72	0.00	0.00	0.09	0.88	0.00	0.00
65.00	0.96	8.90	0.00	0.00	0.00	0.00	0.00	0.00
66.00	0.96	7.16	0.00	0.00	0.00	0.00	0.00	0.00
67.00	0.96	6.99	0.00	0.00	3.20	1.53	0.00	0.00
68.00	0.98	8.67	0.00	0.00	3.29	0.32	0.00	0.00

Table A.2: Line data

From bus	To bus	Resistance (pu)	Reactance (pu)	Line charging (pu)
54.00	1.00	0.00000	0.0181	0.0000
58.00	2.00	0.00000	0.0250	0.0000
62.00	3.00	0.00000	0.0200	0.0000
19.00	4.00	0.00070	0.0142	0.0000

From bus	To bus	Resistance (pu)	Reactance (pu)	Line charging (pu)
20.00	5.00	0.00090	0.0180	0.0000
22.00	6.00	0.00000	0.0143	0.0000
23.00	7.00	0.00050	0.0272	0.0000
25.00	8.00	0.00060	0.0232	0.0000
29.00	9.00	0.00080	0.0156	0.0000
31.00	10.00	0.00000	0.0260	0.0000
32.00	11.00	0.00000	0.0130	0.0000
36.00	12.00	0.00000	0.0075	0.0000
17.00	13.00	0.00000	0.0033	0.0000
41.00	14.00	0.00000	0.0015	0.0000
42.00	15.00	0.00000	0.0015	0.0000
18.00	16.00	0.00000	0.0030	0.0000
36.00	17.00	0.00050	0.0045	0.3200
49.00	18.00	0.00760	0.1141	1.1600
50.00	18.00	0.00120	0.0288	2.0600
68.00	19.00	0.00160	0.0195	0.3040
19.00	20.00	0.00070	0.0138	0.0000
68.00	21.00	0.00080	0.0135	0.2548
21.00	22.00	0.00080	0.0140	0.2565
22.00	23.00	0.00060	0.0096	0.1846
23.00	24.00	0.00220	0.0350	0.3610
68.00	24.00	0.00030	0.0059	0.0680
54.00	25.00	0.00700	0.0086	0.1460
25.00	26.00	0.00320	0.0323	0.5310
37.00	27.00	0.00130	0.0173	0.3216
26.00	27.00	0.00140	0.0147	0.2396
26.00	28.00	0.00430	0.0474	0.7802
26.00	29.00	0.00570	0.0625	1.0290
28.00	29.00	0.00140	0.0151	0.2490
53.00	30.00	0.00080	0.0074	0.4800
61.00	30.00	0.00095	0.0092	0.5800
30.00	31.00	0.00130	0.0187	0.3330
53.00	31.00	0.00160	0.0163	0.2500
30.00	32.00	0.00240	0.0288	0.4880
32.00	33.00	0.00080	0.0099	0.1680
33.00	34.00	0.00110	0.0157	0.2020
35.00	34.00	0.00010	0.0074	0.0000
34.00	36.00	0.00330	0.0111	1.4500
61.00	36.00	0.00110	0.0098	0.6800
68.00	37.00	0.00070	0.0089	0.1342
31.00	38.00	0.00110	0.0147	0.2470
33.00	38.00	0.00360	0.0444	0.6930
41.00	40.00	0.00600	0.0840	3.1500
48.00	40.00	0.00200	0.0220	1.2800
42.00	41.00	0.00400	0.0600	2.2500
18.00	42.00	0.00400	0.0600	2.2500
17.00	43.00	0.00050	0.0276	0.0000
39.00	44.00	0.00000	0.0411	0.0000
43.00	44.00	0.00010	0.0011	0.0000
35.00	45.00	0.00070	0.0175	1.3900
39.00	45.00	0.00000	0.0839	0.0000
44.00	45.00	0.00250	0.0730	0.0000
38.00	46.00	0.00220	0.0284	0.4300
53.00	47.00	0.00130	0.0188	1.3100
47.00	48.00	0.00125	0.0134	0.8000

From bus	To bus	Resistance (pu)	Reactance (pu)	Line charging (pu)
46.00	49.00	0.00180	0.0274	0.2700
45.00	51.00	0.00040	0.0105	0.7200
50.00	51.00	0.00090	0.0221	1.6200
37.00	52.00	0.00070	0.0082	0.1319
55.00	52.00	0.00110	0.0133	0.2138
53.00	54.00	0.00350	0.0411	0.6987
54.00	55.00	0.00130	0.0151	0.2572
55.00	56.00	0.00130	0.0213	0.2214
56.00	57.00	0.00080	0.0128	0.1342
57.00	58.00	0.00020	0.0026	0.0434
58.00	59.00	0.00060	0.0092	0.1130
57.00	60.00	0.00080	0.0112	0.1476
59.00	60.00	0.00040	0.0046	0.0780
60.00	61.00	0.00230	0.0363	0.3804
58.00	63.00	0.00070	0.0082	0.1389
62.00	63.00	0.00040	0.0043	0.0729
64.00	63.00	0.00160	0.0435	0.0000
62.00	65.00	0.00040	0.0043	0.0729
64.00	65.00	0.00160	0.0435	0.0000
56.00	66.00	0.00080	0.0129	0.1382
65.00	66.00	0.00090	0.0101	0.1723
66.00	67.00	0.00180	0.0217	0.3660
67.00	68.00	0.00090	0.0094	0.1710
53.00	27.00	0.03200	0.3200	0.4100

Table A.3: Synchronous generator parameters

Mac No.	Bus No.	Base MVA	X_l (pu)	R_a (pu)	x_d (pu)	x'_d (pu)	T'_{d0} (s)	x_q (pu)	x'_q (pu)	T'_{q0} (pu)	H (s)
1.00	1.00	100.00	0.01	0.00	0.10	0.03	10.20	0.07	0.03	1.50	42.00
2.00	2.00	100.00	0.04	0.00	0.30	0.07	6.56	0.28	0.06	1.50	30.20
3.00	3.00	100.00	0.03	0.00	0.25	0.05	5.70	0.24	0.05	1.50	35.80
4.00	4.00	100.00	0.03	0.00	0.26	0.04	5.69	0.26	0.04	1.50	28.60
5.00	5.00	100.00	0.03	0.00	0.33	0.07	5.40	0.31	0.06	0.44	26.00
6.00	6.00	100.00	0.02	0.00	0.25	0.05	7.30	0.24	0.05	0.40	34.80
7.00	7.00	100.00	0.03	0.00	0.30	0.05	5.66	0.29	0.05	1.50	26.40
8.00	8.00	100.00	0.03	0.00	0.29	0.06	6.70	0.28	0.05	0.41	24.30
9.00	9.00	100.00	0.03	0.00	0.21	0.06	4.79	0.21	0.05	1.96	34.50
10.00	10.00	100.00	0.02	0.00	0.17	0.05	9.37	0.12	0.05	1.50	31.00
11.00	11.00	100.00	0.01	0.00	0.13	0.02	4.10	0.12	0.02	1.50	28.20
12.00	12.00	100.00	0.02	0.00	0.10	0.03	7.40	0.10	0.03	1.50	92.30
13.00	13.00	200.00	0.00	0.00	0.01	0.00	5.90	0.01	0.00	1.50	496.00
14.00	14.00	100.00	0.00	0.00	0.02	0.00	4.10	0.02	0.00	1.50	300.00
15.00	15.00	100.00	0.00	0.00	0.02	0.00	4.10	0.02	0.00	1.50	300.00
16.00	16.00	200.00	0.00	0.00	0.02	0.00	7.80	0.02	0.00	1.50	450.00